Enhancing the Fretting Fatigue strength of Titanium alloys, Ni-based superalloys, and Magnesium alloys by reducing stress at contact and by making composites

Ph.D. thesis

By

Sangam Sangral
(1701205007)

DEPARTMENT OF METALLURGY ENGINEERING AND MATERIALS SCIENCE

INDIAN INSTITUTE OF TECHNOLOGY INDORE

May 2022

Enhancing the Fretting Fatigue strength of Titanium alloys, Ni-based superalloys, and Magnesium alloys by reducing stress at contact and by making composites

A THESIS

Submitted in partial fulfillment of the requirements for the award of the degree
of

DOCTOR OF PHILOSOPHY

by

Sangam Sangral
(1701205007)

Under the Supervision of

Dr. Jayaprakash Murugesan

DEPARTMENT OF METALLURGY ENGINEERING AND MATERIALS SCIENCE

INDIAN INSTITUTE OF TECHNOLOGY INDORE

May 2022

INDIAN INSTITUTE OF TECHNOLOGY INDORE

CANDIDATE'S DECLARATION

I hereby certify that the work which is being presented in the thesis entitled **"Enhancing the Fretting Fatigue strength of Titanium alloys, Ni-based superalloys, and Magnesium alloys by reducing stress at contact and by making composites"** in the partial fulfillment of the requirements for the award of the degree of DOCTOR OF PHILOSOPHY and submitted in the DEPARTMENT OF METALLURGY ENGINEERING AND MATERIALS SCIENCE, **Indian Institute of Technology Indore** is an authentic record of my own work carried out during the time period from December 2017 to April 2022 under the supervision of Dr. Jayaprakash Murugesan (Assistant Professor) at IIT Indore.

The matter presented in this thesis has not been submitted by me for the award of any other degree of this or any other institute.

Signature of the student with date
(NAME OF THE Ph.D. STUDENT)
Sangam Sangral

This is to certify that the above statement made by the candidate is correct to the best of my knowledge.

Signature of the Supervisor

(Dr. Jayaprakash Murugesan)

ACKNOWLEDGEMENTS

First of all, I would like to thank each and everyone who supported me directly or indirectly in accomplishing my Ph.D. journey fruitfully. Being a mechanical engineer, I never thought of stepping into the world of Metallurgy and Materials Science. But the interest in this realm of Materials Engineering was initially fueled by my M. Tech project supervisor **Dr. Kartik Prasad**, by his informative, interesting, and enthusiastic lectures during my post-graduation (2016-2017) at Defence Metallurgical Research laboratory (DMRL), Hyderabad. His lectures really inspired me to a great extent and motivated me to pursue my higher studies in the domain of Materials Engineering.

I convey special thanks to my Ph.D. thesis supervisor **Dr. Jayaprakash** for providing me a platform to work as a doctoral student in the Department of Metallurgy Engineering and Materials Science at IIT Indore. I am grateful to my supervisor for his esteemed guidance and continuous support throughout the Ph.D. program. The cool nature and crisply simplifying things are admirable in **Dr. Jayaprakash Murugesan.** Sir, your valuable suggestions during the presentations, in addressing the review comments helped me a lot. Moreover, you gave me a wonderful opportunity to work as a research exchange student at Nagaoka University of Technology, Japan. Sir, thank you for providing me with international exposure. Sir your enthusiasm for research and your energy levels and your unique hard-working nature is highly inspirable. I am really fortunate to work with you. I would also like to thank **Dr. M. Okazaki** for accepting me as a research exchange student at Nagaoka University of Technology, Japan and providing continuous support during the experimental work.

I must take this opportunity to thank the previous and current Directors (**Prof. Mathur**), (**Prof. Neelesh Kumar Jain**) and (**Prof. Suhas S. Joshi**) of **IIT Indore** and **Head** (**Dr. Vinod Kumar**) of the **Department of Metallurgy Engineering and Materials Science** for providing me enough facilities and support during my research work. I express my sincere thanks to the Ph.D. Students Progress Committee (PSPC) members **Dr. Anand Parey** and **Dr. Hemant Borkar** for their valuable inputs during the comprehensive research evaluations. I thank MHRD, Govt. of India for Teaching Assistantship (TA) position. I would like to thank **Dr. Sumanta Samal** for giving the access to various facilities in his lab.

I would like to express special thanks to my lab mates (Mr. Achyuth Kulkarni and Mr. Mahesh Patel), my beloved friends (Mr. Sharath Kumar, Mr. Sandeep Jain, Mr. Reliance Jain, Mr. Bhavesh Chaudhary, Mr. Akhalesh Sharma, Mr. Mahendar, Mr. Mukul Kumar, Mr. Santosh Bimli and Mr. Satyam Singh), for the support and experimental assistance during my research work. Without having a good ambiance inside the laboratory, it is very difficult to achieve the research goals. Therefore, I thank both the lab members for making my stay pleasant and healthy. I thank **Mr. Mayur Dhake** and **Sophisticated Instrumentation Centre (SIC), IIT Indore** for assisting during the FESEM characterization facility.

Last but not the least, I would like to express my heartfelt gratitude to my parents Smt. Chanan Devi and Sh. Des Raj for their unconditional love, caring, and financial as well as moral support from my childhood. Without them, I am nobody today. Finally, I would like to thank my dearest brothers, Mr. Mukesh Kumar, and Mr. Pawan Sangral, for their love, motivation, and encouragement. They always used to tell me to do something different during my Ph.D. and they used to say to work on real-time problems for the betterment of society.

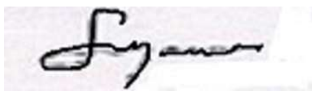

(Sangam Sangral)

Dedicated to…

My Parents

Shri Des Raj Sangral

&

Smt. Chanan Devi

&

(To my Late Grandparents)

ABSTRACT

The investigation embodied in the thesis entitled “Enhancing the Fretting Fatigue strength of Titanium alloys, Ni-based superalloys, and Magnesium alloys by reducing stress at contact and by making composites” was initiated in Dec 2017 in the Department of Metallurgy Engineering & Materials Science, Indian Institute of Technology Indore.

Fretting damage is one of the major problems encountered between the contact surfaces in the mechanical systems, aircraft, and automobile components that are subjected to a synergistic action of load and small amplitude (<300 μm) oscillatory vibrations. Due to fretting, wear can takes place at the contact which causes the loss of fit and leads to heavy noise, vibration, and ultimately fracture in some of the systems. The fretting wear accelerates the fretting fatigue by the initiation of cracks in localized areas. Due to fretting fatigue, the fatigue strength of the component is reduced drastically more than 50 %. Therefore, my thesis work aims in improving the fatigue strength of Titanium alloys and Ni-based superalloys by reducing the stress at the contact during fretting and by fabricating magnesium metal matrix composite (MMC) to improve the fretting fatigue life of the component. The primary objectives of the thesis work are listed as follows:

1) To enhance the fretting fatigue life by reducing the stress or wear damage on the contact surface by introducing soft or porous material.
2) Fabrication of composite by incorporation of hard metal reinforced particles into the matrix to improve the fretting fatigue strength of the alloy.

This thesis comprises 5 chapters in total. **Chapter-1** includes the introduction to fretting fatigue, engineering alloys and their applications in aerospace and automobile industries and literature review. **Chapter-2** describes the effect of contact pad geometry on the fretting fatigue behavior of titanium alloy by experimental and finite element analysis. In this chapter, the effect of two different contact pad geometries were examined in detail. **Chapter-3** illustrates the effect of introducing porous material in the contact pad on the fretting fatigue behavior of nickel-based

superalloys. This chapter specifically deals with the effect of fretting on fatigue behaviour of Ni-based superalloys using slit contact pad with porous material and co-relate results with slit contact pad and flat contact pad. While **Chapter-4** discusses the fretting fatigue behavior of magnesium metal matrix composite fabricated through friction stir processing using nickel reinforced particles. In this study, a metal matrix composite was fabricated through friction stir processing (FSP) to get a proper distribution of particles and avoid intermetallic. In **Chapter-5** conclusions and future scope of this thesis work have been discussed in the field of enhancement of fretting fatigue life of various alloys.

LIST OF PUBLICATIONS

Publications from the Ph.D. Thesis

1. **S Sangral**, P Maheandera Prabu, M Jayaprakash, Experimental and Finite Element Analysis of Measuring the Effect of Fretting on Fatigue Behavior of IMI 834 Titanium Alloy, Journal of Failure Analysis and Prevention, 2022; 22: 609–622 DOI: 10.1007/s11668-022-01343-7
2. **S Sangral**, M Jayaprakash, Evaluating the effect of contact pad geometry on the fretting fatigue behavior of titanium alloy by experimental and finite element analysis, Journal of Failure Analysis and Prevention, 2022; 22: 773–784 DOI: 10.1007/s11668-022-01369-x
3. **S Sangral**, M Patel, M Jayaprakash, Fretting fatigue behavior of Magnesium Metal Matrix Composite Fabricated through Friction Stir Processing using Nickel Reinforced Particles, Journal of Failure Analysis and Prevention, 2022 DOI: 10.1007/s11668-022-01393-x
4. **S Sangral**, K Achyuth, M Patel, M Jayaprakash, Effect of Fretting on Fatigue Behavior of Al Alloys Considering Environmental Effect, Materials Today: Proceedings, 2019; 15: 119-125. DOI: 10.1016/j.matpr.2019.05.033
5. **S Sangral**, M Patel, M Jayaprakash, Fabrication of Magnesium Matrix Composite using Nickel Particles as Reinforcement through FSP with Improve Mechanical Properties, Journal of Materials Engineering and Performance. (Under review)
6. **S Sangral**, M Jayaprakash, Effect of Introducing Porous Material in the Contact Pad on the Fretting Fatigue Behavior of Nickel Based Superalloys, Tribology International. (Under review)

Publications apart from the Ph.D. Thesis

1. M Patel, **S Sangral**, K Achyuth, M Jayaprakash, Fretting Wear Behavior of The Hardfaced Structural Steel Under Corrosive Environment, Materials Today: Proceedings, 15, 2019, 96-102. DOI: 10.1016/j.matpr.2019.05.030

2. K Achyuth, M Patel, **S Sangral**, M Jayaprakash, Fretting wear degradation behavior of Al-Si-Ni based cast Aluminium alloy under different environment, Materials Today: Proceedings, 15, 2019, 103-108. DOI: 10.1016/j.matpr.2019.05.031

3. M Patel, **S Sangral**, M Jayaprakash, Study on Microstructure and Mechanical Properties of Hybrid Aluminium Matrix Composite with Zro_2 and Ni Particles as Reinforcement Fabricated through FSP Route, Advanced Composite Materials, 2022, 1-17. DOI: 10.1080/09243046.2022.2120729

4. M Patel, **S Sangral**, M Jayaprakash, Effect of Friction Stir Processing on Plain Fatigue and Fretting Fatigue Behavior of the AA6063 Alloy, Tribology International. (Submitted)

5. M. Jayaprakash, K. Achyuth, M. Patel, **S Sangral**, Fretting Fatigue Behavior of Aluminium Alloy, Structural Integrity Assessment, 683-690. (Book Chapter)

TABLE OF CONTENTS

Page No.

Contents

LIST OF FIGURES

LIST OF TABLES

ACRONYMS

RT – Room Temperature

OM – Optical Microscopy

XRD – X-Ray Diffraction

FESEM – Field Emission Scanning Electron MicroscopyEDS – Energy Dispersive Spectroscopy

FW – Fretting Wear

R_a – Average RoughnessWt% - Weight %

CoF – Coefficient of Friction3D – 3 Dimensional

YS – Yield Strength

UTS – Ultimate Tensile Strength

FSP – Friction Stir Processing

FEA – Finite Element Analysis

EDM – Electrical Discharge Machining

MMC – Metal Matrix Composite

Chapter 1

Introduction to fretting fatigue, engineering alloys and their applications in aerospace and automobile industries.

1.1. Introduction to Fretting wear and fretting fatigue

Fretting is one of the major problems encountered between the contact surfaces in the mechanical systems, aircraft, and automobile components that are subjected to a synergistic action of load and small amplitude (<300 μm) oscillatory vibrations. Due to fretting, wear takes place at the contact which causes the loss of fit and leads to heavy noise, vibration, and failure of the component. The fretting wear accelerates the fretting fatigue by the initiation of cracks in localized areas. Due to fretting, the fatigue strength of the component is reduced drastically more than 50 %. Fretting fatigue failures are common in turbine blades, bolted assembly, wire ropes, human hip joint etc [1-7]. As a result, investigations to prevent fretting and to develop fretting tests takes place in many different areas of science and industry. Few examples of the parts that were experienced fretting fatigue damage are shown in Fig.1.1.

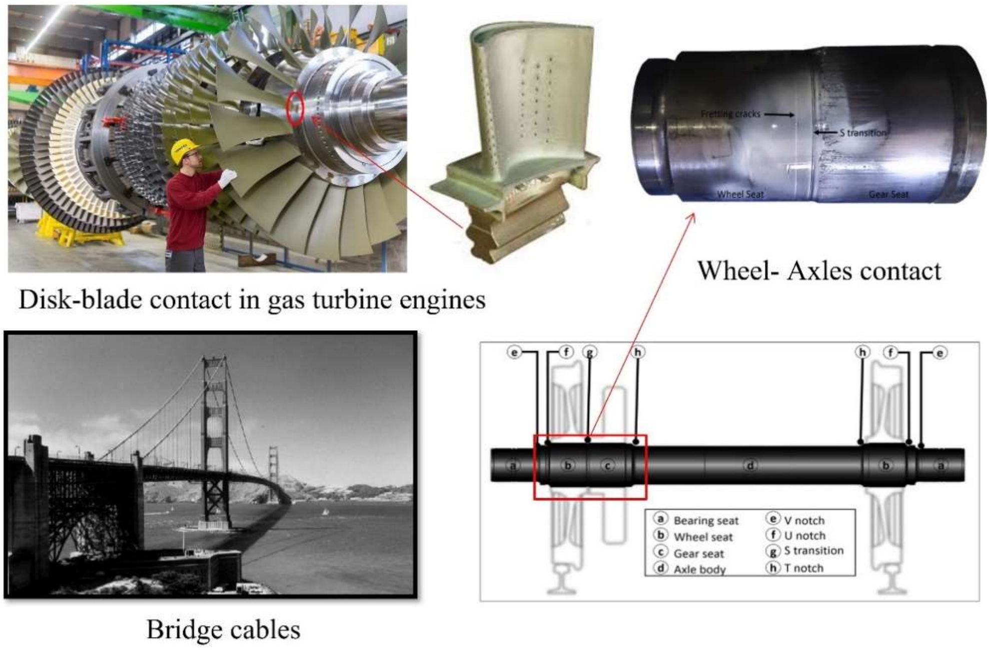

Fig. 1.1 Examples of fretting fatigue damage in various components [3, 8, 13, 44]

There are numerous research findings on fretting fatigue, where researchers have tried to understand the effect of fretting fatigue parameters, also many fretting fatigue strength prediction methods has been proposed [6-10]. However due to the complex interaction of multiple fretting fatigue variables like, contact pressure, coefficient of friction, relative slip amplitude, specimen geometry, complexity in stress distribution during loading etc., still fretting fatigue problem remains fully unsolved.

1.2. Introduction to Engineering alloys

One of the most critical areas where fretting fatigue failure occurs in actual applications is at blade/disc dovetail joints in turbines, among many other situations as shown in Fig. 1.2. (a). Because of their high strength, outstanding heat resistance capabilities, and microstructure stability at room temperature and high temperatures, IMI 834 titanium alloys and Ni-based super alloys are frequently utilised in compressor discs and blades for gas turbine engines [6, 23]. However, the high cost of raw materials and processing limits its use to military and aerospace applications. Fretting fatigue is a major concern in magnesium alloys, which are widely used in automobiles to attach components using nut bolts [52-55]. Due to intense vibrations and repetitive loading in certain circumstances during operation, there is a very tiny amplitude relative displacement between the components, resulting in damage to the surface in contact and component failure as shown in Fig. 1.2. (b). One of the most critical issues in aviation engine and automobile components is fretting fatigue. It is critical to investigate the fretting fatigue behavior of these alloys and to develop an effective approach for extending their fretting fatigue life. According to reports, the largest tangential stress is generated along the contact edge, which causes the fretting fatigue crack to originate and shatter at this position.

1.3. Factors affecting fretting fatigue

From the previous reports on fretting fatigue, it has been clearly understood that the early crack initiation and accelerated crack propagation in fretting fatigue is due to frictional stress (tangential stress) at the contact. Many researchers reported the fretting fatigue strength prediction based on stress at contact. Fretting fatigue strength enhancement methods has been reported by reducing tangential stress at contact using stress relief groove at contact, by reducing the contact rigidity and by using different surface modifications techniques, etc. Previous studies on fretting behavior of engineering alloys suggests that the most significant parameters that influence the fretting fatigue behavior includes [16-20]:

i. Coefficient of Friction
ii. Surface roughness
iii. Contact geometry
iv. Contact pressure
v. Relative Slip amplitude
vi. Temperature

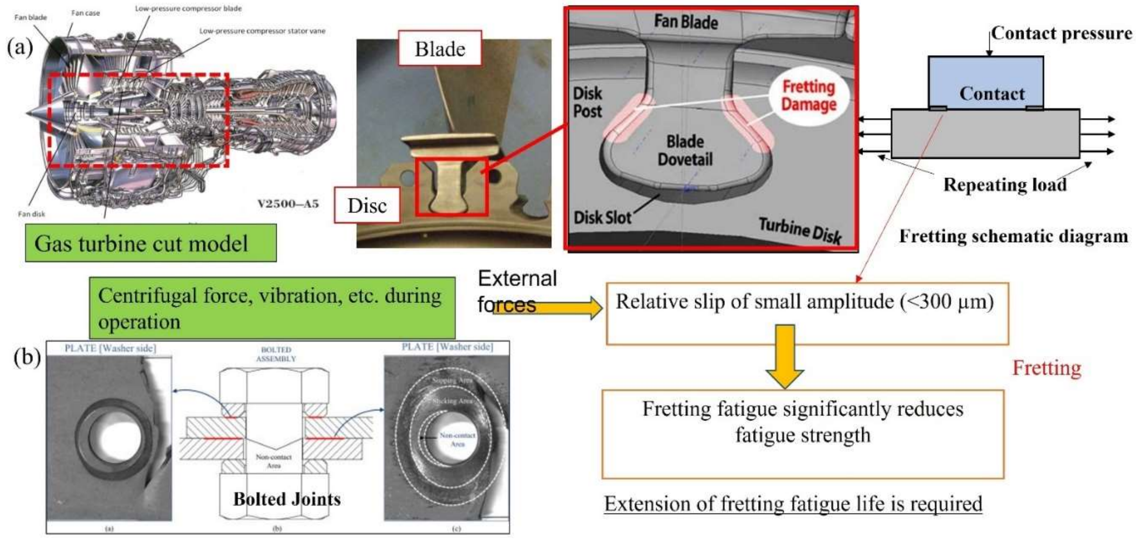

Fig. 1.2 (a) Gas turbine engine with disc-blasé arrangement [15, 23] (b) The bolted assembly (damage due to fretting fatigue) [9, 18]

1.4. Methods to reduce fretting fatigue

Many researchers used different approaches or methods to improve the fatigue strength of the material. However, one of the major challenges that are limiting the wider application of these engineering alloys is the inherent poor mechanical and wear properties at increased fretted duration [21]. From the literature, it is clear that the contact geometry and the material in contact plays a very vital role in altering the fretting fatigue strength. So, it is important to identify a suitable method or surface modification techniques to reduce the damage on the surfaces in contact and enhance the fatigue strength of the component, to effectively use these alloys in wider applications. Some of the surface modification techniques or methods are mentioned as follows:

(1) Case hardening: Nitriding (Laser nitriding and Plasma nitriding), carburizing, cyaniding, Induction and Flame hardening (can improve the surface wear properties)

(2) Shot peening, wet peening and laser peening (can reduce the crack number and prevent the crack propagation)

(3) Surface mechanical attrition treatment (modification of subsurface microhardness, surface morphology, roughness).

(4) Ultrasonic nanocrystalline surface modification.

(5) Low plasticity burnishing.

(6) Laser surface texturing.

These techniques were used to improve the fatigue life of the component by Inducing a residual compressive stress, decreasing the coefficient of friction, increasing the surface hardness or by altering the surface chemistry. The combined effect of shot peening and plasma sprayed CuNiIn coating surface treatment was explored by Yang et al., who discovered that the coating was gradually destroyed by fretting wear, and its protective efficacy diminished or altogether disappeared as the fretting time grew [49]. As a result, research into fretting fatigue behaviour employing a soft contact pad that reduces surface damage is required in order to improve fretting fatigue strength.

1.5. Status on enhancement in fretting fatigue life of Titanium alloy and Ni-based superalloy through contact geometry

Several studies on the fretting fatigue behaviour of various steels [17, 20], Al alloys, and other high strength alloys [23-27] have been published. However, there have been few research on the fretting fatigue behaviour of high temperature superalloys, particularly Ni-based superalloys. Waterhouse chronicles the methodical examination of the fretting phenomena and gives classic illustrations of fretting damage in his keynote article. He emphasises that in laboratory investigations, test settings as well as critical mechanical variables such as the amplitude of slip between the two surfaces and the normal load applied to the surfaces must be regulated. To avoid links and elastic deformation of load arms from becoming causes of testing error, allowances must be made. Waterhouse points out that the practical scenarios in which fretting can occur are so diverse that the investigator must choose which equipment or approach best approximates the practical application [3].

There is a wide range of research on the effect of fretting on fatigue performance, with investigators attempting to comprehend the mechanism of failure by considering various fretting fatigue variables, fracture mechanics approach (crack initiation and propagation), damage models approach (critical plane approach, stress invariant approach, fretting specific parameters, and continuum damage mechanics), and 2-D finite element method techniques. Jayaprakash et al. discovered that increasing pad stiffness enhanced relative slip and tangential stress in the proximity or surrounding area of the contact side, and that the strength owing to fretting is dependent on the combined influence of tangential and compressive stress ranges. The fatigue strength reduced as contact stress increased, which could be due to a modest increase in the tangential force [15, 16, 18]. Noraphaiphipaksa et al. used a FEA model to forecast relative slip, which matched the experiment well, and the crack route was evaluated using the maximum tangential stress range criterion. During cyclic loading, cracks opened as a result of compressive bulk stress, a phenomenon known as fretting-contact-stimulated crack opening. The fatigue lives predicted by using the active stress intensity factor range were shorter than those predicted by using the maximum stress intensity factor range due to fretting, and they were in good agreement with the experimental end results [19, 20, 21]. The results of an experimental research and a damage model for fretting fatigue were compared by Walvekar et al. [22]. To approximate the fretting fatigue life, a FEA model was suggested, which was in good agreement with the experimental end results. Jayaprakash et al. [23] investigated the elevated temperature fatigue performance of titanium alloy due to fretting and found that with increasing temperature, there was a decrease in fatigue life due to fretting, which could be due to an increase in tangential stress coefficient and relative slip amplitude. The FEA model was also created to evaluate stress distribution and relative slide. Using FEM analysis, Shah et al. [24] investigated the influence of notch and fretting on bending fatigue. Single point fretting with double notch and double point fretting with single notch were used in the study. When compared to the other conditions, it was discovered that single point fretting with double notches had a greater impact on fatigue life. Based on experimental and FEA data, Li et al. [25] proposed the fretting-related damage (FRD) parameter. The tangential force, Q, was found to be linked to the impact of fretting. The anticipated fatigue life utilising the damage parameter agreed well with the experiment, indicating that fretting can provide accurate crack initiation position, crack alignment, and fatigue life prediction results. To describe the fretting fatigue damage initiation or initiation life, Nadeem Ali Bhatti [26] and Magd Abdel Wahab [27] used alternative methodologies and damage models, as mentioned earlier. The majority of the studies measured fracture opening lengths ranging from 10 microns to 1mm in depth, with crack angles ranging from 25 to 50 degrees. Because the damage and crack begin on the micro-scale under the contact section. It was confirmed that proper modelling of the fretting fatigue problem remains a challenge. They also employed traditional point and volume averaging methods in conjunction with the quadrant averaging method to determine the crack orientation and component life. The McDiarmid (MD) and Fatemi Socie (FS) damage parameters were used to investigate the differences in fracture alignment and initiation life between all of the approaches. When compared to other methods, the quadrant averaging method provided more accurate and reasonable findings. Diego et al. [28] used numerical simulations to investigate the effect of heterogeneity on crack development in fretting circumstances using two micro-void distributions. The numerical results show that a fracture develops largely at micro-voids closer to the contact boundary, resulting in a decrease in the expected crack initiation life. Guillaume et al. [29] suggested a novel three-dimensional model to better explain component behaviour and service life. The development of a nonlinear incremental model to forecast the growth of the intensity factors and velocity field evolution at the contact boundary, as well as partial slip zone behaviour, was given. Finally, the experimental end findings were compared to the introduction of crack and fatigue life due to fretting. It has been reported that the maximum tangential stress will be generated near the contact edge, due to which the fretting fatigue crack initiated at this location and final fracture occurred. To reduce the tangential stress at the contact and enhance the fretting fatigue life, stress relief grooves techniques were reported. Also effect of contact pad geometry has been reported by many researchers. The contact pad with less rigidity can enhance the fretting fatigue strength, which can be done by drilling hole or making slit in the contact pad. Reducing contact rigidity would reduce tangential stress at contact, which would decrease surface damage and enhances fretting fatigue lives [15-21].

As a result, reducing the stress concentration at the contact is critical to ensuring the components' long-term serviceability. The mating material combination, frequency (Hz), normal load (N), fretting amplitude (m), and environment all have an impact on fretting fatigue behaviour. Many studies have found that fretting fatigue damage between mated objects can be reduced by 1) introducing residual compressive stresses and 2) lowering the CoF at the interfaces. 3) By enhancing the hardness of the surface 4) By lowering surface roughness and 5) by changing the surface chemistry.

1.6. Status on strengthening of Magnesium alloy by making metal matrix composites through various techniques

In recent years, magnesium alloys have become increasingly popular for advanced industrial applications. Because of increased environmental concerns and rising fuel prices, magnesium alloys are a promising material of interest in the automotive and aerospace industries because of its lightweight, high manufacturability, and recycling capabilities. These alloys have piqued the scientific community's interest since they can be utilized to replace heavy materials (such as steel and aluminium) in structural applications, resulting in reduced fuel consumption and CO2 emissions [52-55]. These alloys, however, are still limited in their employment in vehicle structural components due to their low strength, ductility, and poor wear behavior [56, 57, 58].

Fretting is a severe issue in these alloys, which are frequently used in autos to attach components using a nut bolt system. Due to intense vibrations and frequent loading in most automobile components, there is a very tiny amplitude relative displacement between the components, resulting in damage to the surface in touch. As a result, micro fractures form and propagate as the load is applied, resulting in component failure. Surface modification techniques, alloy microstructure modification, and the addition of any hard material to make composites are just a few of the solutions proposed to address these issues.

Making composites with stronger and tougher reinforced particles has been discovered to tackle this problem in numerous research. Creating magnesium alloy-based composites with superior features has proven to be difficult due to a large number of variables such as matrix composition, type, size, volume percentage, and the shape of reinforced particles. Powder metallurgy [55], casting [56], extrusion [58], and friction stir processing [61-64] have all been used to fabricate magnesium matrix composites (MMCs) with various reinforcing particles. In various approaches, the operating temperature is exceedingly high, and the substance becomes liquid. Any operation or treatment in a liquid condition is challenging and results in a reaction between the matrix and reinforcement. As a result, it is preferred to execute these procedures or treatments in a solid-state environment. Several magnesium alloys from the AZ series were employed as matrix materials, and several ceramic particles were used as reinforced particles, to generate MMCs successfully. The results demonstrated an appropriate distribution of reinforced particles with microscopic grains and higher mechanical capabilities, but the ductility of the MMCs was considerably reduced.

Researchers then revealed that metallic particles with a higher melting point may hold the key to solving the problem. Various magnesium alloys from the AZ series were used as matrix materials with various metal-reinforced particles (Ti, Ni, W, and Mo) to successfully make MMCs via powder metallurgy, casting, and pressure infiltration, but microstructural characterization revealed objectionable features such as non-homogeneous distribution, particle accumulation, micropores, poor bonding at the interface, coarse grains, and intermetallic compounds, all of which affect the strength of the MMCs [65, 66]. Friction stir processing (FSP) has therefore emerged as one of the most promising solid-state technologies for developing MMCs with improved particle dispersion and mechanical properties. Prior investigations for reinforcing magnesium alloys showed ceramic particles to be the focus of interest, while other metal particles were likely explored as reinforcement with amazing results as well.

Hassan et al. used powder metallurgy and a hot extrusion process to make a magnesium-based MMC with a 1.5 percent and 3.2 percent volume fraction of nickel in prior investigations. According to the findings, a tiny amount of nickel can improve the hardness (30%) and ultimate tensile strength (16%) of pure magnesium, but it substantially reduces the ductility by 60% due to the development of intermetallics [61, 67]. As a result, the injection of nickel reinforced particles into the magnesium matrix in a solid state at low processing temperature might totally rule out this intermetallic formation between magnesium and nickel. There is very little study on metal particle reinforced MMCs produced by friction stir processing, according to the literature. However, no research has been done on producing MMCs with nickel reinforcement by FSP to improve the fretting fatigue life of these magnesium alloys.

1.7 Motivation of the study

From the literature, it is understood that the contact geometry and the material of contact greatly affects the fretting fatigue life of the component. It has been reported that during fretting fatigue the tangential stress (frictional stress) will be generated at the contact interface, which is responsible for surface damage, early crack nucleation and accelerated propagation. It has been reported that the maximum tangential stress will be generated near the contact edge, due to which the fretting fatigue crack initiated at this location and final fracture occurred. To reduce the tangential stress at the contact and enhance the fretting fatigue life, stress relief grooves techniques were reported. Also effect of contact pad geometry has been reported by many researchers. The contact pad with less rigidity can enhance the fretting fatigue strength, which can be done by drilling hole or making slit in the contact pad. Reducing contact rigidity would reduce tangential stress at contact, which would decrease surface damage and enhances fretting fatigue lives. So, there is a need to study fretting fatigue behaviour using soft contact pad to reduce contact stresses or by fabricating metal matrix composite to reduce surface damage in order to achieve improved fretting fatigue strength. As we know, fretting damage occurs in between the contact surface with very small relative slip amplitude due to which it very difficult to understand mechanism of failure through experimental work only. To understand the damage mechanism and stress distribution at the contact clearly, FEA modelling needs to be explored. There is very limited study available on co-relation of experimental and FEA 3D model to understand the stress distribution at the contact region and fretting fatigue damage mechanism. There is no study found on the fabrication of magnesium metal matrix composite using nickel reinforced particles to improve fretting fatigue life through friction stir processing. As fretting wear is a complex phenomenon, thus reducing the overall lifespan and performance of the engine components due to fatigue failure. Therefore, investigating the fretting fatigue behavior is very important.

1.8 Objectives of the thesis

Titanium alloys and Ni based superalloys mostly used in aircraft engines/gas turbine engines. These are always connected as disc-blade arrangement or work as a dove-tail assembly in the turbine section. Due to high temperature gases and vibration involved during application, fretting damage takes place at the contact and results in failure of the component. Whereas Magnesium alloys is widely used in automobile section and the components are mostly connected with the help of bolted joints or rivets. As the fretting duration increases, wear takes place at the contact section and cause reduction in fatigue strength of the alloys. The current thesis work aims to improve the fretting fatigue strength of Titanium alloy, Ni-based superalloy and magnesium alloy for aerospace and automobile applications through two different techniques. Enhancing the fretting fatigue properties by introducing a soft material at the contact surface and by adding hard metal reinforcement into the matrix through friction stir processing technique in order to get homogeneous distribution of the powder particles. The effect of contact pad geometry, mechanical properties and fretting fatigue behavior have been examined in detail. It has been reported that the maximum tangential stress will be generated near the contact edge causes more damage at the mating surfaces, due to which the fretting fatigue crack initiated at this location and final fracture occurred. The primary objective of the thesis is to reduce the tangential stress at the contact and enhance the fretting fatigue life. To reduce the tangential stress and wear damage at the contact surface and enhance the fretting fatigue life, two different methods were adopted as (1) Enhancing the fretting fatigue life by reducing stress distribution at the surface in contact by introducing soft material at the contact interface. (2) Fabrication of composite by incorporation of metal reinforced particles into the matrix to improve the mechanical properties (less surface damage) and fretting fatigue life. Plain fatigue and fretting fatigue tests are conducted at room temperature in the experimental investigation. Under fretting conditions, the evolution of frictional tractions and fatigue lifetimes is examined. In light of the aforementioned experimental findings, a mechanism-based computational model was suggested to study the stress distribution over the contact surface and calculate the crack initiation stress state as a result of fretting forces at the contact.

Based on this study, it has been identified that by using slit + porous contact pad, the fretting damage can be reduced and thereby, it might be possible to enhance the fretting fatigue life. The presence of a significantly harder and stronger reinforcement phase, as well as tiny grain size, exacerbated the matrix's localized deformation during loading. The fretting fatigue life can be enhanced by producing MMCs using friction stir processing, according to this research.

1.9 Outline of the thesis

Chapter 1: Introduction to fretting fatigue, engineering alloys and their applications in aerospace and automobile industries.

Chapter 2: Evaluating the effect of contact pad geometry on the fretting fatigue behavior of titanium alloy by experimental and finite element analysis

Chapter 3: Effect of introducing porous material in the contact pad on the fretting fatigue behavior of nickel-based superalloys

Chapter 4: Extension of fretting fatigue life by fabricating Magnesium Metal Matrix Composite through Friction Stir Processing using Nickel Reinforced Particles

Chapter 5: Conclusion and the scope for future work.

Chapter 2

Evaluating the effect of contact pad geometry on the fretting fatigue behavior of titanium alloy by experimental and finite element analysis.

2.1 Introduction

There has been a lot of study on fatigue failure of different components due to fretting but few studies are reported on the prevention methods to avoid failure and recommended as a future scope for the researchers. There are numerous variables involved in causing fretting fatigue failure due to which the mechanism is still unclear. The predominant factors which affect the most in this type of failure are the coefficient of friction, surface roughness, contact geometry, contact pressure, relative slip amplitude. Major factors necessary to cause fretting fatigue failure are the local stress arising from the relative slip of the surfaces of the two elements in contact under pressure and the total cyclic stress on the component.

In this chapter, fretting fatigue experiments with two different contact pad geometries, namely flat pad (flat contact interface) and groove pad (groove contact interface), are used to assess the influence of rectangular grooves at the fretting contact on the fretting fatigue behavior of IMI 834 titanium alloy (rectangular grooves at the contact interface). To further understand the effect of fretting on the fatigue behavior of IMI 834 titanium alloy, a plain fatigue test (without fretting) was also carried out. The damage processes were also studied using a finite element analysis (FEA) model that analyzed stress distribution at the contact interface. A scanning electron microscope and electron microscopy were used to examine the fracture surface and fretting region of the test object. The results showed that fretting fatigue lifetimes with a contact pad with grooves at the fretting contact were substantially longer than those with a flat contact pad. The findings were addressed using the results of the experimental testing, as well as the stress distribution at the contact.

2.2 Experimental Details

2.2.1 Material, composition, and specimen dimensions:

The specimens utilised in this study for plain fatigue and fretting fatigue tests were constructed of IMI834 titanium alloy. The fretting fatigue contact pads (groove pad and flat pad) were also made of IMI 834 titanium alloy. The materials employed in this study are commonly used in disc-blade combinations in gas turbine engines. The chemical composition and mechanical properties were confirmed through EDS technique and tensile testing by using FESEM and UTM. The chemical composition and mechanical parameters of the IMI 834 titanium alloy used are shown in Table 2.1(a) and (b). The size of the fatigue test specimen and the contact pad used are shown in Fig. 2.1. The gauge length, width, and thickness of the test specimen are 30 mm, 5 mm, and 4 mm, respectively. The flat type contact pad utilized has a contact length of 2mm, a contact width of 5 mm, and a foot height of 1mm. The fretting contact in the case of groove pad was made with rectangular grooves with a depth of 0.5 mm and a width of 0.33 mm. Before each test, the contact surfaces of all specimens and contact pads used in the study were polished with 1500-grit emery paper and then cleaned with acetone.

Table 2.1(a) The chemical composition of IMI 834 Titanium alloy

Chemical composition (wt. %)	Al	Sn	Zr	Nb	Mo	Si	C	Ti
	5.8	4	3.5	0.7	0.5	0.35	0.06	Bal.

Table 2.1(b) The mechanical properties of IMI 834 Titanium alloy

Mechanical properties of IMI 834 Titanium alloy	Modulus of Elasticity (GPa)	Yield Strength (MPa)	Ultimate Tensile Strength (MPa)	Elongation (%)	Density (g/m^3)	Hardness (Hv)
	120	910	1030	12	4.5	350

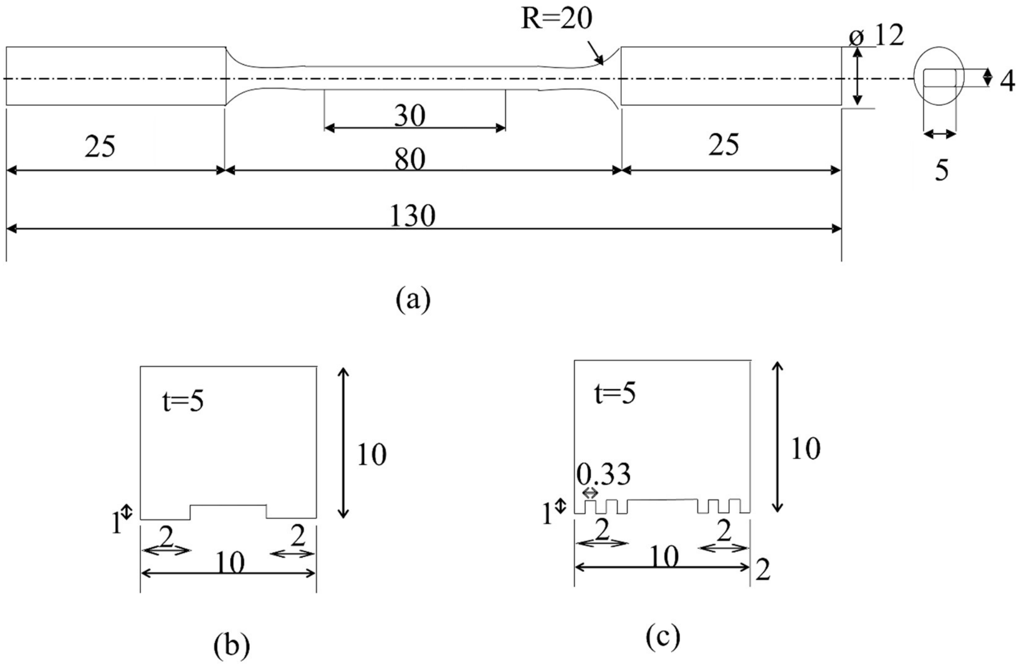

Fig. 2.1 (a) Shape and dimension of fatigue test specimen (plain fatigue and fretting fatigue)
(b) Flat pad (c) Groove pad (All dimensions in mm)

2.2.2 Fretting fatigue test of IMI834 titanium alloy:

Fretting fatigue tests for IMI834 titanium alloy were carried out using a servo-hydraulic testing machine in accordance with JSME standard S015 [50] at a stress ratio of 0.1 and a frequency of 10 Hz. For comparison, a simple fatigue test was performed (without fretting). Power screws were employed to apply contact pressure, and a calibrated proving ring was used to assure a consistent contact pressure of 100 MPa on the contact pads. The cyclic load was applied to the specimen, and the tangential force between the contact pad and the test specimen was measured with a calibrated strain gauge pasted to the contact pad's gauge section. Fig. 2.2(a) depicts a schematic illustration of a fretting fatigue test setup for a groove pad on a flat contact configuration, whereas Fig. 2.2(b) depicts the experimental test system employed in this study.

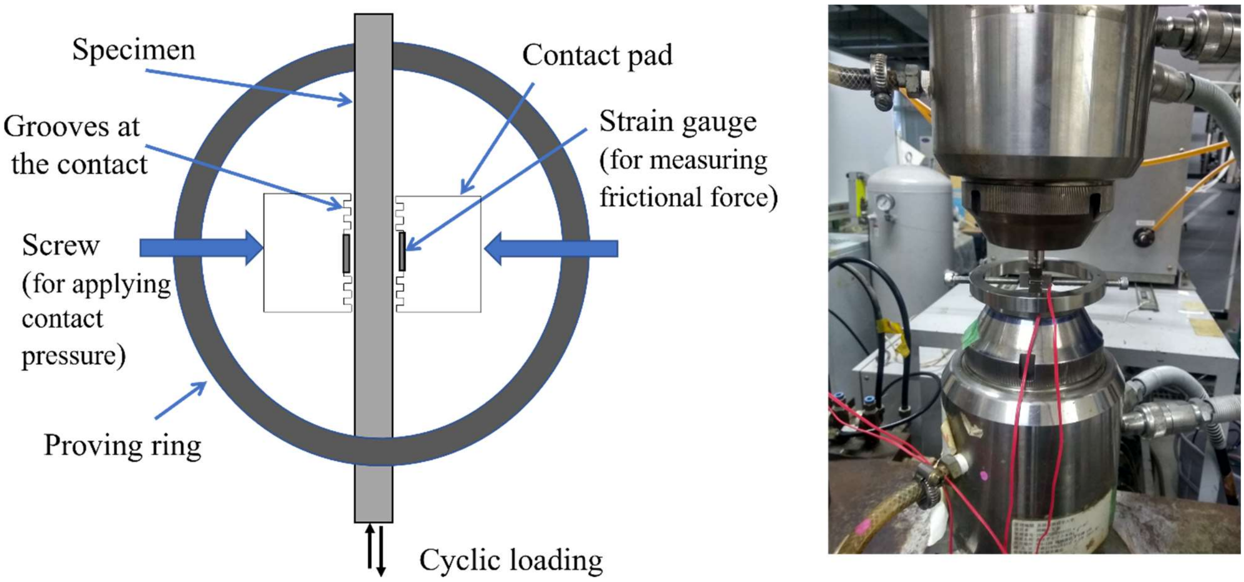

Fig. 2.2 (a) Schematic of fretting fatigue test for groove pad (b) Photograph of experimental setup for fretting fatigue test.

2.2.3 Fretted area, roughness measurement, and fracture surface observation:

The specimen's surface was damaged during fretting. Electron microscopy was used to investigate the fretted surfaces on the flat surface of the fatigue specimen. The surface roughness of flat and groove pads was assessed using coherence scanning interferometry at the fretting area (the contact region on the specimen that was in touch with the pads). The fracture surface of the tested specimen was cleaned with an ultrasonic vibrator in acetone for 15 minutes following the fatigue test before being studied with a scanning electron microscope. The fretted surfaces on the flat surface of the fatigue specimen were investigated using electron microscopy.

2.2.4 Finite element analysis:

ANSYS software was used to generate FEA models of flat pad and groove pad on the flat surface of a tested specimen, as shown in Fig. 2.3, to estimate the distribution of stresses at the contact interface. The structural analysis was employed and the tetrahedron element type was used in the present model as it gives convincing results in many types of engineering calculations. The simulation of the current investigation was solved as a linear isotropic material model with given material properties. Since material data is crucial to accurate fatigue results, Workbench Simulation readily allows the input of this information to new or existing materials by hand or through load history files. Material properties include density, Young's modulus, Poisson's ratio, and Ultimate tensile strength were included in the engineering data file. Materials in the Workbench Simulation material library may include a fatigue stress-life curve populated with data from engineering handbooks. The Fatigue Tool will then use the information in the stress-life curves for each material in the model when calculating stress distribution, damage, life, etc. The boundary conditions adopted for the present fretting fatigue test were also applied for this analysis based on the experimental study. In the first step, the contact pressure of 100MPa was applied by both the contact pads (top and bottom) to make contact with the smooth surface of the specimen. In the next step, the load was applied to the specimen by choosing a stress ratio of 0.1 for one second and the contact between the elements was given as frictional contact, f=0.8. FEA 3-D model analysis was performed for all the stress amplitude values used for the fretting fatigue test.

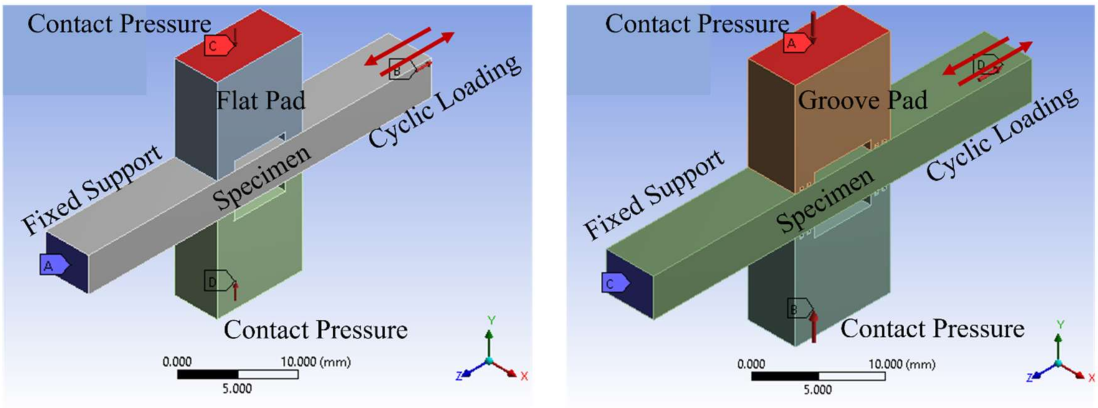

Fig. 2.3 FEA model for different contact pads using Ansys 14.5 (a) Flat pad (b) Groove pad

2.2.5 Grid study for numerical analysis:

The grid test was carried out at 250 MPa for both the flat pad and the groove pad, with the mesh size of the elements being adjusted in all directions (x, y, and z) to improve accuracy and numerical results. Similar boundary conditions were applied in the current study. The S-N curve and other mechanical characteristics were also incorporated to the software from the engineering data file. Depending on the shape of the contact interface and the number of mesh points used, the stress value in the contact region changes. As a result, the grid research must be conducted using trial and error analysis with various mesh size models in order to fully understand its behavior for various contact analyses. Five different combinations of tetrahedron meshes were utilised to ensure that the behaviour of the produced model matched that of the practical test. For flat pad analysis, the best mesh size (case 3) MS=1 mm, mesh size at contact i.e., CS=0.15 mm was chosen, and for groove pad analysis, the best mesh size (case 4) MS=1 mm, mesh size at contact i.e., CS=0.2 mm was chosen, as shown in Fig. 2.42.4(b) and (c). The results of the meshing used in this study matched the results of the experimental testing quite well.

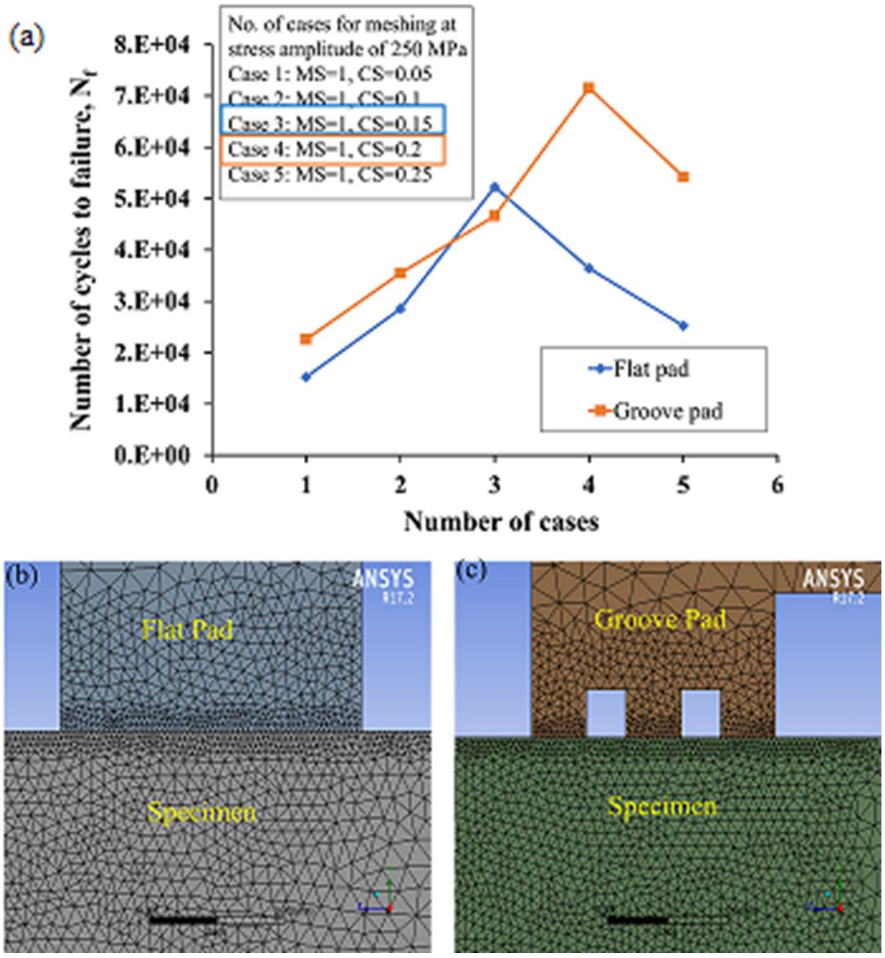

Fig. 2.4 (a) The grid study of the 3-D finite element analysis model for both type of contact pads. (b) Mesh size for flat pad. (c) Mesh size for groove pad.

2.3. Results and discussion

2.3.1 Plain fatigue and fretting fatigue behaviour of IMI titanium alloy:

Experimental test findings show that fretting greatly affects the fatigue strength of IMI 834 titanium alloy, as shown in Fig. 2.5. (a). A groove pad has a longer fretting fatigue life than a flat pad, as demonstrated in the diagram. It is generally known that the material's fretting fatigue strength reduces as the contact area rises. In this study, the groove type of contact pad has a smaller contact area than the flat kind, which reduces surface damage at the contact interface. The fretting fatigue life of a flat type contact pad is 3.8x105 at 150 MPa, while the fretting fatigue life of a groove type contact pad is 8x105. When grooves are added to the fretting contact, the fretting fatigue life is more than doubled compared to a flat pad. Because of the contact pad's interaction with the specimen, significant frictional stress has been recorded in the contact region, resulting in severe surface damage on the in-touch surface and a reduction in the component's fretting fatigue strength [15, 16]. To figure out why the groove pad enhanced fretting fatigue strength, the tangential force exerted at the fretting contact was measured using a calibrated strain gauge. The relationship between tangential force and stress amplitude for both contact pads is depicted in Fig. 2.5(b). According to the figure, flat type contact pads have a higher tangential force than groove type contact pads, which causes more stress at the contact and may be one of the reasons for the reduced fretting fatigue strength, i.e., the flat pad has the shortest fretting fatigue life. However, in order to gain a better understanding, the fretted surface must be examined as well as the damage at the interface.

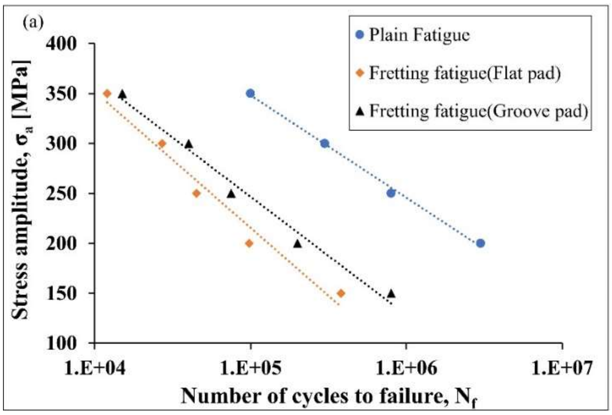

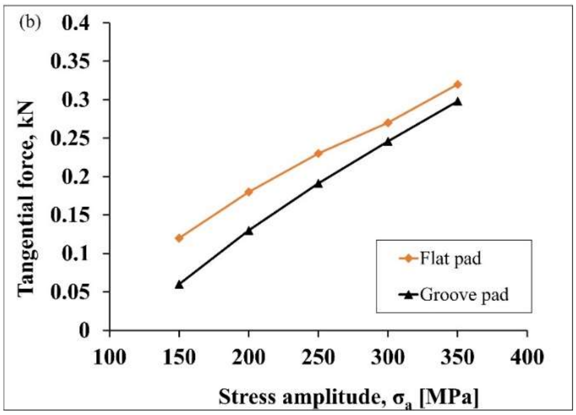

Fig. 2.5 (a) S-N curve for plain fatigue and fretting fatigue with flat pad and groove pad. (b) Relationship between tangential force and stress amplitude for both contact pads.

2.3.2 Surface roughness and characterization:

The contact of two mating surfaces at the contact interface causes fretting. As a result, contact fretting and surface roughness play a substantial role in the material's fatigue strength loss. Figures 2.6 and 2.7 show fretting surface views and roughness profiles, respectively. In this study, the surface damage induced by flat type contact pads at the fretting contact is more than that generated by contact pads with grooves. As shown in Figs. 2.6 and 2.7, the maximum average surface roughness values for flat type contact pads and groove type contact pads at 250 MPa are 3.5053 µm and 2.4677 µm, respectively. The average surface roughness value of flat pads is likewise larger than the value of groove pads. The depth profile at the fretting contact could be seen at both the inner and outer borders (inside and outside) in both situations, as shown in Fig. 2.8. And it was revealed that the depth is greater near the outside borders of the contact region in both cases (flat pad and groove pad), but the depth value was higher in the flat type contact pad (9.2 µm) than in the groove type contact pad (8.6 µm).

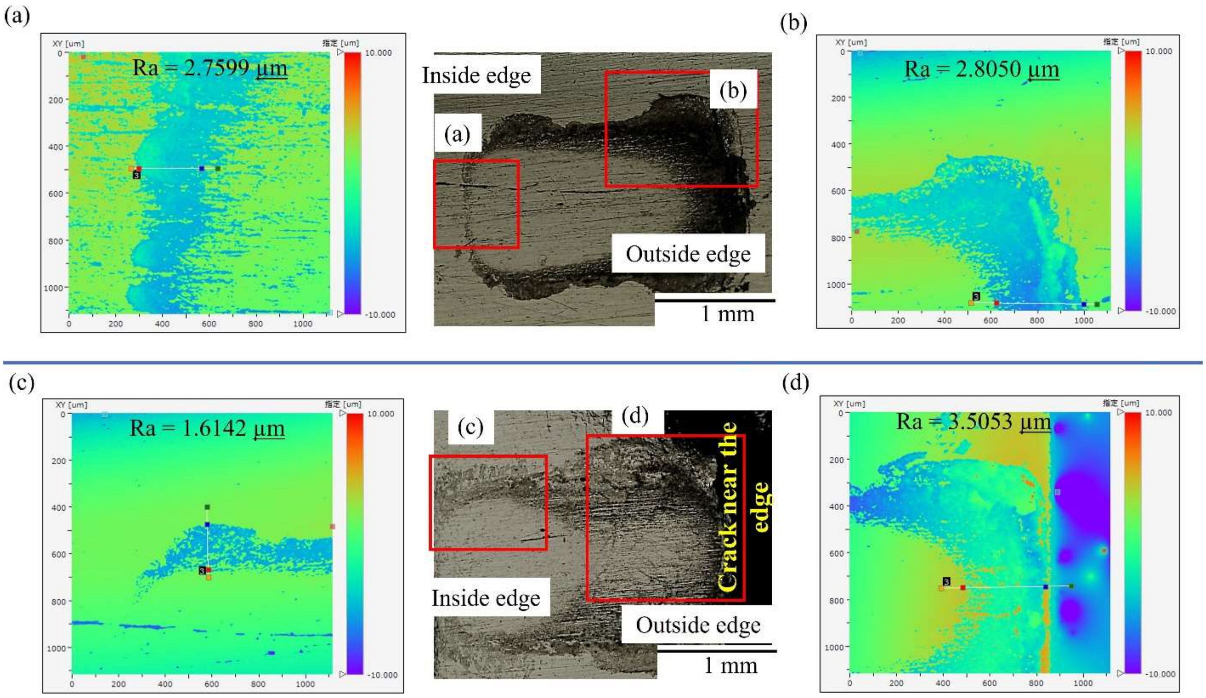

Fig. 2.6 Surface roughness profiles and damage surface observation on fretted area using coherence scanning interferometry and electron microscopy at stress amplitude of 250 MPa in case of flat pad.

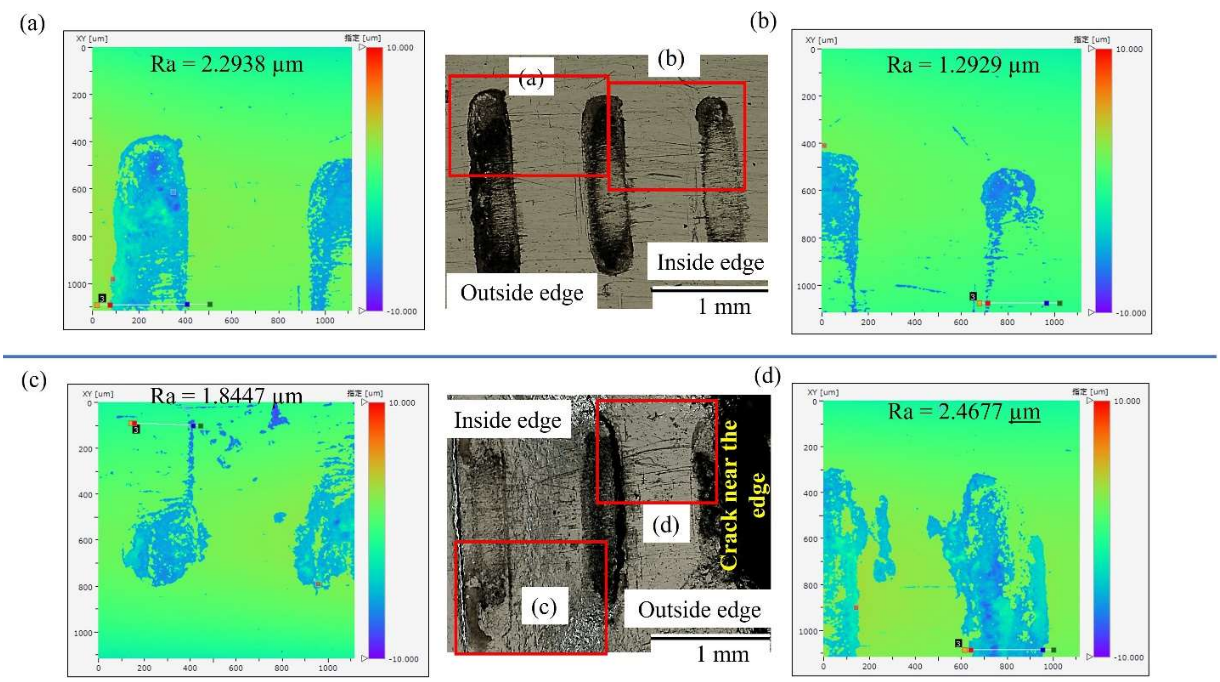

Fig. 2.7 Surface roughness profiles and damage surface observation on fretted area using coherence scanning interferometry and electron microscopy at stress

amplitude of 250 MPa in case of groove pad.

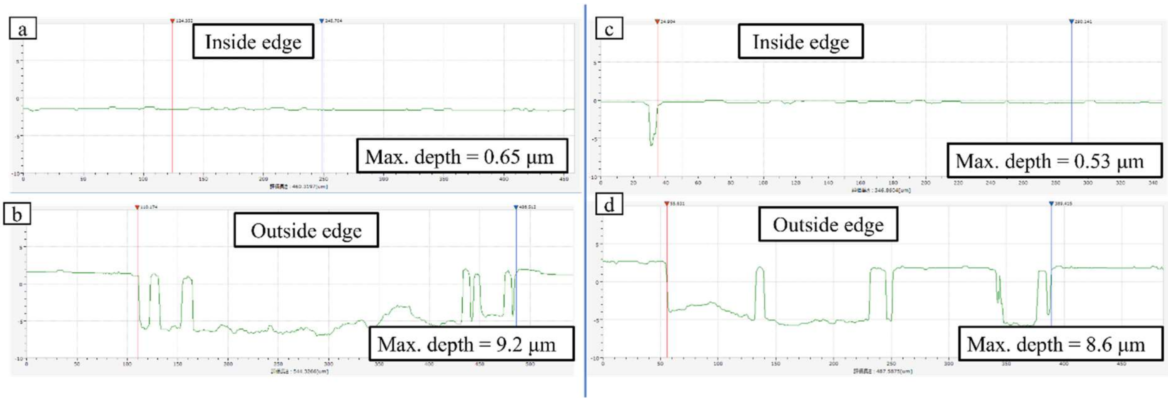

Fig. 2.8 Depth profiles on fretted area using coherence scanning interferometry at stress amplitude of 250 MPa in case of (a), (b) Flat pad and (c), (d) Groove pad.

The crack begins on the outside edge of the contact pad, where there is a large concentration of tension or friction stress. As revealed by fracture surface observations, the contact area of a flat type contact pad is higher than that of a groove type contact pad, resulting in significant surface damage and the nucleation of a crack from the specimen's contact edge. The fracture surface of the tested specimen at 250 MPa is shown in Fig. 2.9 for flat type contact pads and groove type contact pads The crack begins on the specimen's surface under the fretting contact and expands throughout the thickness of the specimen, according to the findings. The fracture surface of the tested specimens (at 250 MPa), as well as the crack nucleation site and crack propagation direction, are also shown in Fig. 2.9. The crack initiation location in Fig. 2.9(c) and (f) revealed a modest number of flat facets and striations, which were indicated by yellow arrows. The primary α-phase cleavage fracture of the titanium alloy under cyclic loading produced these facets.

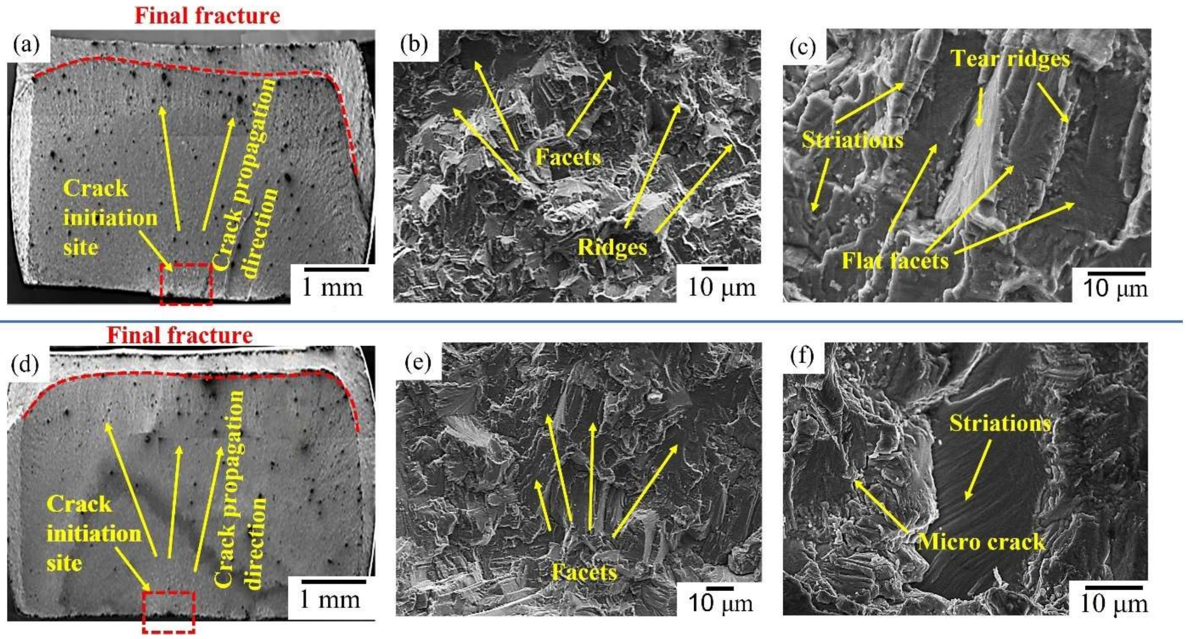

Fig. 2.9 Fracture surface of fretting fatigue tested IMI834 specimens using different contact pads at σ_a = 250 MPa. (a), (b) and (c) represents flat pad and (d), (e) and (f) represents groove pad.

2.3.3 Finite element analysis results:

In section 2.2.4, the details of the FEA model and boundary conditions employed in this investigation are described. To examine the mechanism behind the higher fretting fatigue strength due to the integration of grooves at the fretting contact, different models were created, and the results were compared to experimentally obtained values. Fig. 2.10 depicts the effect of stress amplitude values on fretting fatigue life. The experimental lifetimes are compared to the FEA-estimated lives. The experimental end findings are in good agreement with the projected FEA outcomes, as shown by the co-relation. After comparing the data, the average percentage error is less than 25%, which is very low when compared to the errors recorded in prior studies by numerous academics.

The loads were applied to the model in three stages during

FEA. The contact pad was clamped to the specimen using a constant contact pressure of 100 MPa in the first step. The maximum cycle stress was then applied, and the tangential stress at maximum load was then measured. For various pad types, the relationship between tangential stress and distance from the contact (one end of the contact pad) is shown in Fig. 2.11. The tangential stress value is largest on the outside edge of a flat type of contact pad, which is consistent with the experimental data. The relative slip amplitude between the contact pad and the test specimen was computed using FEM for both types of contact pads and depicted in Fig. 2.12. As the stress amplitude increases, the amplitude of relative slip increases for both contact pads. The relative slip amplitude for flat pad is the largest as compared to groove pad [31]. This could also explain why the tangential stress value of flat type contact pads is higher.

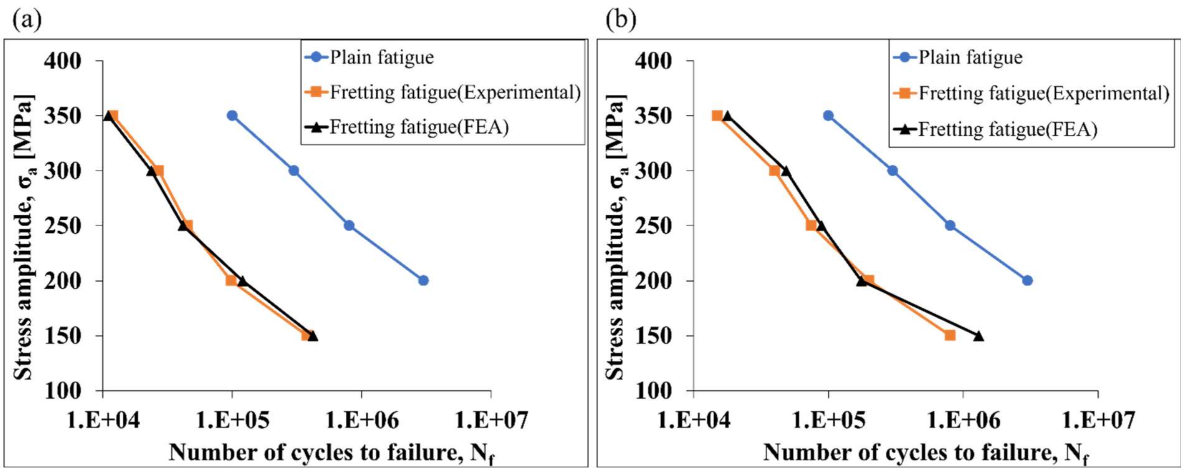

Fig. 2.10 S-N curve for Experimental results vs FEA results. (a) Flat pad and (b) Groove pad.

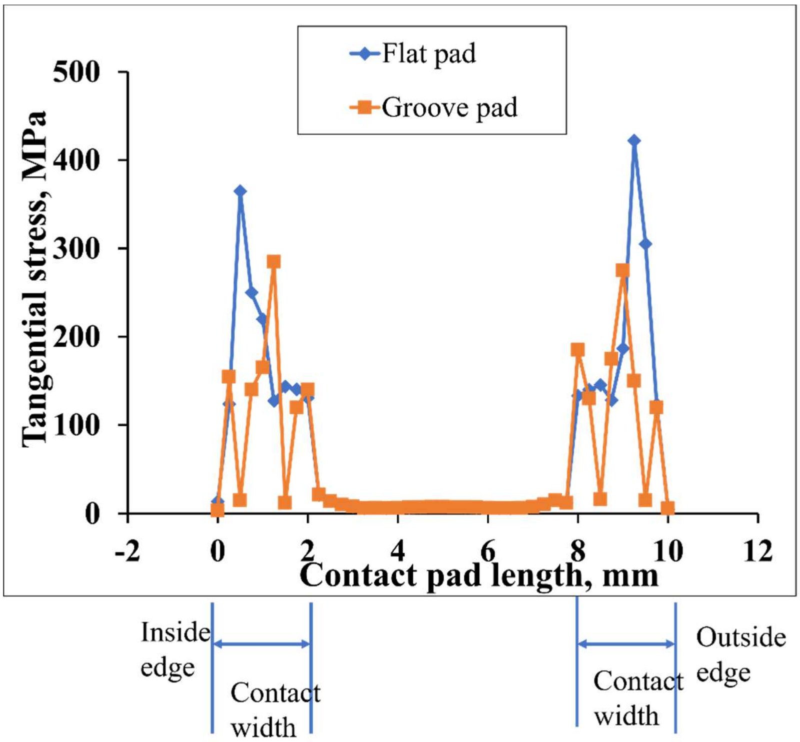

Fig. 2.11 Tangential stress distribution along the contact pad using the FEA model for flat pad and groove pad.

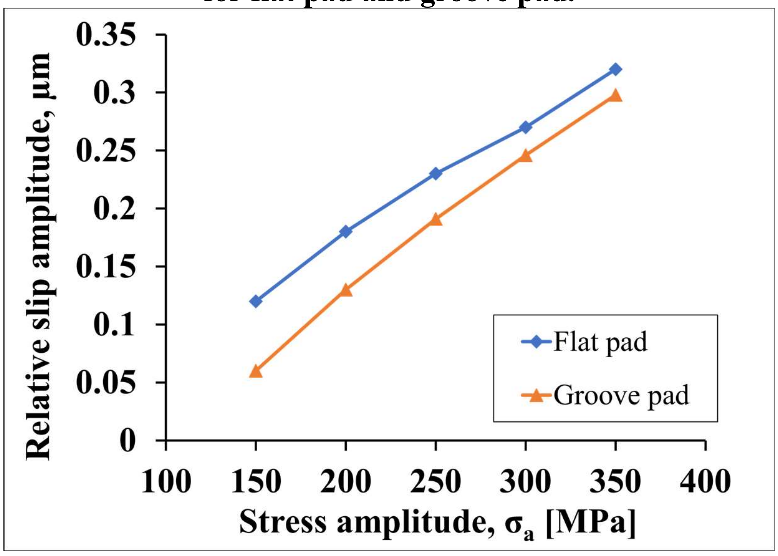

Fig. 2.12 Relationship between relative slip amplitude and stress amplitude in case of flat pad and groove pad.

The distribution of stresses along the contact region was investigated using finite element analysis with both flat pad and groove pad geometries, and the results were compared to experimentally measured values to determine the mechanism behind the increased fretting fatigue strength due to the incorporation of grooves at the fretting contact. Figure 2.13 depicts the stress distribution along the contact pads using a FEA model with a 250 MPa stress amplitude. And, when comparing flat and groove contact pads, the stress value is found to be higher in the case of flat contact pads. The flat type contact pad's peak stress was higher than the groove type contact pad's stress value, and it was detected at 0.2 mm from the contact edge, whereas the groove pad's peak stress was discovered at 0.4 mm, as shown in Fig. 2.14. As a result, the peak stress location in the groove pad was slightly further away from the outside contact edge than in the flat pad, which might be attributed to the greater contact area and higher tangential stress in the groove pad. In Fig. 2.15, the fatigue life due to fretting was examined using the FEA model at stress amplitudes of 250 MPa for the flat pad and groove pad. The fretting fatigue life of the component is found to be reduced in the case of flat type contact pad as compared to groove type contact pad in the figure, which could be due to the high stress value observed in the case of flat type contact pad.

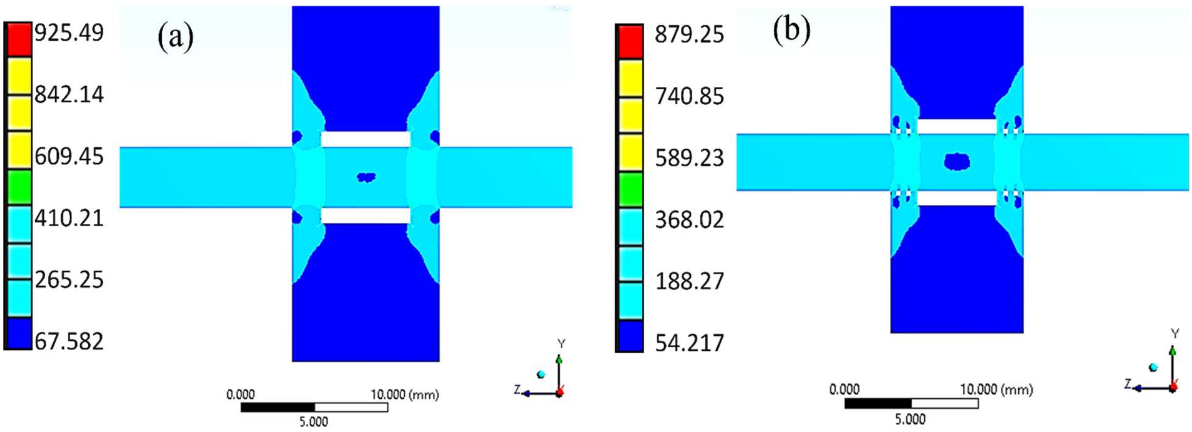

Fig. 2.13 Equivalent alternating stress distribution along the contact pads by using the FEA model at stress amplitudes of 250 MPa (a) Flat pad (b) Groove pad.

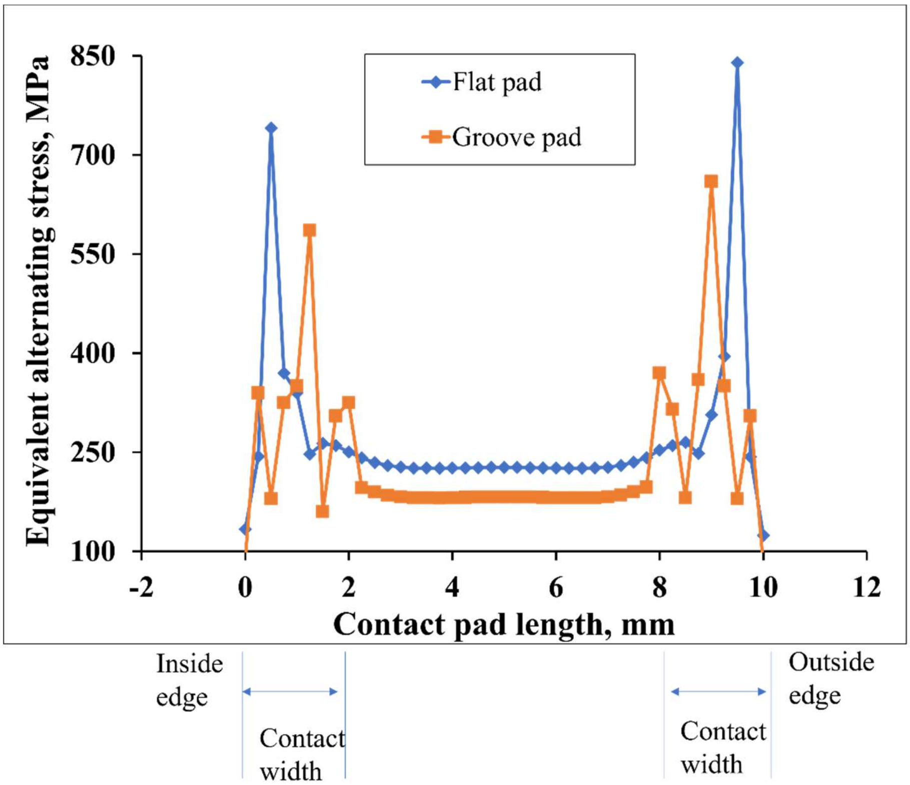

Fig. 2.14 Stress distribution curve along the contact pad using FEA with flat pad and groove pad.

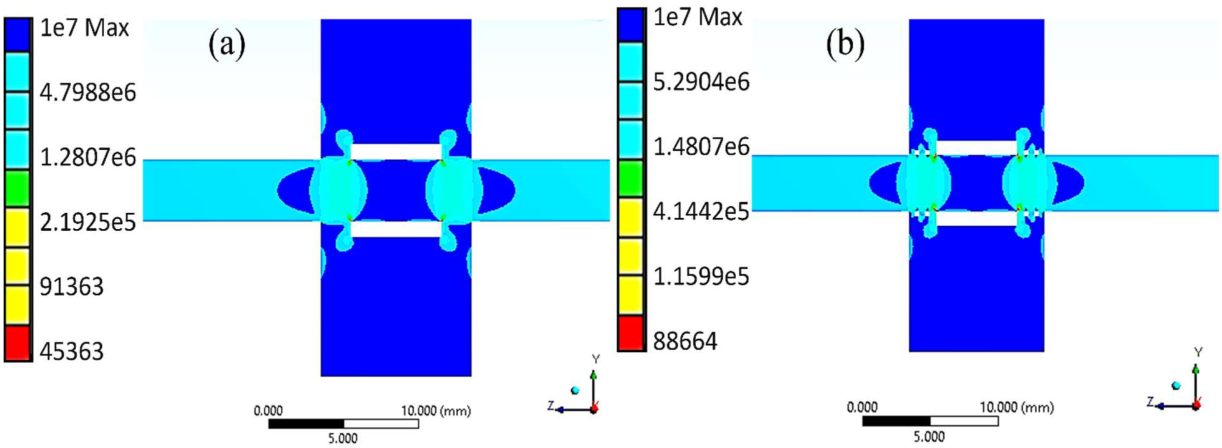

Fig. 2.15 The fretting fatigue life by using FEA model at stress amplitude of 250 MPa (a) Flat pad (b) Groove pad.

At a stress amplitude of 250 MPa, the fretting scar region of the fretting fatigue tested IMI834 alloy is shown in Figs. 2.6 and 2.7 for both contact pads. As seen in Fig. 2.9 for flat type contact pads, the fretting damage was greatest along the contact's outside edge, where the crack began and fractured. The fretting damage was most severe near the outside edge of groove type contact pads, as shown in Fig. 2.7, where the cracking and fracture began. The maximum tangential stress measured by FEA is quite comparable to the position of the fracture as viewed with an optical microscope. If the relative slip amplitude is considerable, the tangential stress is large, the surface damage is greater, and early fracture initiation and fretting fatigue life are limited, according to several researchers [24, 25]. In this study, the same thing happened. When compared to a groove pad, the tangential stress was the highest and the fretting fatigue life was the lowest when a flat type contact pad was employed for fretting fatigue testing. Based on this research, it was determined that fretting damage can be reduced, and fretting fatigue life can be extended by introducing rectangular grooves at the contact interface.

2.3.4 Crack initiation and crack angle measurement using FEA:

To determine the location of fracture start and propagation, many researchers used stress averaging methods such as the point method, line method, volume stress averaging method, and quadrant averaging method [32, 33]. To assess the position of crack start and fatigue life, the critical plane approach is often utilised. The adoption of a stress averaging technique is essential in this investigation due to the considerable stress concentration around the contact zone. The crack position and angle were estimated using the line stress averaging approach after the contact analysis was completed. Taking one or two points along selected radial lines in the critical damage zone is the goal of this technique. In fretting fatigue difficulties, the Findley parameter (FP) is used to calculate the start of a crack. According to this characteristic, the crack begins on a plane where the highest shear stress amplitude and normal stress are both greatest [35]. To calculate fracture initiation position and angle, only FS characteristics are used in this study. The plane, where the damage parameter (FS) achieves its highest value, is designated as the critical plane. Findley parameter is established on stresses and can be stated as

$$FP = \Delta\tau_{max}/2 + k\sigma_n^{max} \ldots\ldots(1)$$

Where $\Delta\tau_{max}/2$ and σ_m^{max} are the maximum shear stress amplitude and normal stress on the critical plane. The material constant k acts as an influencing factor to the normal stress component.

Along these lines, the Findley parameter value is averaged; the highest parameter value represents the fracture initiation point, and the line with the highest parameter is labelled as the crack initiation angle. Fig. 2.16 demonstrates the evaluation of fracture start site and crack angle in a FEA model for stress amplitudes of 250 MPa for flat and groove pads using the line approach. When the stress amplitude is 250 MPa, the Findley parameter value for flat pad is larger at = 56°, whereas the parameter value for groove pad, which reflects the crack angle, is larger at = 45°.

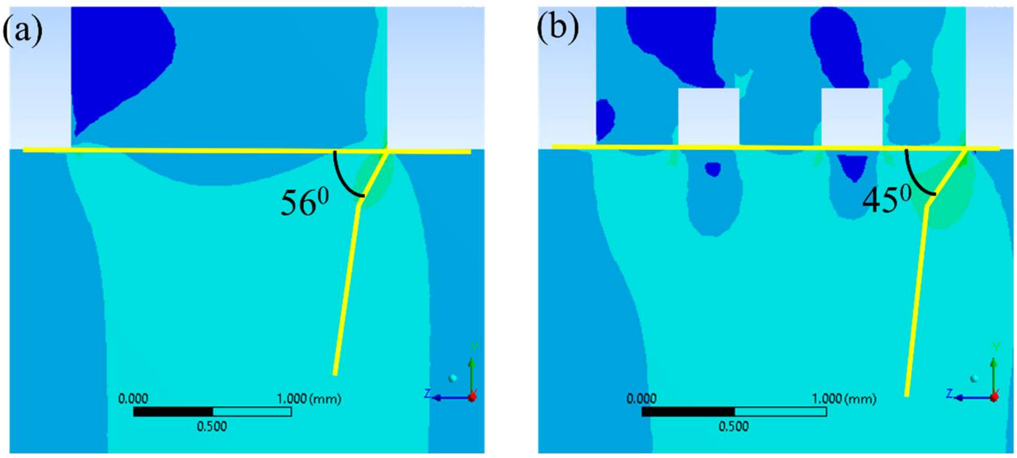

Fig. 2.16 Crack initiation location and crack angle using FEA model at stress amplitude of 250 MPa (a) Flat pad and (b) Groove pad.

The experimental results in this investigation are very similar to the FEA results. In comparison to prior literature [25, 26], the average percentage error in the S-N curve produced from the present model is only 25%. This suggests that the model produced in this work can be utilized to explain the stress distribution along the component's contact zone because it matches the experimental fretting fatigue test very well. The model's accuracy and reliability were evaluated, and the results demonstrate that this numerical simulation technique may be utilized to examine crack initiation and stress distribution between contact pads. This research aims to evaluate the accuracy and reliability of the current model using finite element analysis (FEA) simulations. It can be used to evaluate crack initiation and stress distribution between the contact pad by introducing different contact-shaped geometries to improve the component's fatigue strength during fretting.

2.4. Summary

In the current work, the effect of adding rectangular grooves at the fretting contact on the fatigue behaviour of IMI834 titanium alloy was examined. By assessing the distribution of stresses at the contact regions, crack initiation site, and crack angle, a FEA 3D model has been presented to better understand the damage mechanisms. The following are the conclusions drawn from the preceding findings and discussions:

1. There is a significant reduction (more than 50%) in the fatigue life due to fretting. But due to the incorporation of grooves at the fretting contact, there is a slight improvement in the fretting fatigue life (i.e., 2 times) as compared to the flat pad.
2. The frictional stress increases as the stress amplitude increases and it is noticed that the frictional stress is high in case of flat pad as compared to groove pad.

3. Fretted surface observations and surface roughness measurements for both contact pads revealed that in the case of flat pads, surface damage and average surface roughness values are higher near the contact edge of the pad than in the case of groove pads, resulting in a decrease in fretting fatigue strength.
4. According to the FEA results, the amplitude of relative slip is greater in flat type contact pads, causing more frictional stress at the contact and more damage along the outside contact edge, resulting in a loss in fretting fatigue strength. When the FEA results are compared to the experimental data, they show that they are quite close.
5. The shape at the fretting contact is confirmed to have a significant impact on the component's fretting fatigue behaviour. By lowering the stress concentration at the contact interface with the groove pad, or by inserting grooves at the contact interface in fretting fatigue, the life of the fretting fatigue can be greatly extended.

Chapter 3

Effect of introducing porous material in the contact pad on the fretting fatigue behavior of nickel-based superalloys.

3.1 Introduction

Fretting fatigue is one of the main factors in the failure of most of the material components in our industries such as axle-wheel arrangement in the train, bolted connections in automobile and disc-blade assembly in turbine engine, etc. As we know, this is a contact-type failure with small relative displacement at micro scale between two contact bodies and it is very challenging to understand the mechanism behind failure experimentally. So, there is a need to develop some better numerical fretting fatigue simulation with better accuracy to study the effect of fretting at the contact which can be useful in designing the component with improved life for industrial applications.

In the chapter, the effect of introducing a porous material in the contact pad on the fretting fatigue behavior of two nickel-based super alloys IN718 and CMSX4 has been investigated by performing room temperature fretting fatigue tests with different types of contact pad, i.e., bridge type flat pad (flat pad), bridge type flat pad with slit (slit pad) and bridge type flat pad with slit filled with porous material (slit + porous pad). The fretting fatigue tests were carried out under a constant contact pressure of 100 MPa. For comparison, plain fatigue tests were also performed in these nickel-based super alloys. The fretting damage at the contact interface and the fretting fatigue fracture surfaces were examined using a scanning electron microscope. The results showed that fretting fatigue life in case of slit + porous showed significantly higher compared to slit pad and flat fad. The results were discussed based on the experimental tangential stress measurement, stress evaluation at the contact using finite element analysis (FEA), fretting surface damage examination and fracture surface examination.

3.2 Experimental Details

3.2.1 Materials and Specimens:

In the present study two types of Ni based super alloy i.e., IN718 and CMSX4 were used for specimens. The contact pads for fretting fatigue test of IN718 were made of Inconel 718. The contact pad of fretting fatigue test of CMSX4 was made of CMSX4. The contact combinations used in this study are commonly used for gas turbine blade/ rotor combination in jet engines. The chemical composition and mechanical properties of IN718 and CMSX4 at room temperature are given in Table 3.1 and Table 3.2. Fretting fatigue tests were carried out using three different types of contact pads, for each IN718 and CMSX4. That is, bridge type flat pad (flat pad), bridge type flat pad with slit (slit pad) and bridge type flat pad with slit filled with porous material (slit + porous pad). The shape and dimensions of specimen used for fatigue test (both plain fatigue and fretting fatigue test) is shown in Fig. 3.1. The shape and dimensions of the bridge type contact pads used for fretting fatigue tests are shown in Figs. 3.2 (a-c). Fig.3.2 (a) shows the flat pad (contact pad with flat contact surface), Fig. 3.2 (b) shows the slit pad, i.e., three rectangular grooves (slit) with 0.5 mm depth and 0.33mm width made in the flat pad, Fig. 3.2 (c) shows slit + porous pad i.e., rectangular grooves (slit) with 0.5 mm depth and 0.33 mm width filled with porous metallic IN718. The magnified schematic of slit + porous pad is shown in Fig. 3.2 (d). The porous IN718 material is fixed firmly in the slit using an adhesive bond. After bonding the surface is cleaned and polished and ensured the contact surface is uniform. For both

IN718 and CMSX4 contact pads the slits were filled with porous IN718 material. Before each test, the gauge parts of all specimens and contacting surfaces of contact pads were polished up to 2000 grade emery paper and then supersonically cleaned with ethanol. The surface roughness of the contact surface was R_a = 0.9 μm.

Table 3.1: The chemical composition of Inconel 718 and CMSX-4 used in present study (wt. %).

Elements	Cr	Mo	Nb	Fe	Al	Ti	Ta	W	Co	Re	Hf	C	Ni
IN718	19.0	3.0	5.0	18.0	0.5	0.9	-	-	-	-	-	0.04	Bal.
CMSX4	6.4	0.6	-	-	5.7	1.0	6.5	6.4	9.7	2.9	0.1	-	Bal.

Table 3.2: Mechanical properties of IN718 and CMSX4 used in present study.

Mechanical properties	Modulus of Elasticity (GPa)	Yield Strength (MPa)	Ultimate Tensile Strength (MPa)	Elongation (%)	Density (g/cm^3)	Hardness (Hv)
IN718	205	510	935	44	8.44	470
CMSX4	130	890	930	19	8.7	425

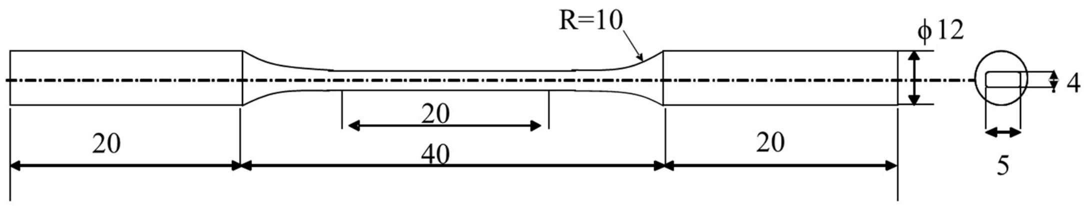

Fig. 3.1 Shape and dimension of fatigue test (plain fatigue and fretting fatigue) specimen.

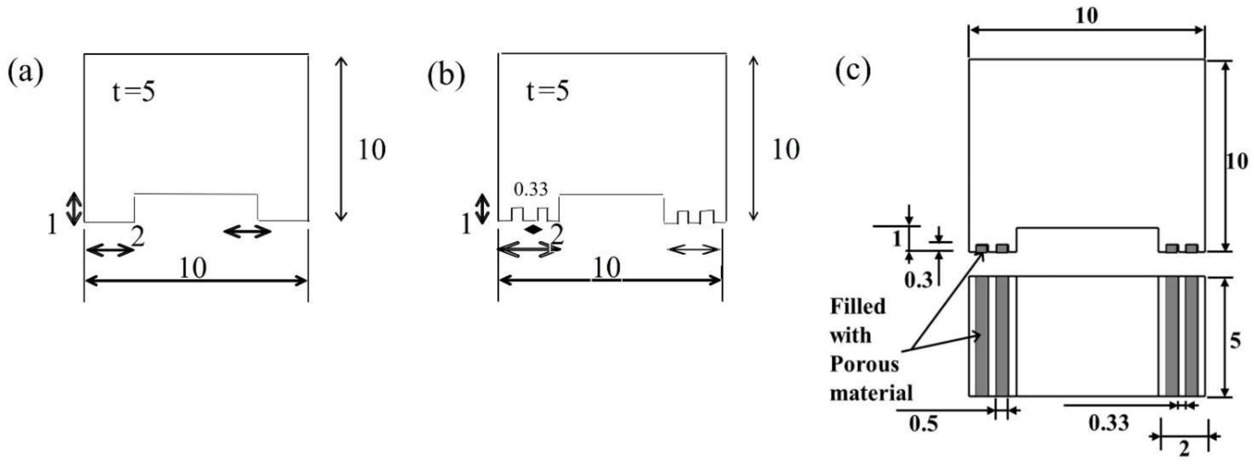

Fig. 3.2 The shape and dimensions of the bridge type contact pads used for fretting fatigue tests (a) flat pad, (b) slit pad, (c) slit+ porous pad (All dimensions in mm).

3.2.2 Fretting fatigue test:

Fretting fatigue tests for both the Ni based super alloys were conducted on a servo-hydraulic test machine at room temperature with a stress ratio of 0.1 and frequency of 10 Hz as per JSME standard S015 [4, 50]. To apply and maintain contact pressure, a calibrated proving ring was used. Fretting fatigue test were carried out at a constant contact pressure of 100 MPa. For comparisons plain fatigue tests of IN718 and CMSX4 were were also carried out. The schematic of fretting fatigue test setup is shown in the Fig. 3.3 (a). During the fretting fatigue test the tangential force between the contact pad and the specimen were measured by using a calibrated strain gauge pasted in the gauge portion of the contact pad as shown in Fig. 3.3 (a). The photograph of fretting fatigue test assembly used in the present study is shown in Fig. 3.3 (b).

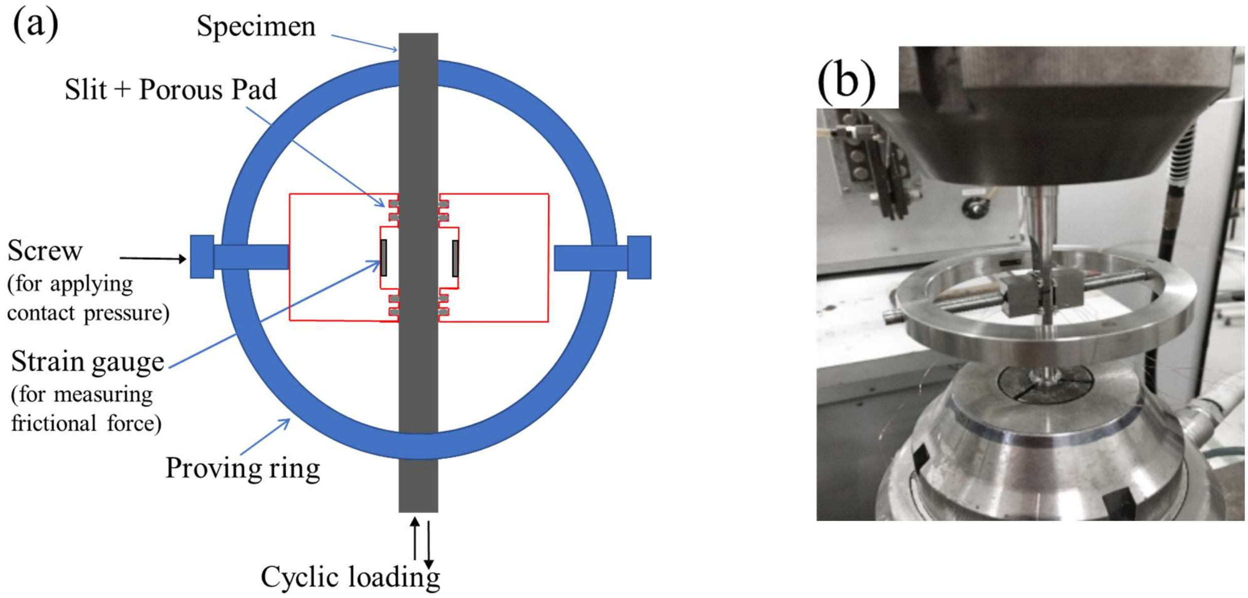

Fig. 3.3 (a) Schematic of fretting fatigue test (b) Photograph of fretting fatigue test experimental setup.

3.2.3 Fretting surface and fracture surface examination:

The fretting scar (fretted surface) was observed using an optical microscopy. Roughness on the fretted surface was examined using TR200 surface roughness tester. The fracture surfaces of the fretting fatigue tested sample were examined using a scanning electron microscope.

3.2.4 Finite Element Analysis:

Finite element analysis was carried out using commercial FEM software ANSYS to evaluate the stress distribution in the contact region and to evaluate the relative slip amplitude. In the model quadrilateral elements were used. The minimum mesh size used at the contact region was 5µm. Boundary conditions were applied along the two symmetrical axes, and loading conditions were given as the same as the fretting fatigue test conducted in the present study. Analysis was carried out by assuming a linear elastic body under plane strain condition. Contact elements were introduced at the contact interface. Loads were applied to the model in three steps. In the first step, a contact pressure was applied on the top of pad for clamping the pad to the specimen. In the second step the maximum cyclic stress was applied. In the third step the minimum cyclic stress was applied. The friction coefficient of 0.6 was used in the present analysis, based on the experimental result in gross slip region. Young's modulus, Poisons ratio and thermal coefficient of expansion used were 210 GPa, 0.33 and 1000 respectively. Separate material properties were provided in porous region and the Young's modulus used for porous material incorporated in between the slits was 60 MPa. The FEA models used in the present study for three different contact pad geometries are shown in Figs. 3.4 (a)-(c). The procedure for evaluation of tangential stress using FEA was explained in section 3.3.3. The relative slip is determined as the difference of relative displacements in the horizontal direction of contact points between the pad and the specimen [51].

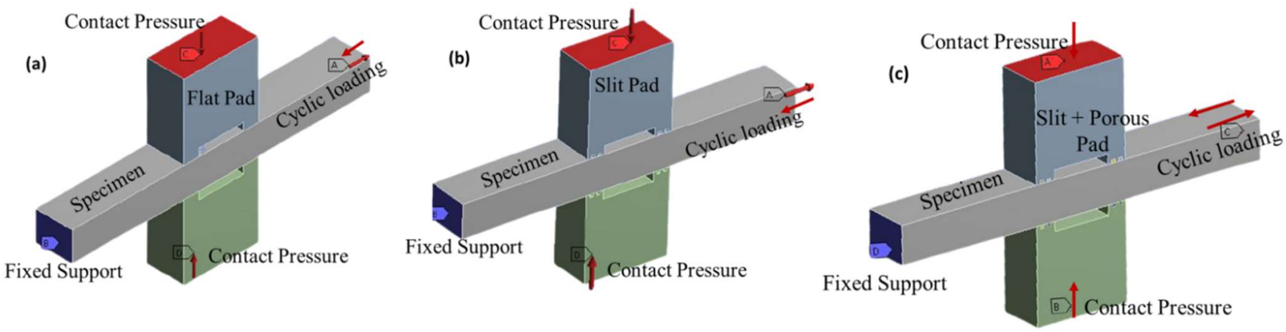

Fig. 3.4 FEA model for different contact pads using Ansys 14.5 (a) flat pad (b) slit pad (c) slit + porous pad.

3.3 Results and discussion

3.3.1 Plain fatigue and fretting fatigue behaviour of Nickel based super alloys:

The plain fatigue and fretting fatigue test results of IN718 and CASX4 are shown in Fig. 3.5. As it can be observed from the figure for both IN718 and CASX4 the fatigue life reduced significantly (more than 50 %) regardless of contact pad type due to fretting. However, compared to

IN718, in CMSX4, the reduction in fatigue lives due to fretting is lower. The reduction in fatigue lives might be due to the accelerated crack nucleation at the contact influenced by high tangential stress at contact interface [15].

Effect of using different contact pad types, i.e., flat pad, slit pad and slit + porous pad for fretting fatigue behavior of IN718 are shown in Fig 3.5. As observed from the figure, the slit pad showed significant enhancement in fretting fatigue life compared to flat pad, slit + porous pad showed further significant enhancement in fretting fatigue life compared to slit pad and flat pad. The same behavior was observed for CMSX4. In fretting fatigue test of CMSX4 using different contact pad types at 250 MPa stress amplitude, slit + porous pad showed higher fretting fatigue life, followed by slit pad and flat pad, as seen from Fig 4. For CMSX4 fretting fatigue test was carried out at only one stress amplitude (250 MPa) just to conform the effect of different contact pad types, i.e., flat pad, slit contact pad and slit + porous, on fretting fatigue life. The results followed the same trend as fretting fatigue of IN718, i.e., slit + porous pad showed significant enhancement in fretting fatigue lives compared to slit pad and flat pad. In case of CMSX4, the effect of fretting on fatigue strength is slightly less compared to IN718, as per the results obtained in the present study.

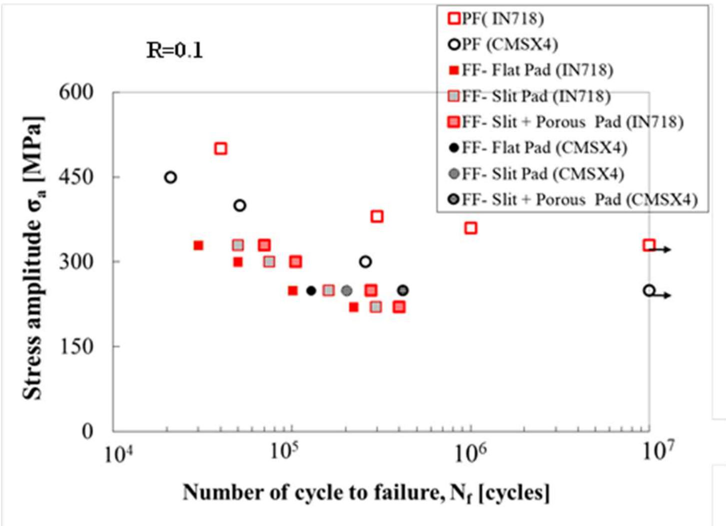

Fig. 3.5 S-N curve for plain fatigue (PF) and fretting fatigue (FF) test of IN718 and CMSX4 (arrow indicates runout)

3.3.2 Effect of contact pad type on tangential stress generated at contact:

To understand the reason behind the enhancement in fretting fatigue strength with slip + porous pad, tangential stress generated at the fretting contact during fretting fatigue test were measured using calibrated strain gauge bonded at the gauge portion of contact pad as mentioned section 3.2.3. The relationship between tangential stress coefficient (tangential stress coefficient = tangential stress / contact pressure) and stress amplitude for different pad types for the fretting fatigue test of IN718 are shown in Fig 3.6. As seen from the figure tangential stress increases with increase in stress amplitude for all type of contact pads. The tangential stress coefficient is highest for flat pad, followed by slit pad, followed by slit + porous pad. The slip + porous pad showed a lowest tangential stress value.

The fretting fatigue test of CMSX4 with different contact pad types also showed a similar trend in tangential stress values as IN718. That is the tangential stress is highest for flat pad, followed by slit pad, followed by slit + porous pad. The slip + porous pad showed a lowest tangential stress value. The summary of measured tangential stress values for IN718 and CMSX4 material at stress amplitude 250 MPa are shown in Fig. 3.7 (a). The summary of fretting fatigue lives for IN718 and CMSX4 material at stress amplitude of 250 MPa are shown in Fig. 3.7 (b). As seen from the figure for both IN718 and CMSX4 the tangential stress is highest for flat pad, followed by slit pad, followed by slit + porous pad. The slip + porous pad showed a lowest tangential stress value. Also, it is observed that for both IN718 and CMSX4 the fretting fatigue life is highest for slit + porous pad, followed by slit pad, followed by flat pad. The flat pad showed a lowest fretting fatigue life.

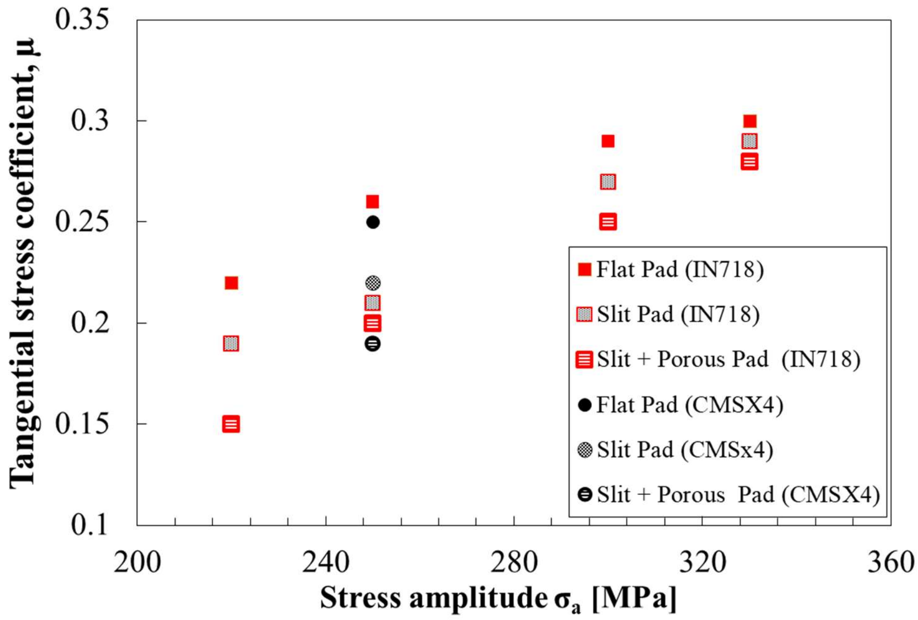

Fig. 3.6 Relationship between tangential stress coefficient and stress amplitude for fretting fatigue test of IN718 and CMSX4.

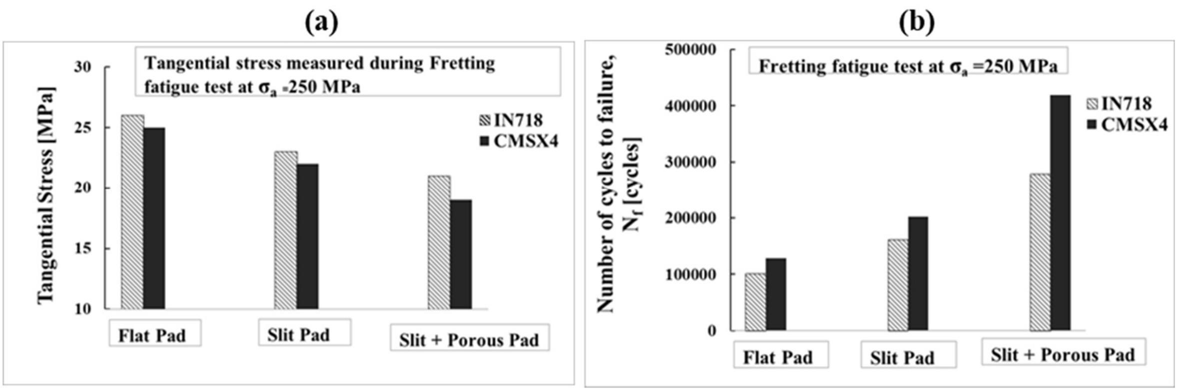

Fig. 3.7 (a) Experimentally measured tangential stress values for Inconel 718 and CMSX4 during fretting fatigue test at σ_a = 250 MPa for different types of pads (b) The summary of fretting fatigue lives for Inconel 718 and CMSX4 material at σ_a = 250 MPa for different types of pads.

3.3.3 Evaluation of tangential stress and relative slip amplitude using FEA:

To identify the location of maximum tangential stress, finite element analysis was carried out. The details of FEA model and parameters used are mentioned in section 3.2.3. In FEA, the loads were applied to the model in three steps. In the first step, a contact pressure was applied on the top of pad for clamping the pad to the specimen. In the second step the maximum cyclic stress was applied, the tangential stress at maximum load was measured. In the third step the minimum cyclic stress was applied, the tangential stress at minimum load was measured. From the maximum and minimum values tangential stress range was calculated. The relation between the tangential stress range and the distance from the contact (one end of contact pad) for different pad types for IN718 are shown in Fig. 3.8 and for CMSX4 are shown in Fig. 3.9. As seen from the figure, for flat pad the tangential stress range was highest near the external edge of contact. For slit pad the tangential stress range was highest near the edge of first slit. For slit + porous pad the tangential stress range was highest near the external edge of contact. The similar trends are observed for both IN718 and CMSX4 alloys.

However, in IN718, the value of peak stress shown was higher compared to CMSX4 alloys, for all the types of pad geometries used in present study as seen from Fig. 3.8 and Fig. 3.9. The location of peak stress in case of IN718 is slightly away from the contact edge compared to CMSX4 alloys. As shown in Fig. 3.8 and Fig. 3.9, the peak stress value for flat pad were identified at 0.3 mm and 0.2 mm from contact edge for IN718 and CMSX4 alloys. For slit pad the peak stress were identified at 0.9 mm and 0.85 mm for IN718 and CMSX4 alloys respectively. Similarly for slit + porous pad the peak stress were identified at 0.2 mm and 0.12 mm from contact edge for IN718 and CMSX4 alloys respectively. These details are clearly shown in Fig. 3.8 and Fig. 3.9. In IN718, the peak stress location was slightly away from the contact edge compared to CMSX4, which might be due to the ductile nature of IN718 compared to CMSX4. The relative slip amplitude between the contact pad and the specimen were evaluated using FEM for different type of contact pads for IN718 and CMAX4 and shown in Fig. 3.10. The relative slip amplitude increases with increase in stress amplitude for all type of contact pads for IN718. For flat pad the relative slip amplitude is highest followed by slip pad, followed by slit + porous pad. The slit + porous pad showed the lowest slip amplitude values. The same trend has been observed for CMSX4 also. However, the values of relative slip obtained in case of IN718 were slightly higher that of CMSX4 alloy. This might be the reason for showing higher tangential stress range values in IN718 as observed in Figs 8 and 9.

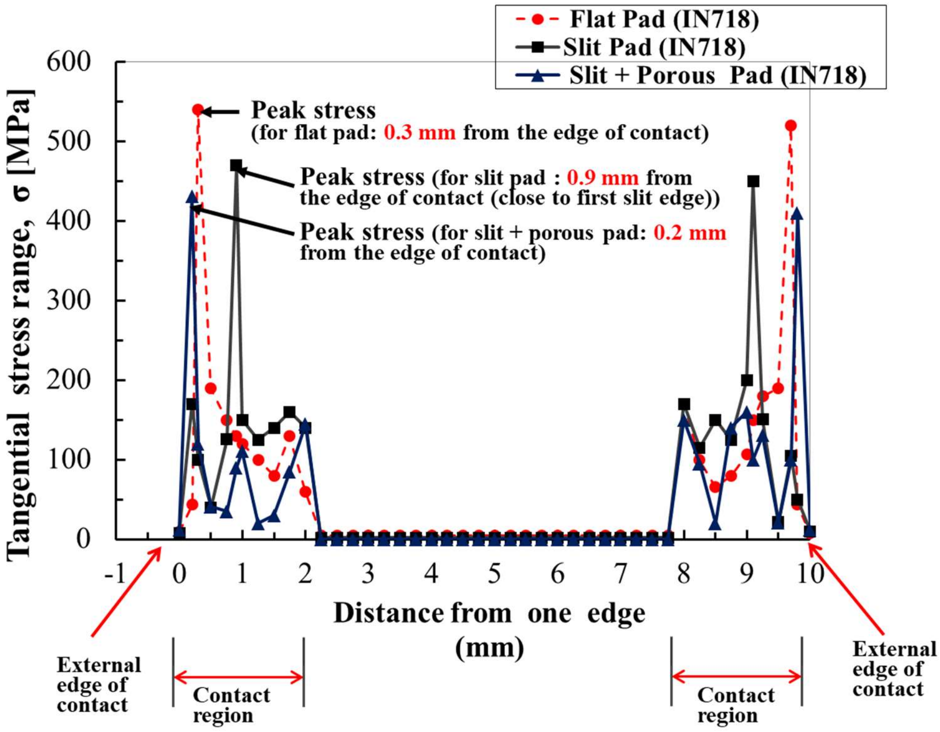

Fig. 3.8 Tangential stress range Vs distance from one edge for IN718 at σ_a = 250 MPa obtained through FEA.

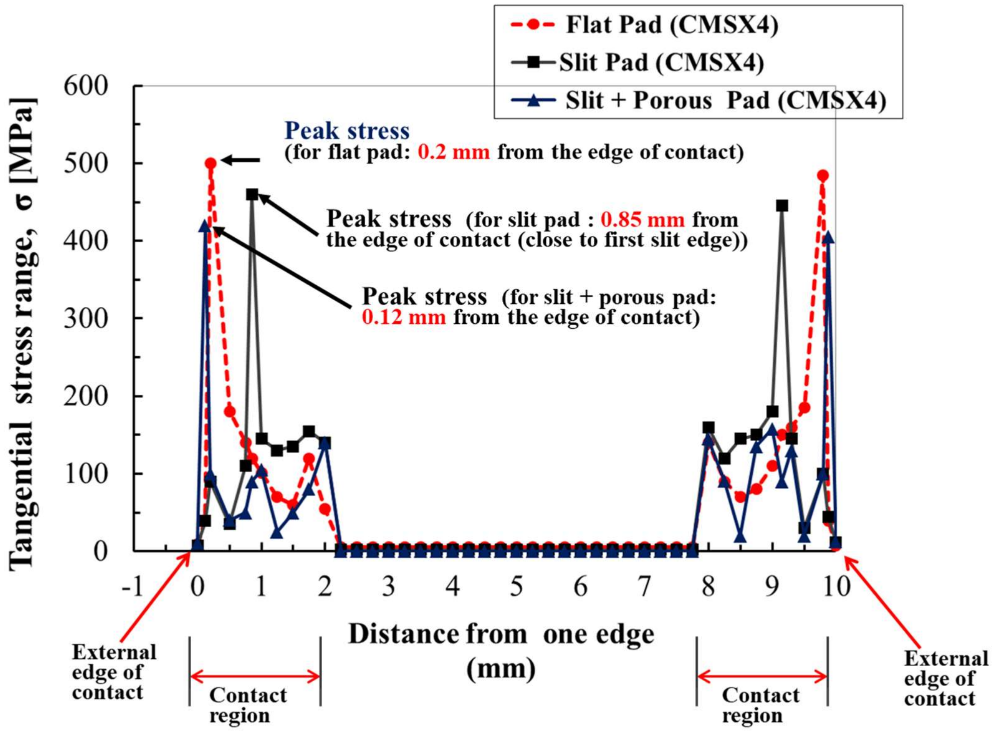

Fig. 3.9 Tangential stress range Vs distance from one edge for CMSX4 at σ_a = 250 MPa obtained through FEA.

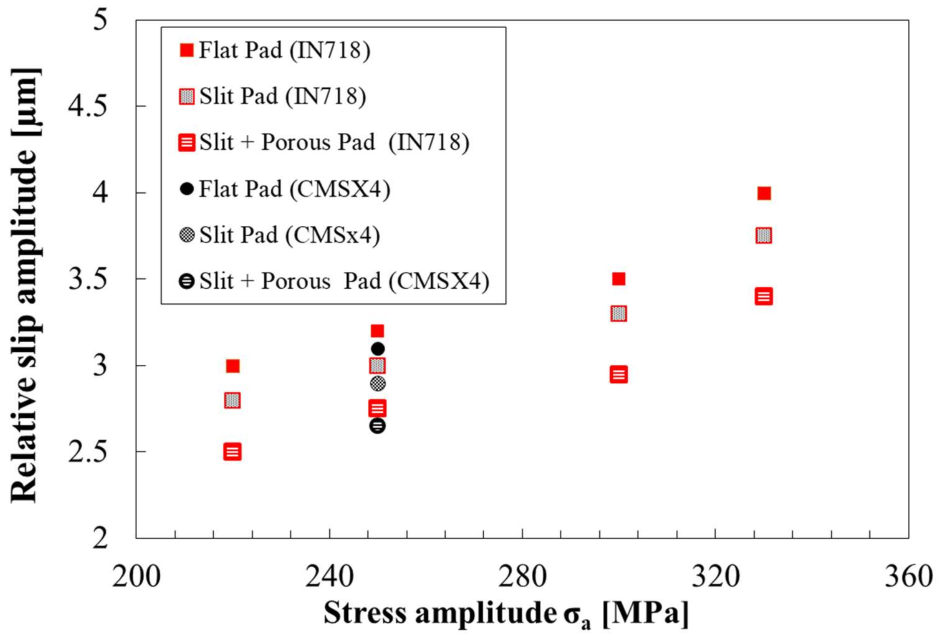

Fig. 3.10 Relationship between relative slip amplitude and stress amplitude for fretting fatigue test of IN718 and CMSX4.

3.3.4 Fretting damage observation:

The fretting scar region of fretting fatigue tested IN718 alloy for different contact pad types are shown in Figs. 3.11 (a-c). As observed form the Fig. 3.11 (a) for flat pad the fretting damage was highest near the external edge of contact, the crack initiation and fracture happened in that location. For slit pad the fretting damage was highest near the edge of first slit, as pointed out in Fig. 3.11 (b), the crack initiation and fracture happened in that location. For slit + porous pad the fretting damage was highest near the external edge of contact, the crack initiation and fracture happened in that location, as shown in Fig. 3.11 (c). The fracture location observed through optical microscope and the maximum tangential stress range location obtained from FEA matches well with each other.

The fretting scar region of fretting fatigue tested CMSX4 alloy for different contact pad types are shown in Figs. 3.12 (a-c). As observed form the Fig. 3.12 (a) for flat pad the fretting damage was highest near the external edge of contact, the crack initiation and fracture happened in that location. For slit pad the fretting damage was highest near the edge of first slit, the crack initiation and fracture happened in that location, as shown in Fig. 3. 12 (b). For slit + porous pad the fretting damage was highest near the external edge of contact, the crack initiation and fracture happened in that location, as shown in Fig. 3.12 (c). In this case also, the fracture location observed through optical microscope and the maximum tangential stress range location obtained from FEA matches well with each other.

Also, from the tangential stress measurement using strain gauge and FEA results, the fretting fatigue test with flat pad showed the highest tangential stress values, followed by slit pad and then slit + porous pad. The fretting fatigue test using slit + porous pad showed the lowest tangential stress values.

As it was reported by many researchers [51], if the relative slip amplitude is high, the tangential stress would be high, the surface damage would be more, results in early crack initiation and reduced fretting fatigue life. The same phenomenon has happened here. The tangential stress was highest for fretting fatigue test with flat pad. It showed lowest fretting fatigue lives. The tangential stress was second highest for fretting fatigue test with slit pad. It showed second lowest fretting fatigue lives. The tangential stress was lowest for fretting fatigue test with slit+ porous pad. It showed highest fretting fatigue lives.

The surface roughness values measured across the fretting damage region for various types of contact pad is given in Table 3.3. As observed in table 3.3, the average surface roughness was highest for fretting fatigue test with flat pad, followed by slit pad and followed by slit + porous pad. Slit + porous pad showed the lowest surface roughness values, which indicates the least surface damage.

Table 3.3: Surface roughness values on fretting scar region of fretting fatigue tested specimen.

Material	Average surface roughness, R_a (μm) of fretted surface at σ_a = 250 MPa		
	Flat Pad	Slit Pad	Slit + Porous pad
IN718	2.15	2	1.65
CMSX4	1.52	1.23	1.1

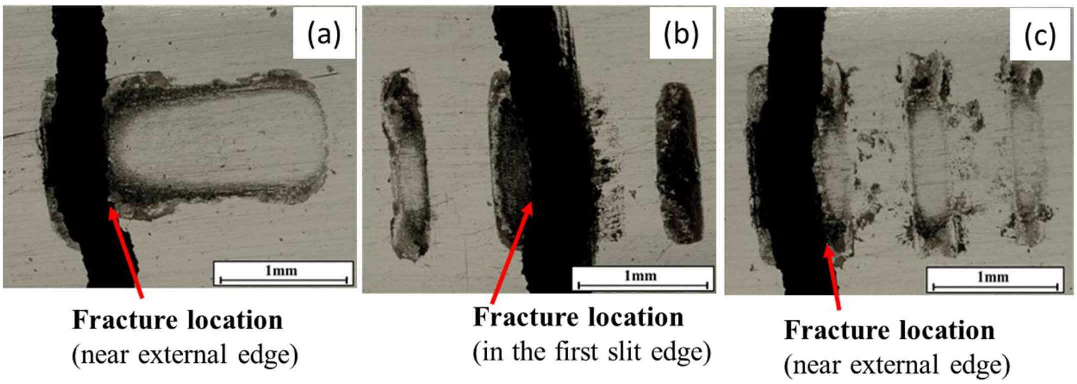

Fig. 3.11 Fretted surface of fretting fatigue tested IN718 specimens using different contact pads at σ_a = 250 MPa (a) Flat pad (b) Slit pad (c) slit + porous pad.

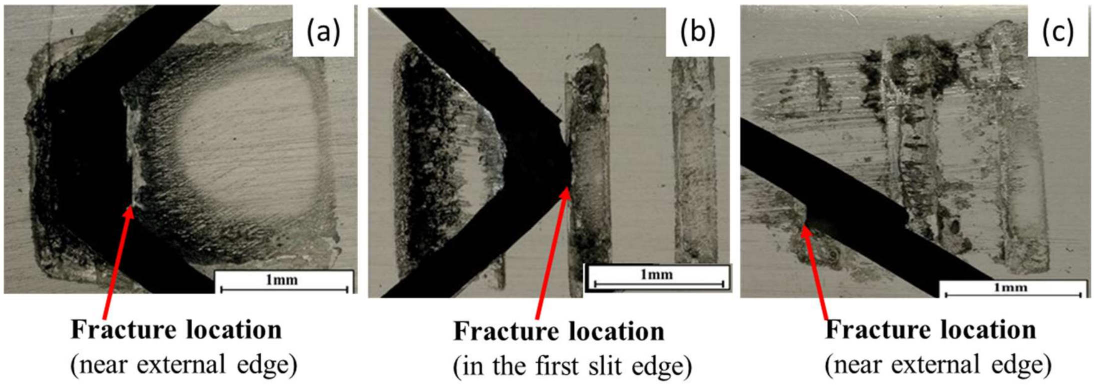

Fig. 3.12 Fretted surface of fretting fatigue tested CMSX4 specimens using different contact pads at σ_a = 250 MPa (a) Flat pad (b) Slit pad (c) slit + porous pad.

Fretting fatigue fracture surface of the fretting fatigue tested specimen with various type of contact pad for IN718 is shown in Figs. 3.13 (a) – (c). As observed form the figure the crack initiated at the contact. The cracks are shown by red arrow and contact region also marked in Fig. 3.13 (a) –(c). For flat pad multiple cracks and more damage at the contact surface were observed due to high tangential stress at the contact. Slit pad has few cracks and surface damage were observed at the contact, but less than flat pad. Slit + porous pad has very few cracks and less surface damage was observed at the contact. The same trends were observed for fretting fatigue fracture surface of the fretting fatigue tested specimen with various type of contact pad for CMSX-4 as shown in Figs. 3.14 (a) – (c). The cracks are shown by red arrow and contact region also marked in Fig. 3.14 (a) –(c). Comparing the fracture surface shown in Figs 3.13 and 3.14, it can be inferred that in CMAX4 the fracture is like quasi cleavage fracture, i.e., brittle compared to Inconel 718. In case of CMSX4, the relative slip amplitude and the tangential stress generated are less compared to IN718 for all types of contact pad for similar stress amplitude (250 MPa), due to tis the surface damage is less in CMSX4, as evident from the surface roughness values measurement from Table 3.3. This might be the reason, for the less reduction of fatigue life due to fretting in CMSX4 compared to IN718.

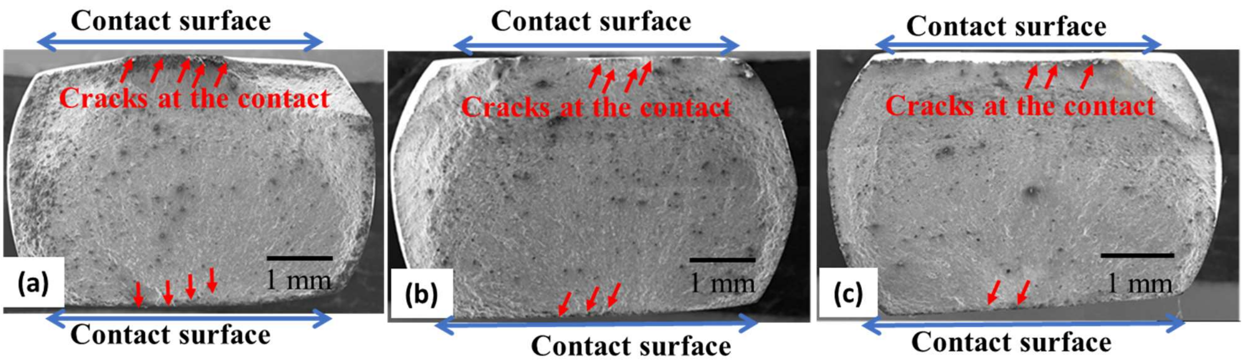

Fig. 3.13 Fracture surface of fretting fatigue tested IN718 specimens using different contact pads at σ_a = 250 MPa (a) Flat pad (b) Slit pad (c) slit + porous pad.

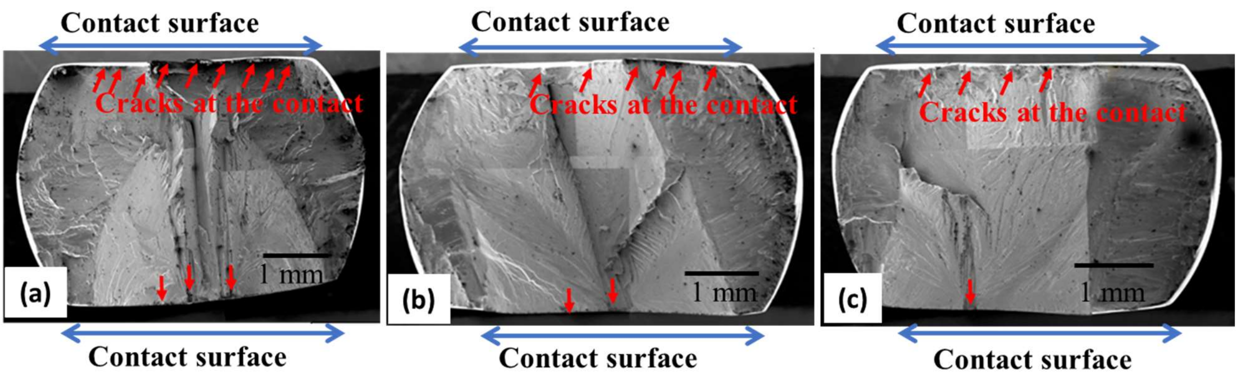

Fig. 3.14 Fracture surface of fretting fatigue tested CMSX4 specimens using different contact pads at σ_a = 250 MPa (a) Flat pad (b) Slit pad (c) slit + porous pad.

3.3.5 Enhancement in fretting fatigue lives with slit + porous pad:

For the fretting fatigue test with slit + porous pad, the relative slip amplitude values are less, the tangential stress generated are less, surface damages are less compared to slit pad and flat pad. For both the Ni based super alloy used in the present study (IN718 and CMSX4), the fretting fatigue life was highest for fretting fatigue test with slit + porous pad. This is due to the lower values of relative slip amplitude, tangential stress at the fretting contact and very less surface damage [25-30]. Based on this study, it has been identified that by using slit + porous contact pad, the fretting damage can be reduced and thereby, it might be possible to enhance the fretting fatigue life. In the present study, only room temperature fretting fatigue behaviour was investigated with slit + porous contact pad, it is equally important to study the high temperature fretting fatigue behaviour using slit + porous pad in future as the materials (IN718 and CMSX4) actual application is at high temperature.

3.4 Summary

In the present study the effect of introducing a porous material in the contact pad on the fretting fatigue behaviour of two nickel-based super alloys IN718 and CMSX4 has been investigated by performing room temperature fretting fatigue tests at a constant contact pressure of 100 MPa using different types of contact pad, i.e., flat pad, slit pad and slit + porous pad, the main conclusions obtained from this study are summarized as follows:

1. Due to fretting, for both IN718 and CMSX-4, the fatigue lives were reduced significantly (more than 50 %). The reduction in fatigue lives were due to the accelerated crack nucleation at the contact influenced by high tangential stress at contact interface.
2. From the experimental tangential stress measurement, the tangential stress is highest for flat pad, followed by slit pad, followed by slit + porous pad. The slip + porous pad showed a lowest tangential stress value.
3. From the FEA analysis results, it is confirmed that the tangential stress is highest for flat pad, followed by slit pad, followed by slit + porous pad. The slip + porous pad showed a lowest tangential stress

value. For flat pad the tangential stress range was highest near the external edge of contact. For slit pad the tangential stress range was highest near the edge of first slit. For slit +porous pad the tangential stress range was highest near the external edge of contact. The similar trends are observed for both Inconel 718 and CMSX-4 alloys.

4. From the fretting scar (fretting surface) observation, of fretting fatigue tested IN718 and CMSX4 alloy for different contact pad types reviled that, for both the alloys for the flat pad the surface damage is very high, followed by slit pad + porous pad. The location of maximum tangential stress identified using FEA matches well with the fracture location in the fretting fatigue tested specimens for all the types of contact pad in both the alloys.
5. Relative slip amplitude evaluated using FEA showed that for flat pad the relative slip amplitude is highest, followed by slit pad, followed by slit + porous pad. The slit + porous pad showed the lowest relative slip amplitude values for both IN718 and CMSX4. For CMSX4 alloy compared to IN718, the relative slip amplitude is less, the tangential stress value generated is less, surface damage is less due to which the effect of fretting on reduction of fatigue lives is less in CMSX4 alloy.
6. For the fretting fatigue test with slit + porous pad, the tangential stress generated were less, surface damages were less compared to slit pad and flat pad. For both the Ni based super alloy used in the present study, the fretting fatigue lives were highest for fretting fatigue test with slit + porous pad. This is due to the lower values of relative slip amplitude, lower tangential stress at the fretting contact and very less surface damage. Using the slit + porous, i.e., by introducing porous material at the contact interface in fretting fatigue, the fretting fatigue lives can be significantly enhanced.

Chapter 4

Extension of fretting fatigue life by fabricating Magnesium Metal Matrix Composite through Friction Stir Processing using Nickel Reinforced Particles

4.1 Introduction

In this chapter, magnesium metal matrix composites (MMCs) were fabricated using Nickel particles as reinforcement and AZ31 alloy as a matrix through the FSP route. The volume fraction of the reinforcement was varied 9%, 12%, and 15% to fabricate the MMCs. The number of passes in FSP was varied to get a homogeneous distribution of reinforced particles. The microstructure characterization was accomplished using an optical microscope (OM) and scanning electron microscope (SEM) which revealed refined equiaxed grains due to combining the action of dynamic recrystallization and pinning effect. The distribution of reinforced particles (Ni particles) all over the stir zone was uniform and created a suitable interface with the matrix. The hardness of the composite was evaluated using a micro-Vickers hardness tester. The tensile properties and fretting fatigue behavior of the MMCs were also studied in detail. From the results, the hardness and tensile strength of the MMCs were improved with a rise in volume fraction (vol. %) of reinforced particles with optimized parameters and helped to enhance the fretting fatigue life of the alloy. Fracture surfaces were also examined using SEM equipped with EDS to identify the failure mechanism.

4.2 Experimental procedure

4.2.1 Fabrication of AZ31/Ni MMCs

For this current research work, a Magnesium alloy AZ31 plate was purchased having a size of 800 mm x 600 mm x 3.3 mm. This plate was cut into small rectangular section plates of size 200 mm x 100 mm x 3.3 mm which was used as base material to produce the Ni reinforced magnesium matrix composites. The composition and mechanical properties of the magnesium alloy used are shown in Table 4.1 and Table 4.2. Pure (99.9%) nickel powder (grain size of ≈40 microns) was used as reinforced particles to produce metal matrix composites (MMCs). Fig. 4.1 shows an SEM micrograph, elemental mapping using energy dispersive spectroscopy (EDS), size distribution of Ni particles, and XRD pattern of nickel powder used in the present study.

Table 4.1 Composition of AZ31 magnesium alloy.

Element	Al	Zn	Mn	Si	Fe	Cu	Ni	Mg
Wt. %	3	1	0.5	0.0075	0.003	0.0025	0.0007	Bal.

Table 4.2 Mechanical properties of AZ31 Magnesium alloy.

Elastic Modulus (GPa)	Yield Strength (MPa)	Ultimate Tensile Strength (MPa)	Elongation (%)	Density (g/cm^3)	Hardness ($HV_{0.1}$)
40	110	196	12	1.8	54

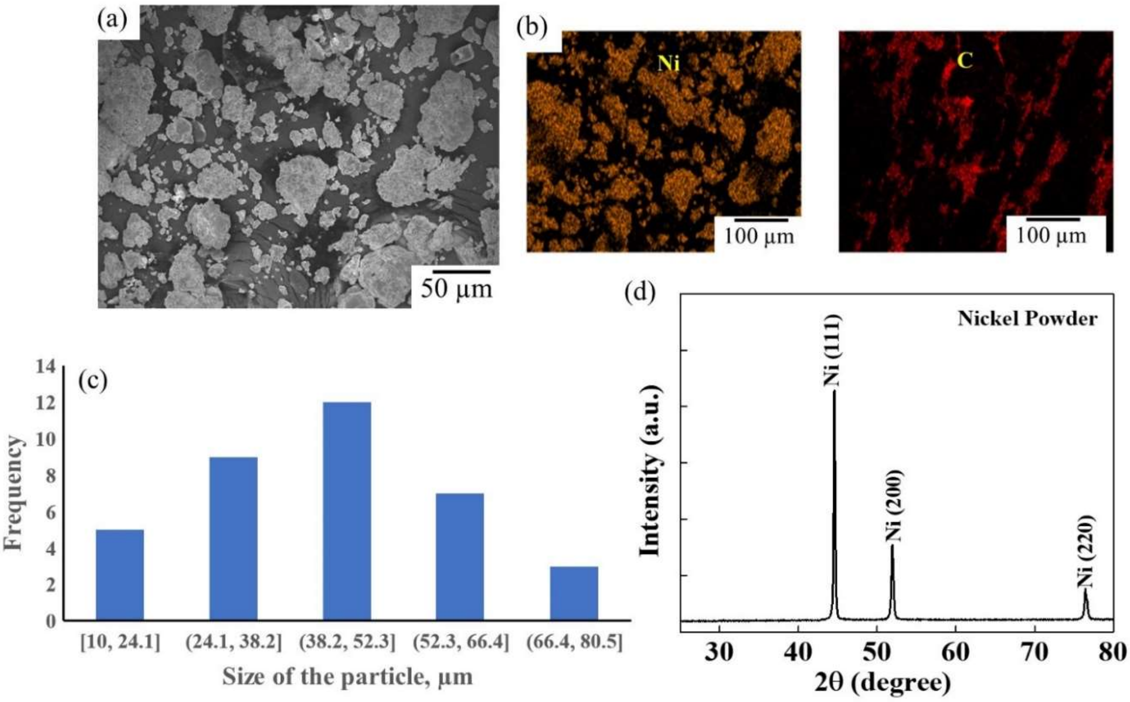

Fig. 4.1 (a) SEM micrograph of pure nickel powder. (b) EDS mapping of nickel particles. (c) Particles size distribution. (d) XRD pattern of pure nickel powder.

The schematic illustration of experimental work conducted in this study is demonstrated in Fig. 4.2. In FSP, initially on the surface of small size plates (200 mm x 100 mm x 3.3 mm), different rectangular shape grooves having a breadth of 0.6 mm, 0.8 mm, and 1 mm were created to a product in three different kinds of volume fraction (9%, 12%, and 15%) with the same depth of 1.8 mm using traditional vertical milling machine with the help of threaded blade cutter. The particles (Nickel powder) were sensibly packed into these machined grooves. Initially, these grooves were closed by running the pinless tool on the surface of the plate at a rotational speed of 600 rpm and a traverse speed of 30 mm/min. to avoid the outflow of powder during processing as represented in Fig. 4.2(a). In the next step, a rigid pin tool was used to distribute the particles into the matrix as shown in Fig. 4.2(b) and the final composite plate was produced as mentioned in Fig. 4.2(c). The FSP tool used in this study was prepared from a mild steel rod of 30 mm diameter. A conical shaped tool pin was preferred of height

3.1 mm to accelerate the constant distribution of reinforced particles into the matrix. The diameter was changing from 3.5 mm at the shoulder end to 3 mm at the free end. As we understand from the previous studies, there are many variables involve in friction stir processing [54] but in the present study, experiments were conducted by varying volume fraction of reinforced particles with multiple passes as mentioned in Table 4.3. The conventional vertical milling machine used for fabricating MMCs is shown in Fig. 4.3 (a). The rotational speed of the tool (950 rpm) and traverse speed (30 mm/min.) was maintained constant which was used from the optimized condition mentioned in previous studies for processing [61, 62]. The processed plates for base Mg alloy and MMCs at different volume fractions are shown in Fig. 4.3(b). The plate was allowed to cool after every experiment. These processed plates were cut in a direction perpendicular to the tool direction to obtain specimens for various microscopic observation and testing as shown in Fig. 4.2(d) and (e).

Table 4.3 Process parameters used for friction stir processing.

Parameter	**Values**
Rotational speed (rpm)	950
Transverse speed (mm/min.)	30
No. of passes	2, 4
Tool shoulder diameter (mm)	15
Pin diameter (mm)	3.5
Pin length (mm)	3.1
Groove width (mm)	0.6, 0.8 and 1
Groove depth (mm)	1.8
Ni content (Vol. %)	0, 9, 12 and 15

4.2.2 Microstructure

Mounting of the sample was done initially and then polish the specimen using an automatic polishing machine. Fine polishing was achieved using a diamond paste of 1 micron and spray. A chemical etchant consisting of 25 ml ethanol, 2.5 ml acetic acid, 2 g picric acid in 10 ml water for 1 to 3 seconds was used to expose the microstructural features. Micrographs were observed using an OM and SEM to investigate the distribution of the reinforced particles and interface integrity. The average grain size of base magnesium alloy with different numbers of passes was measured using ImageJ software.

4.2.3 XRD and residual stress

The X-ray diffraction pattern of AZ31 Mg alloy and AZ31/Ni MMCs at different volume fractions (9 %, 12 %, and 15 %) was extracted to confirm the presence of Mg and Ni-related phases, which were obtained by comparing the Bragg angles and interplanar spacing values to the standard values. An X-ray diffractometer was used to assess the residual stress of the as-received AZ31 Mg alloy and the AZ31 Mg alloy with numerous passes. The diffraction angle of crystal planes (202) 104.2° was used as a measuring criterion.

Bragg's law (eq. 1) states that the lattice spacing, d, is proportional to the diffraction angle, and that any change in 'd' shifts the diffraction angle to the left or right. The residual stress can be calculated using the diffraction angle (2θ) shifts. To determine the residual stress components, the sample should be tested in several orientations in order to obtain all of the stress values [59].

$n\lambda = 2d\sin\theta$ ………………………………………………… (1)

The most used method for stress determination is the sin2 ψ method. Several XRD measurements were made at different psi (ψ) tilts. By altering the tilt of the specimen within the diffractometer, measurements of planes at an angle ψ can be made and thus the strains along that direction can be calculated using

$\varepsilon = (d_\psi - d_o) / d_o$ ……………………………………………… (2)

From Hooke's law we know that

$\sigma = E\,\varepsilon$ ………………………………………………… (3)

If we consider the strains in terms of inter-planar spacing, then the stress can then be calculated from such a plot by calculating the gradient of the line and with basic knowledge of the elastic properties of the material using the equation as follows [60].

$\sigma = E/(1+\nu)\,\sin^2\Psi\,((d_\Psi - d_o)/d_o)$ …………………………… (4)

4.2.4 Hardness and tensile behavior

A rectangular sectioned specimen from the fabricated plate was cut for the hardness test. The micro-Vickers hardness of the basic material (AZ31 magnesium alloy) and the composites (AZ31/Ni MMC) at various volume fractions was determined under a load of 100g for a dwell time of 10s. The E834 standard test method [65] was used to assess the material's micro indentation hardness. The ASTM D638-V standard [74] was utilised to prepare tensile specimens with wire EDM. As shown in Fig. 4.2, tensile specimens with a gauge length of 9.5 mm, a width of 3.18 mm, and a thickness of 3 mm were obtained from the treated region (d). The test was performed at a cross head speed of 0.5 mm/min [76], with the results compared at the conclusion. Tensile testing was carried out with the help of a fully integrated servo-hydraulic test system/machine (UTM), as shown in Fig. 4.4. (a). SEM was employed after the test to inspect the fracture surface and determine the failure mechanism.

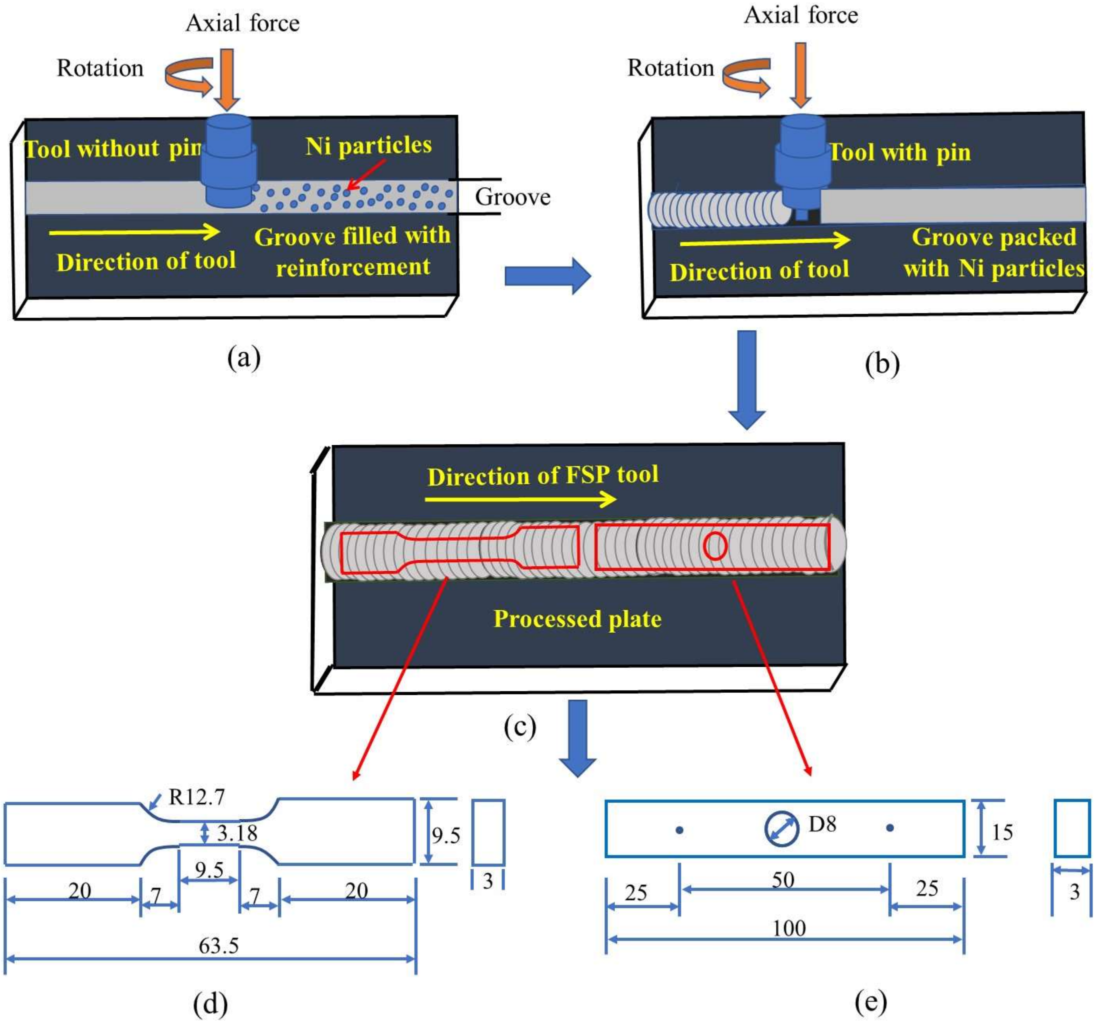

Fig. 4.2 Schematic diagram of friction stir processing. (a) Nickel particles packed inside the groove using a pinless tool (b) FSP using rigid pin tool (c) Processed plate (d) Tensile test specimen. (e) Bending test specimen. (All dimensions are in mm)

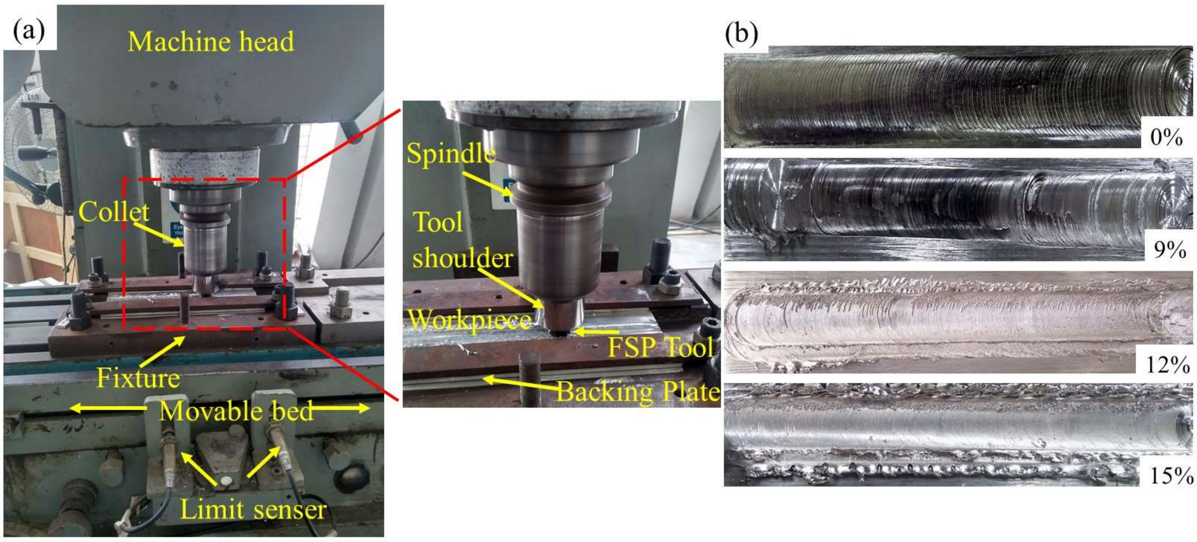

Fig. 4.3 (a) Experimental setup for conventional vertical milling machine with a magnified view. (b) Processed plates for different volume fractions (AZ31/0%Ni, AZ31/9%Ni, AZ31/12%Ni, and AZ31/15%Ni).

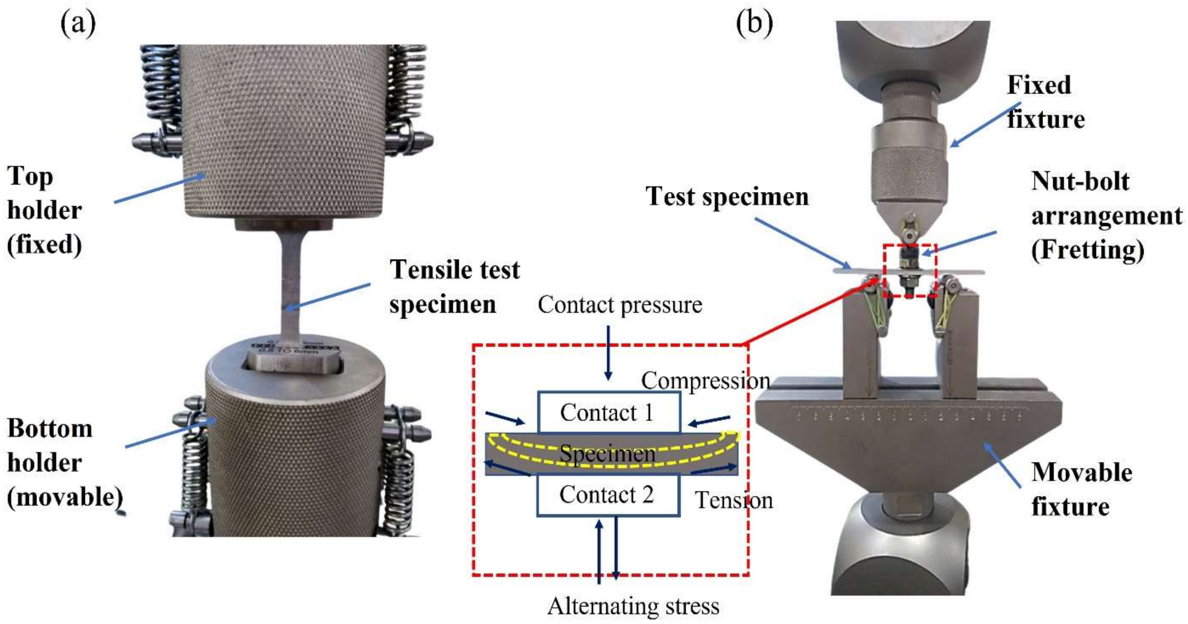

Fig. 4.4 (a) Tensile test setup and (b) Fretting fatigue test setup.

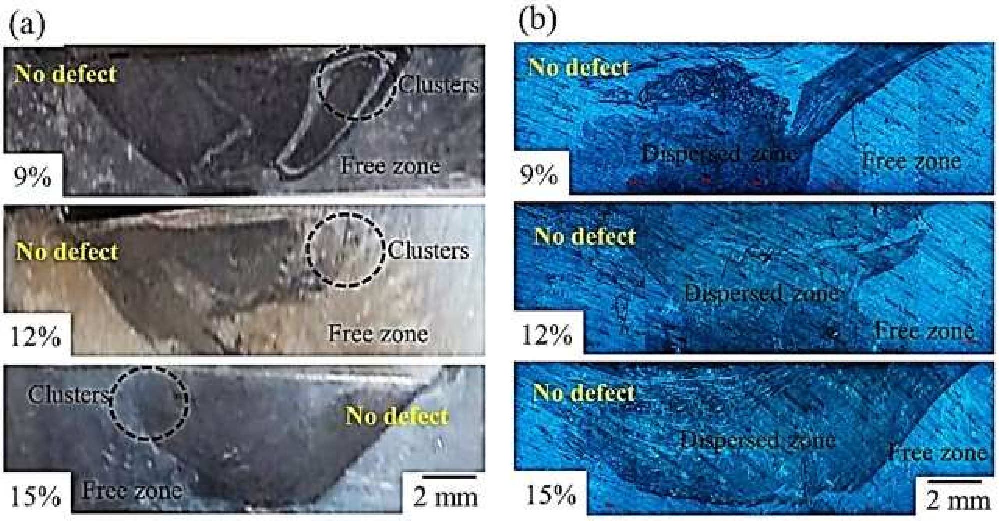

Fig. 4.5 Macrographs of stir zone without defects at different volume fraction (9%, 12% and 15%).
(a) 2 pass (b) 4 Pass.

4.2.5 Fretting fatigue behavior

As shown in Fig. 4.2(e), the specimen was manufactured in accordance with ASTM D790 utilising wire EDM with a length of 100 mm, a width of 15 mm, and a thickness of 3 mm. After that, a drill was used to make an 8 mm hole in the specimen's centre. This hole was created to introduce the nut-bolt assembly with washer so that the fretting effect could be understood during the testing. This fretting fatigue test was generally performed on a universal testing machine using the required 3-point bending test fixture. As illustrated in Fig. 4.4(b), the specimen with nut-bolt arrangement was placed on two supporting cylindrical pins, with one cylindrical pin situated midway from the top at the bolt head. The test was performed with a constant stress ratio of R = 0.1 (r_{min}/ r_{max}) and a uniaxial sinusoidal load control of 5 Hz [79]. A constant contact pressure of 110 MPa was applied by tightening the bolt. The stress reduced from a level corresponding to a fatigue life of less than 10^5 cycles to a level below the fatigue strength stress (125 MPa to 75 MPa, each time decrease by 25 MPa). 'Run outs' are specimens that have not failed after a set number of cycles ($2x10^6$ cycles), while others are stopped until the core component breaks. The results of these tests can be used to look at the effects of processing, surface condition, and stress on the fatigue resistance of materials subjected to flexural stress over a large number of cycles, which is what can be expected from actual device handling and assembly.

4.3 Results and discussion

4.3.1 Microstructural characteristics of AZ31/Ni MMCs:

There are no defects in the MMCs at the macroscopic level, such as pinholes or tunnels. Fig. 4.5 shows macrographs of the stir zone at different volume fractions (9 %, 12 %, and 15 %) over numerous runs. Based on the selection of process parameters, a defect-free stir zone is obtained, which aids in particle spreading and strength retention during testing. It was discovered that there existed a strong permanent contact between the matrix and the reinforced particles. The density of the composite was evaluated using weight and size after MMCs were manufactured. The theoretical (by rule of mixture) and experimental density of MMCs produced by FSP are shown in Fig. 4.6. It was discovered that the density of MMCs did not vary significantly during FSP when compared to the theoretical density, implying that no reinforced particles were wasted throughout the process. The maximum density of nickel at 15% volume fraction is 2.4 g/cm3, which is lower than that of other structural alloys.

As per Table 4.3, the microstructure of all the experiments was studied. The optical micrographs of base Mg alloy and alloy with multiple passes (2 and 4) are shown in Fig. 4.7. From the ImageJ software, the average grain size for the base magnesium alloy was found to be 31.7 ± 2.6 µm. Similarly, the base alloy with 2 passes and 4 passes was found to be 14.9 ± 1.8 µm and 8.2 ± 0.7 µm. From the ImageJ analysis, it is understood that there is a noteworthy reduction of 53% and 74% in the average grain size was observed for base magnesium alloy in the case of 2 passes and 4 passes respectively. As a result, as the number of passes increases, the grain refinement is confirmed. Because no flaws were discovered in the processing zone. The absence of macroscopical flaws, on the other hand, does not guarantee a uniform distribution of reinforced particles. Using a conical tool with a stiff pin, Ni particles are put in the machined groove to make the composite. An ideal MMC should have a correct distribution of reinforced particles after processing in order to display enhanced and higher mechanical properties.

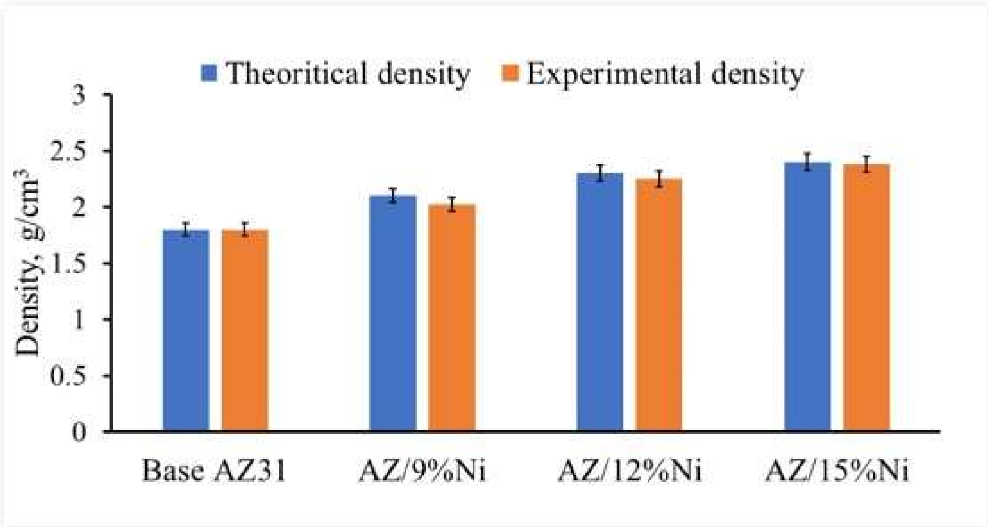

Fig. 4.6 Comparison of the theoretical density and experimental density of MMCs at different volume fraction.

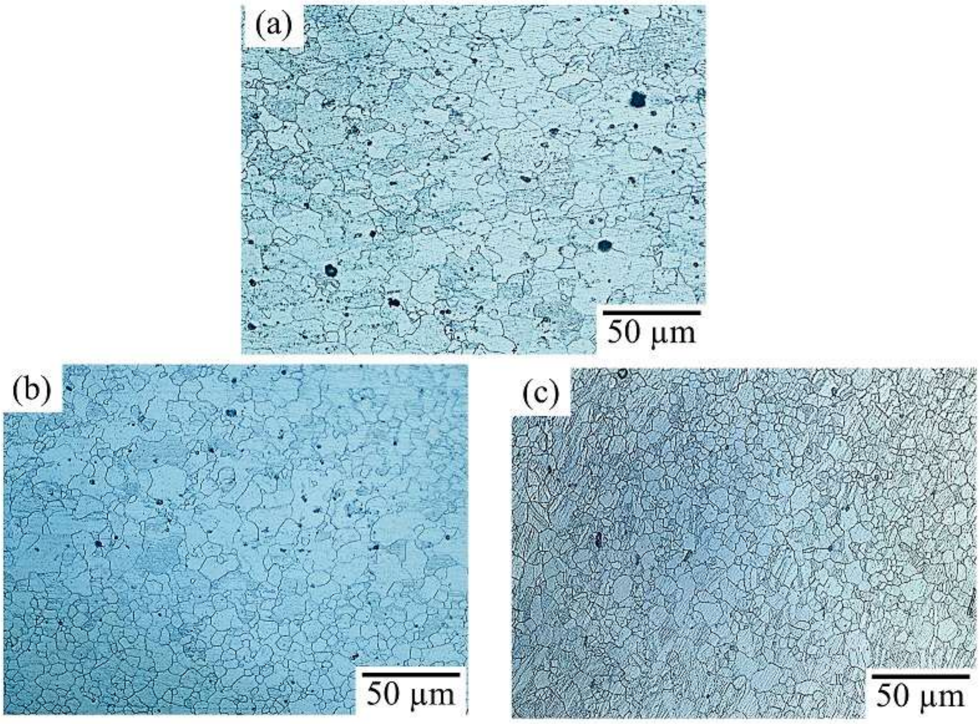

Fig. 4.7 Optical micrographs of base material (AZ31 magnesium alloy). (a) AZ31 magnesium alloy (as received). (b) AZ31 magnesium alloy (no. of passes = 2). (c) AZ31 magnesium alloy (no. of passes = 4).

As in the case of 2 passes, the distribution was not homogenous in the stir zone. So, it is not easy to represent a single micrograph for each test. The observed microstructures can be categorized into different zones such as free zone (Fig. 4.8(a), (b) and (c)), dispersed zone (Fig. 4.8(d), (e) and (f)), layered zone (Fig. 4.9(a), (b) and (c)) and clustered zone (Fig. 4.9(d), (e) and (f)). In the free zone, there are hardly any particles, or zero particles present which can be observed near the interface zone (Fig. 4.8). The MMCs are stronger as a result of the correct particle distribution. However, as the volume percentage increases, segregation of Ni particles may be observed in some spots due to substantial variations in the density of reinforced particles and the matrix, as shown (by arrow) in Fig (4.8). The layered zone is present at the base of the stir zone. In this zone, the particles are arranged in curved form due to the vertical material flow as represented (dotted arrows) in Fig. (4.9). And clustered zone shows a random dispersion of particles with a small interparticle distance between them. There is a broad gap between clusters present in certain places as represents in Fig. (4.9). In this zone, the bonding of Ni particles to the matrix is insufficient to absorb any external load. Because there are more particles in this area, the grain size is smaller. Due to the lack of diffusion between ceramic particles during processing, this microstructure is not achievable in MMCs containing ceramic particles. Because the reinforced particles and the matrix in the dispersed zone are well bonded, the big size is unneeded for strengthening because the number of passes is reduced. The micro-Vickers hardness of this zone was 90 Hv, indicating that the particles were appropriately distributed and sintered in this type of zone as a result of the frictional heat and stirring action.

Both frictional heat and mechanical stirring are affected by the number of passes. The reduction in the number of passes causes a reduction in frictional heat and mechanical stirring action, resulting in less particle dispersion and a lower degree of plasticization. As a result, the circulation of particles was seen to be improved and homogeneous after four passes, as illustrated in Fig. 4.10. Except for the dispersed zone, there are no additional zones in the microstructure. At two passes, the amount of clustered zone was observed to be greater. Another variable that was used in this investigation was the volume fraction. The quantity of powder packed in the machined groove is determined by the volume fraction. To modify the volume fraction of particles in the matrix, different sizes of grooves were created. Because higher particulate material obstructs particle mobility and results in a poor distribution of reinforcement, increasing groove dimension increased the difficulty of plasticization. As a result, at a volume fraction of 15%, with 4 passes, a satisfactory distribution was observed. The effect of mechanical stirring is increased by increasing the number of passes, which improves distribution across the stir zone. Because of the repetitive action of mechanical stirring, the material's plastic flow prompted the smashing of clustered and sintered particles. However, the process parameters (rotational and traverse speed) are constant, the more number of passes leads to fresh recrystallization because of repetitive plastic deformation of the previously recrystallized grains [74, 75]. The repeated deformation and recrystallization cause a reduction in grain size. There is a reduction in grain size after 4 number passes which is 40% as compared to 2 number of passes before adding the reinforcement as mentioned earlier. It was difficult to quantify grain size because numerous particles crossed grain boundaries (intragranular distribution), preventing the formation of a permanent grain boundary after etching, and the fine dispersion made identifying grain boundaries difficult. The onion ring structure in composites produced by friction stir processing is a lamellar arrangement of particles at the base of the stir zone that reduces and increases intensity in a curved or circular pattern [76].

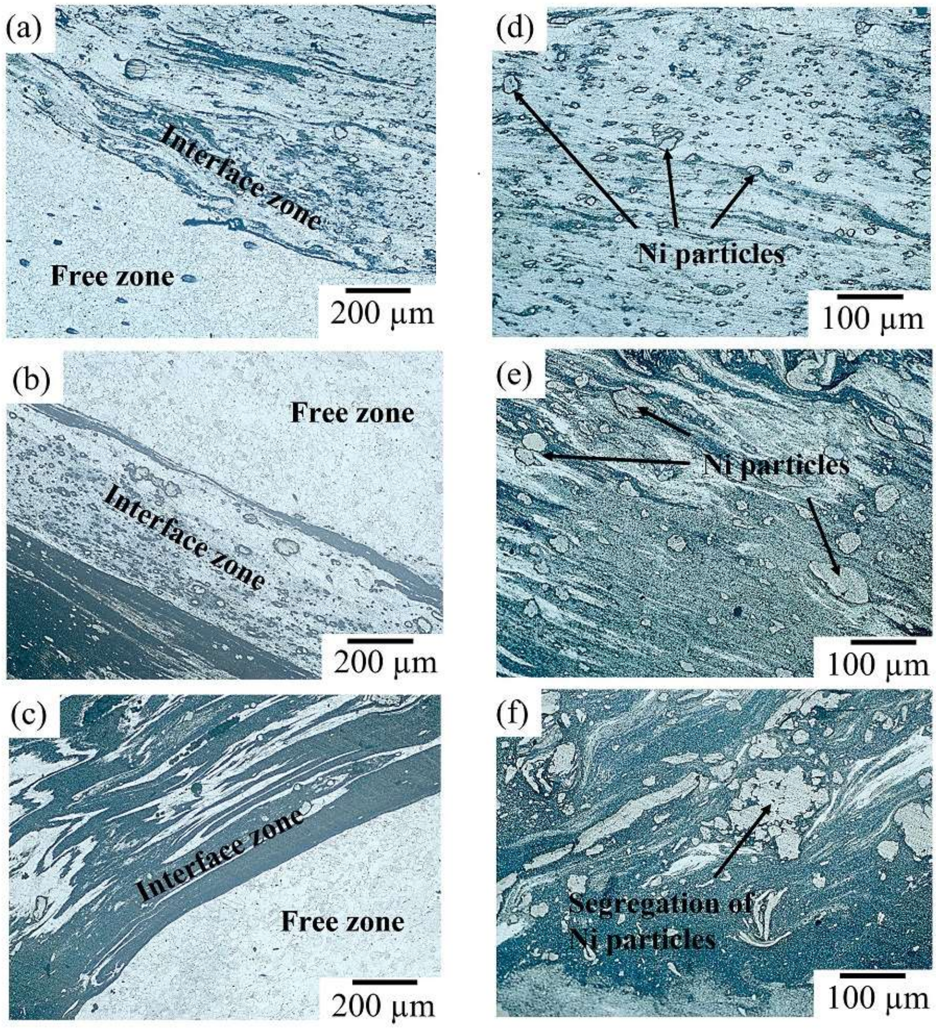

Fig. 4.8 Optical micrographs of AZ31 magnesium matrix composite. (a), (b) and (c) represents interface zone. (d), (e) and (f) represents dispersed zone. (a) and (d) AZ31/9%Ni MMC, (b) and (e) AZ31/12%Ni MMC, and (c) and (f) AZ31/15%Ni MMC (no. of passes = 2 in all cases).

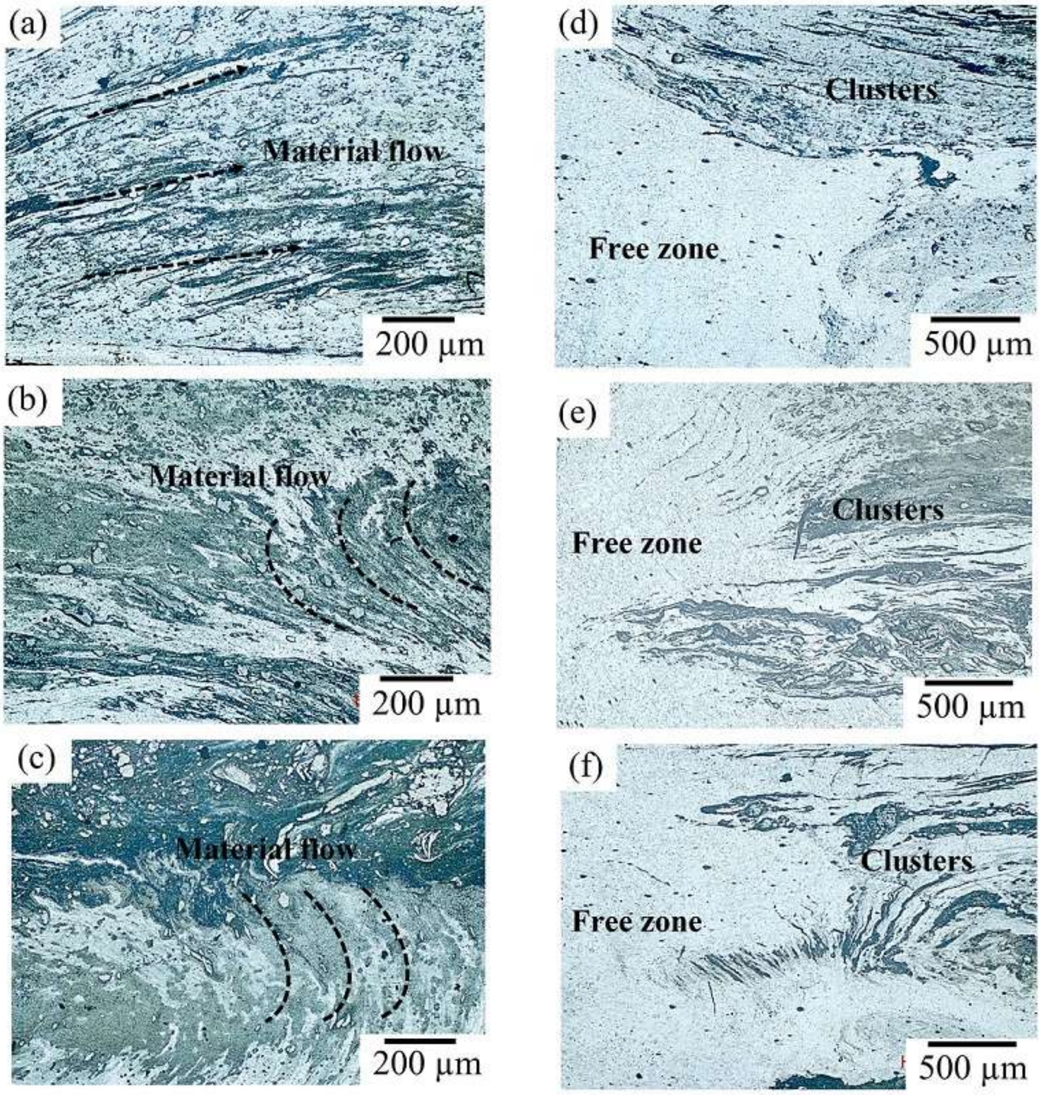

Fig. 4.9 Optical micrographs of AZ31 magnesium matrix composite. (a), (b) and (c) represents layered zone. (d), (e) and (f) represents cluster zone. (a) and (d) AZ31/9%Ni MMC, (b) and (e) AZ31/12%Ni MMC, and (c) and (f) AZ31/15%Ni MMC (no. of passes = 2 in all cases).

Fig. 4 shows SEM micrographs for 2 and 4 passes at varying volume fractions of Ni particles. The presence of nickel particles as white portions in nodular or round shape with uniform distribution and good Ni –Mg interfacial integrity for many passes was indicated by microstructural evaluation of composite specimens. As the volume of powder is raised, they rise in quantity and concentration. The existence of elemental nickel particles as reinforcement was discovered in the microstructure without any evident nickel-magnesium reaction product, which might be attributed to the low processing temperature and mechanical stirring. Because the micrographs do not exhibit any empty gaps or particle aggressiveness, they represent a homogeneous distribution in the case of repeated passes [68]. Due to the homogenous dispersion of reinforced particles, FSP is one of the best ways for forming MMCs. FSP was done up to 2.8 mm in the 3.3 mm substrate plate in this current study. The remaining plate, which is around 0.5 mm thick, increases heat transfer and generates a significant vertical heat flow difference. To achieve homogeneous distribution, the number of passes and volume fraction of Ni particles were changed. Frictional heat causes plasticization, which affects the size of the grains. Mechanical stirring, on the other hand, aids in the deformation of the material, affecting particle mobility. FSP has provided a correct particle dispersion, which aids in the achievement of improved mechanical characteristics. The processing parameters for this approach are numerous. Multiple passes are an important component in avoiding inappropriate distribution and particle-free zones, according to some studies [76, 77]. The inter-particle distance decreases as the number of passes increases, indicating a uniform distribution. Fig. 4.11(f) presents the particle distribution in AZ31/15 vol% Ni composite which confirms the uniform distribution of Ni particles in the MMCsThe nature of the contact produced between Ni particles and the AZ31 magnesium alloy may also be determined using these micrographs. Due to sufficient plasticization of the AZ31 alloy and unimpeded flow over the particles, there is no breakdown or disruption around each particle, and no additional compounds are discovered in the interface. As illustrated in Fig. 4.12, EDS mapping was used to check any form of diffusion or traces of other substances throughout the element mapping process. The existence of Mg, Ni, and other alloying elements is confirmed by the mappingDuring FSP, the reinforced particles are subjected to significant straining, which aids in particle crushing, and there is a change in the form and size of the particles, as observed in various earlier studies [78]. The base material (AZ31 magnesium alloy) is represented by the plane back portion in Fig. 4.12, while the composite (AZ31+Ni particles) is represented by the white area. This shows the nature of Ni particle strengthening and dispersion with other alloying elements.

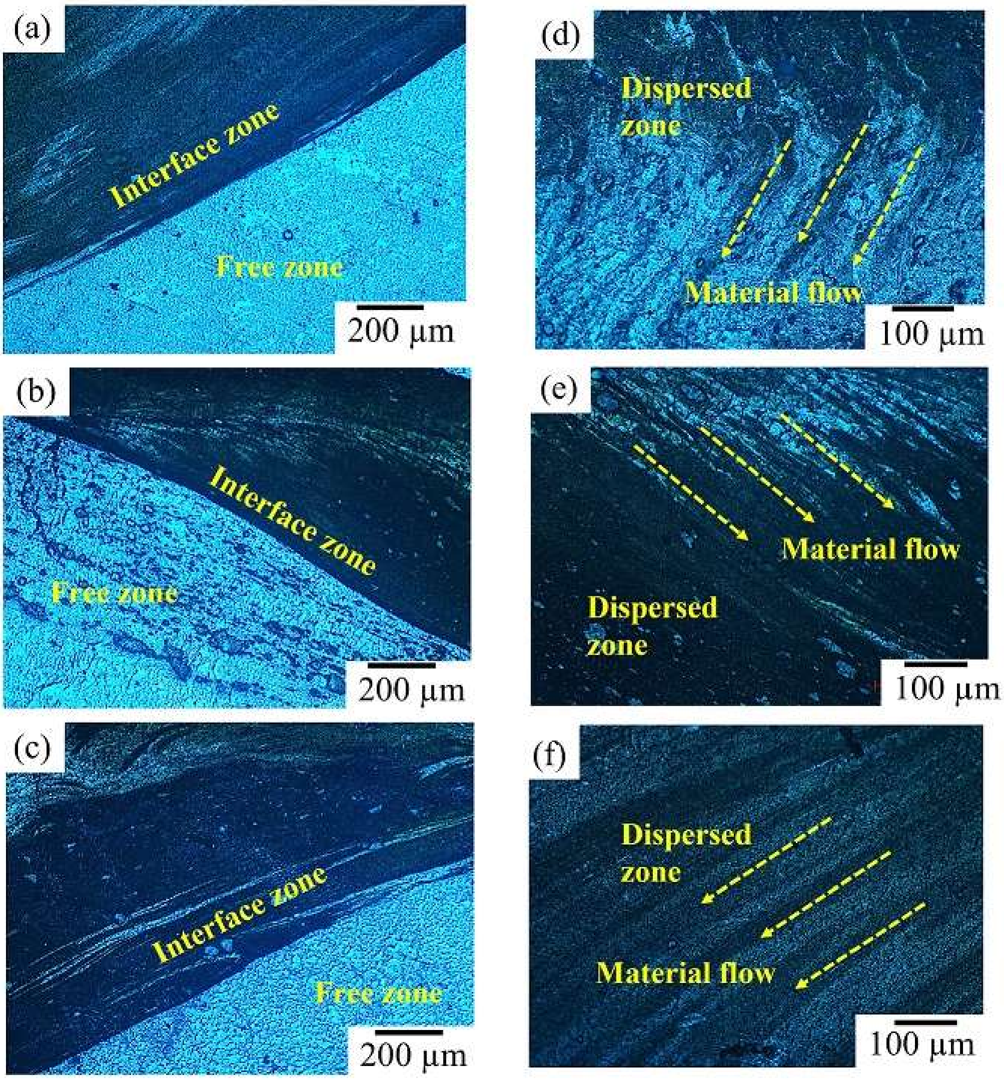

Fig. 4.10 Optical micrographs of AZ31 magnesium matrix composite. (a), (b) and (c) represents interface zone. (d), (e) and (f) represents dispersed zone. (a) and (d) AZ31/9%Ni MMC, (b) and (e) AZ31/12%Ni MMC, and (c) and (f) AZ31/15%Ni MMC (no. of passes = 4 in all cases).

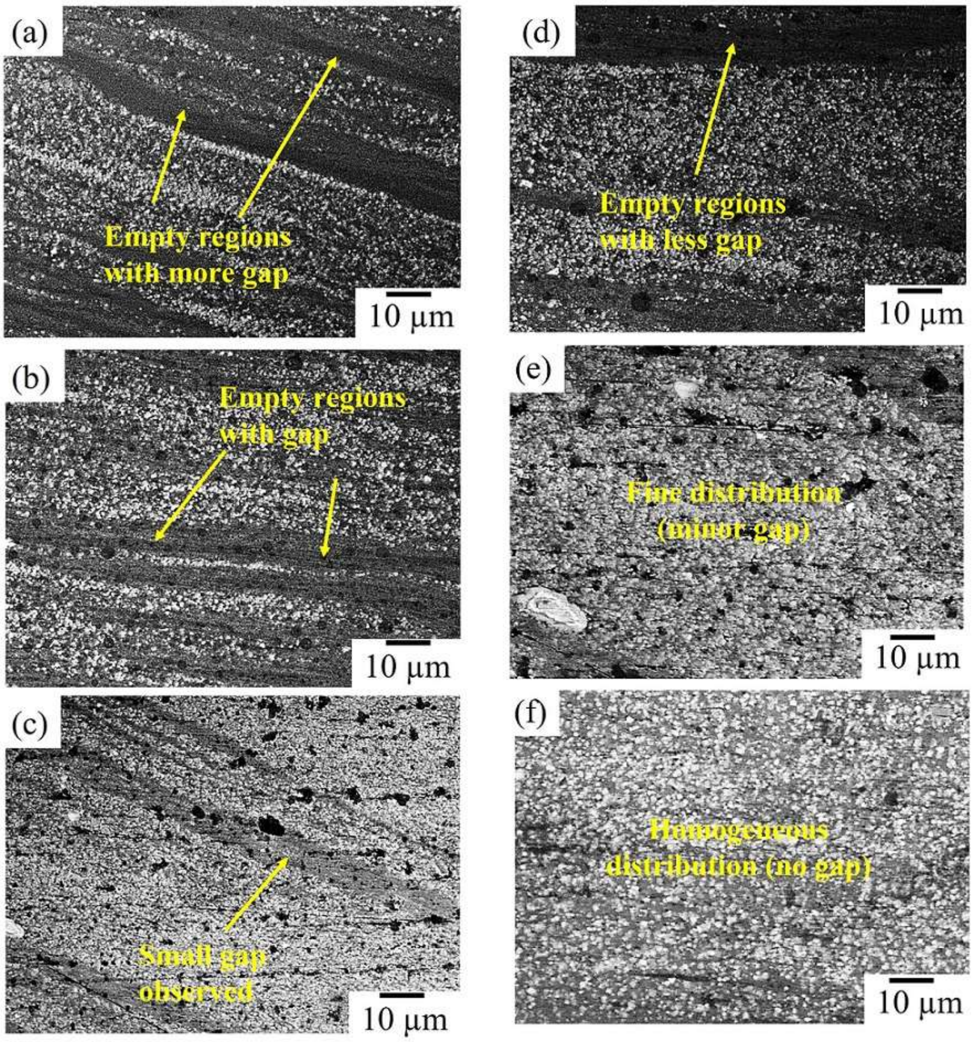

Fig. 4.11 SEM micrographs of AZ31 magnesium matrix composite. (a) AZ31/9%Ni, (b) AZ31/12%Ni, and (c) AZ31/15%Ni represent MMCs with 2 passes. (d) AZ31/9%Ni, (e) AZ31/12%Ni, and (f) AZ31/15%Ni represent MMCs with 4 passes.

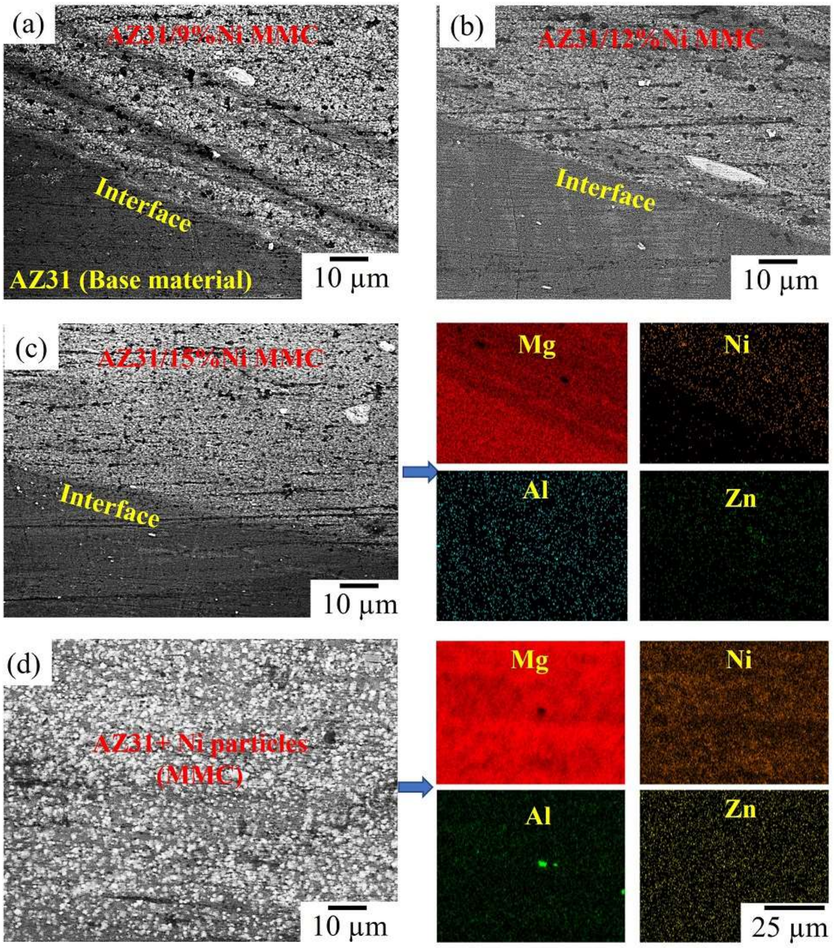

Fig. 4.12 SEM micrographs with EDS mapping of AZ31 magnesium matrix composite. (a) AZ31/9% MMC (b) AZ31/12% MMC (c) AZ31/ 15% MMC (at the interface) (d) Processed area (white portion confirmed the presence of Ni particles).

4.3.2 XRD and residual stress measurement results:

Fig. 4.13 shows the X-ray diffraction pattern for AZ31 Mg alloy and AZ31/Ni MMCs at different volume fractions (9 %, 12 %, and 15 %). As the volume fraction of reinforcement is increased, the number of Ni peaks increases. The elemental peaks of the elements in the composite are recorded in these patterns. The Bragg angle and lattice spacing values for AZ31 Mg alloy, Ni, and many phases were compared to standard values. However, the presence of solely elemental nickel and magnesium was confirmed, implying that the Ni particles were successfully reinforced into the matrix without reaction or the production of undesired phases as a result of the low processing temperature and exposure time. Several XRD measurements were made at different psi (ψ) tilts. By altering the tilt of the specimen within the diffractometer, measurements of planes at an angle ψ can be made and thus the strains along that direction can be calculated using

$\varepsilon = (\mathrm{d}\Psi - \mathrm{d}A = \pi r^2 \mathrm{o}) / \mathrm{do}$ ....

(2) from section 4.2.3

From values of Young's modulus, Poisson's ratio, d-spacing and slope of "d vs $\sin^2\Psi$" after scanning the friction stir welded sample for measuring residual stress using $\sin^2\Psi$ method, one can calculate stress using standard equation which is

$\sigma = \mathrm{E}/(1+v) \sin 2\Psi ((\mathrm{d}\Psi - \mathrm{do}) / \mathrm{do})$ ....

(4) from section 4.2.3

In Fig. 4.14(a), the inter-planar spacing, or 2-theta peak location, is measured and shown as a curve (b). The peak intensity increases with successive passes and slightly moves to the right, confirming the compressive nature of produced residual stress, as seen in Fig. 4.14(a). According to the figure shown in Fig. 4.14(b) using the sin2 ψ approach described in section 4.2.3, the residual stress in the as-received AZ31 Mg alloy was around -14 MPa, which rose with the number of passes until it reached -72 MPa. This processing approach introduces compressive stress to increase the service performance of magnesium alloys, which may improve fatigue and wear resistance [75].

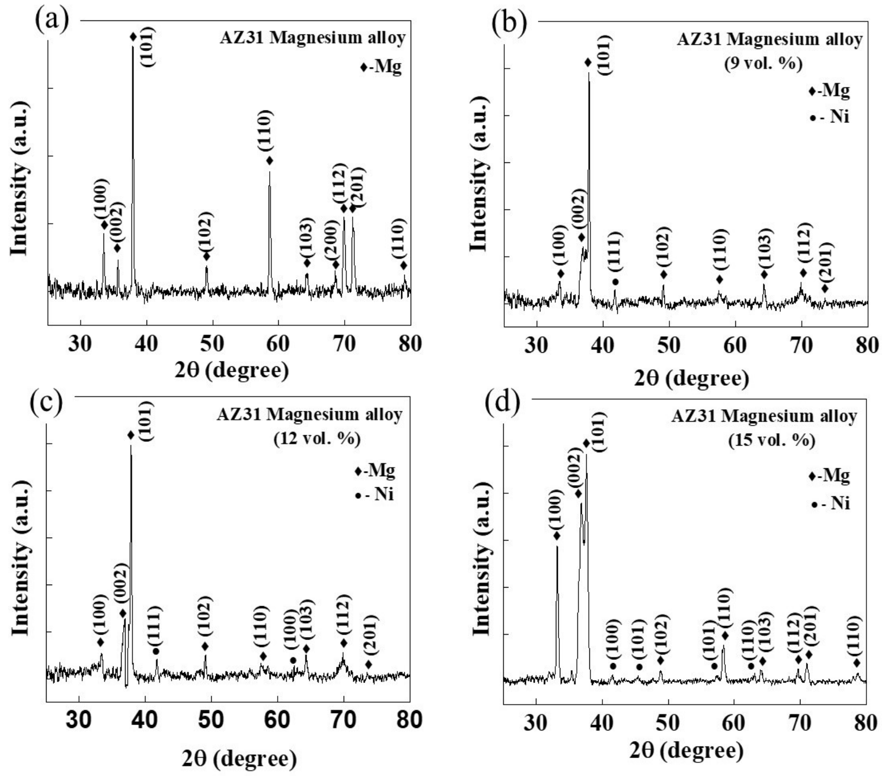

Fig. 4.13 XRD pattern for AZ31 Mg alloy and AZ31/Ni MMCs (a) AZ31 magnesium alloy, (b) AZ31/9%Ni, (c) AZ31/12%Ni and (d) AZ31/15%Ni

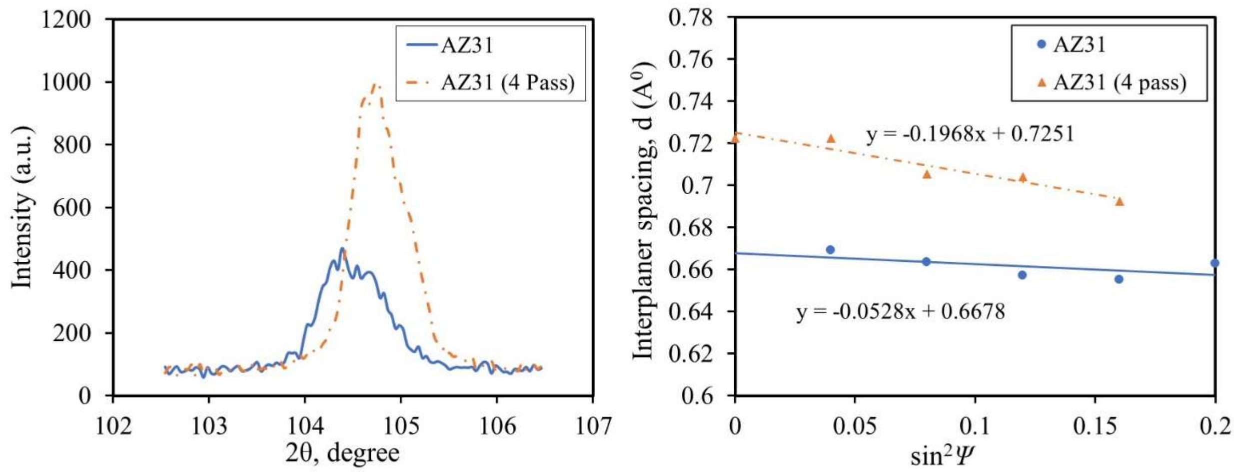

Fig. 4.14 (a) Comparison of peak position for AZ31 Mg alloy and AZ31 Mg alloy after multiple passes. (b) d vs $\sin^2\Psi$ plot for residual stress calculation.

4.3.3 Mechanical behavior of AZ31/Ni MMCs:

From the microhardness test results, there is a significant increment in the hardness of MMCs from 30 to 50% as that of the AZ31 magnesium alloy due to the addition of nickel reinforced particles can predominantly be credited to the presence of comparatively harder and stronger reinforcement phase and refine grain size which amplified obstruction to the localized deformation in the matrix during the indentation. Fig. 4.15(a) and (b) represents the Vickers hardness value of base material (AZ31) and MMCs at different volume fractions used in this study. The hardness results found in this current study are comparable to the findings described in previous studies [79]. From the figures, there is a change in hardness value due to a change in the location in the stir zone. In the case of 2 passes as shown in Fig. 4.15(a), the dispersion of particles is not proper or homogeneous which results in the formation of various zones with different hardness values. Segregation of particles takes place due to less heat generation and material flow during processing. But in case of 4 passes as shown in Fig. 4.15(b), there is a single zone (dispersed zone) present due to the homogeneous distribution of particles throughout the processed area which represents nearly about the same hardness values at all the locations in the stir zone. From the results, the figure shows as the number of passes and volume fraction of powder increases there is an improvement found in the hardness i.e., 55% as that of the AZ31 magnesium alloy.

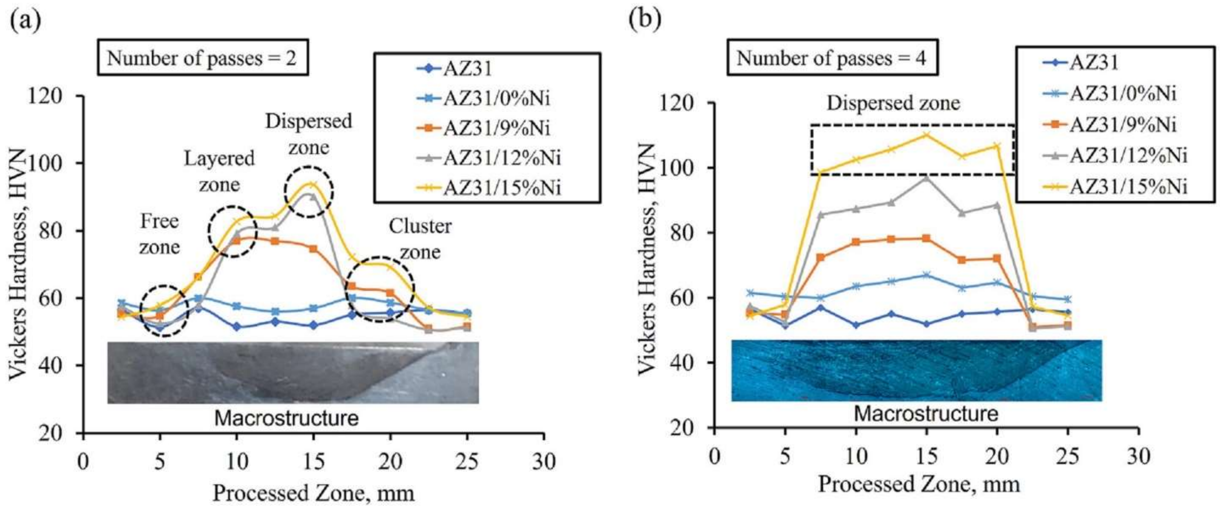

Fig. 4.15 Vickers hardness value of AZ31 magnesium alloy (base material) and AZ31/Ni MMCs in case of 2 and 4 number of passes for different volume fraction.

The stress-strain curve obtained during the tensile test of base material (AZ31) and AZ31/Ni MMCs with 2 and 4 number of passes for different volume fractions are shown in Fig. 4.16(a) and Fig. 4.16(b). The tensile test results for a different number of passes are summarized or compared as shown in Fig. 4.17(a) and 4.17(b). The effect of Ni particle combination into the base Mg alloy is obvious from these plots. From Fig. 4.16(a), it is observed that as compared to the base alloy, there is a significant reduction of UTS from 196 MPa (AZ31) to 150 MPa (AZ31/15%Ni) and % elongation from 10.2% (AZ31) to 5% (AZ31/15%Ni) with 2 number of passes. The percentage reduction in UTS value was found to be 23.4% which is due to the non-homogeneous distribution and coarser grains. From Fig. 4.16(b), it is confirmed that there is an enhancement in UTS from 196 MPa (AZ31) to 254 MPa (AZ31/15%Ni) but a significant reduction is observed in % elongation from 10.2% (AZ31) to 6.3% (AZ31/15%Ni) with 4 number of passes [79, 80]. The increment in the UTS value was observed to be 25% in comparison with the base alloy which is credited to the homogeneous distribution of reinforced particles into the matrix and refined microstructure as evidenced from Fig. 4.10. It is interesting to observe that the overall ductility of the metal-reinforced composite is superior compared to the ceramic reinforced MMCs. However, as the number of passes increases, there is a slight improvement in the % elongation from 5.2% (AZ31/15%Ni) with 2 passes to 6.3% (AZ31/15%Ni) with 4 passes. The Yield strength of the MMCs also increases due to the presence of harder reinforcement and grain refinement with homogeneous distribution which increases the number of obstacles to the dislocation motion. The presence of a high percentage of nickel particles was able to increase the dislocation density and create a barrier to the dislocation movement [81, 82]. However, plastic deformation led to an effective dislocation-nickel particle interaction in the beginning which caused effective strain hardening into the matrix and considerably improve the tensile strength.

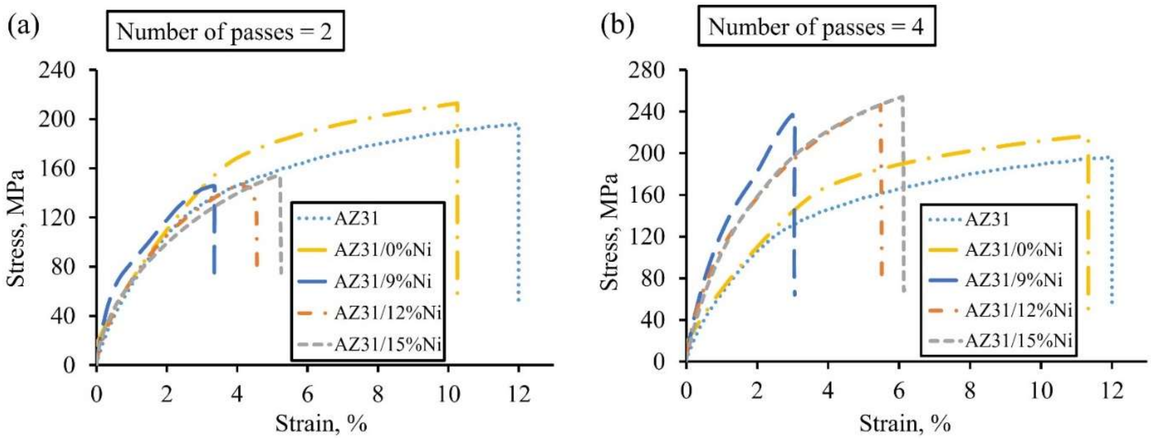

Fig. 4.16 The stress-strain curves were recorded during the tensile test of AZ31 magnesium alloy (base material) and AZ31/Ni MMCs in the case of 2 and 4 passes for different volume fractions.

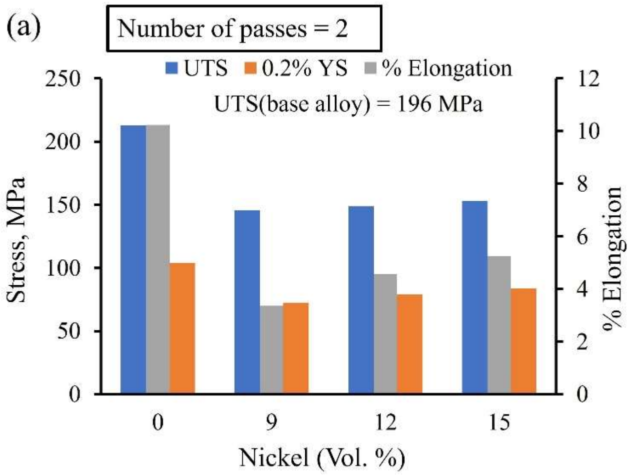

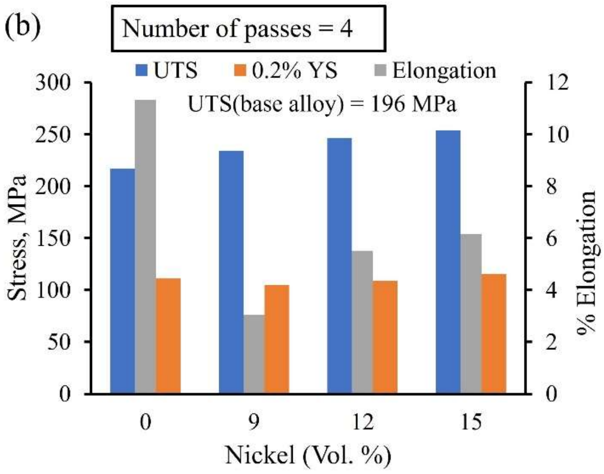

Fig. 4.17 Comparison of results obtained from stress-strain plots with 2 and 4 number of passes for different volume fractions.

4.3.4 Fracture behavior:

After the tensile test, the fracture surfaces of base Mg alloy and the composites (AZ31/Ni) at different volume fraction with 2 pass and 4 passes was observed using SEM to understand the failure mechanism. Fig. 4.18 represents the fracture surfaces of base Mg alloy and MMCs at different volume fractions with 2 passes. Fracture analysis was performed on the tensile fractured samples and the results revealed large size dimples in AZ31 magnesium alloy which confirmed the ductile mode of failure. The fractography of AZ31/0%Ni fractured specimens revealed relatively small size dimples and micro voids present as shown in Fig. 4.18(a). The intergranular particle cracking and debonding of Ni particles were observed in MMCs at volume fractions of 9%, 12%, and 15% Ni as represented in Fig. 4.18(b) and Fig. 4.18(c) and microcracks into the matrix shown in Fig. 4.18(d) were also observed in MMCs justifying a considerable reduction in the strength and ductility. Brittle features with the existence of particle cracking were also detected in the case of nickel reinforced composites. Fracture surfaces of MMCs revealed a ductile-brittle mode of failure which might be the reason for the reduction in UTS and ductility [73]. The fracture surfaces of base Mg alloy and MMCs at different volume fractions with 4 passes are shown in Fig. 4.19. The fracture surface in Fig. 4.19(a) revealed comparatively smaller dimples as observed in 2 passes which confirm the comparable ductility. The debonding of Ni particles without any cracks into the matrix was also observed in MMCs at a volume fraction of 9%, 12%, and 15% Ni as represented in Fig. 4.19(b), (c), and (d). Fracture surfaces of MMCs revealed a ductile mode of failure which justifying the considerable increase in UTS and marginal ductility [31]. SEM micrograph of AZ31/15%Ni MMC (4 passes) with point and map EDS is shown in Fig. 4.20. From EDS mapping, represents various alloying elements present in the MMC and confirmed Ni particle in the matrix. There was a significant grain refinement in the MMCs caused by dynamic recrystallization through mechanical stirring action of the FSP tool causing severe plastic strain which crushed the Ni particles into smaller size particles. Ni particles enhanced the tensile behavior and helped to attain considerable deformation before fracture. Brittle mode of failure was prevented by optimizing the process parameters.

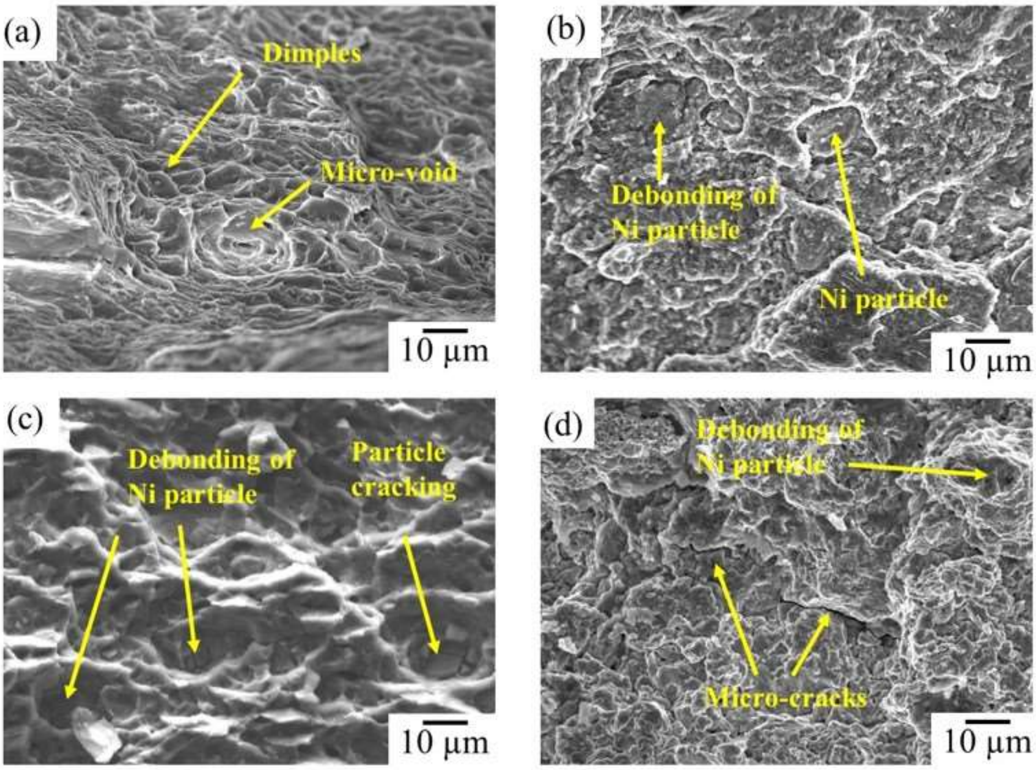

Fig. 4.18 Fractography of fractured samples after the tensile test using SEM in case of 2 pass. (a) AZ31/0%Ni (b) AZ31/9%Ni (c) AZ31/12%Ni (d)AZ31/15%Ni

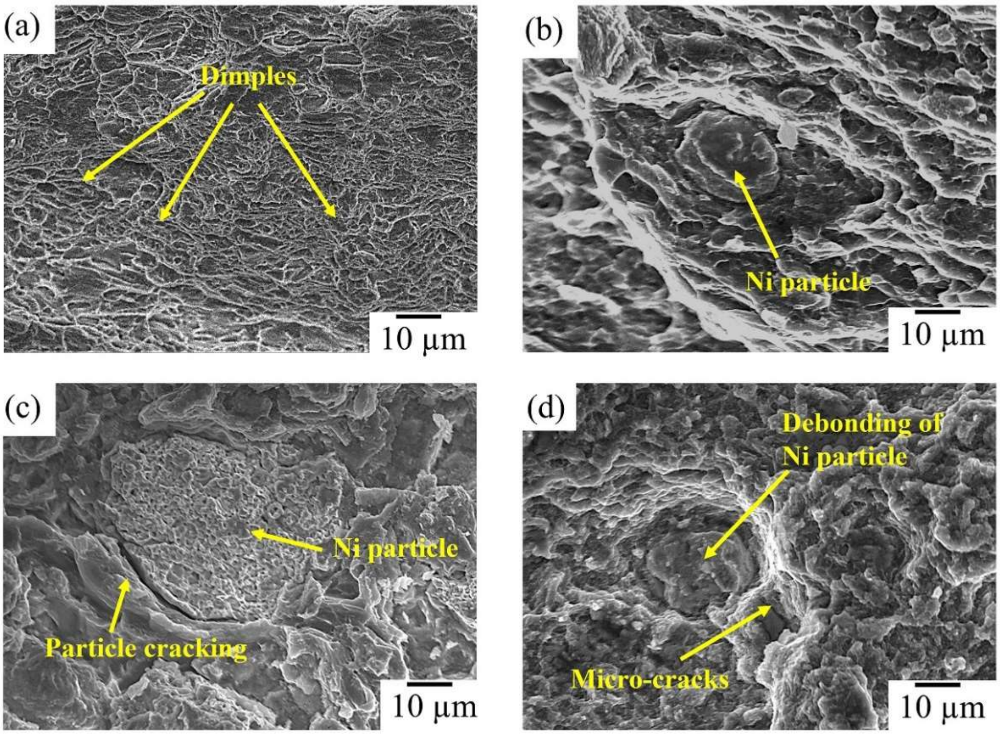

Fig. 4.19 Fractography of fractured samples after the tensile test using SEM in case of 4 pass. (a) AZ31/0%Ni (b) AZ31/9%Ni (c) AZ31/12%Ni (d)AZ31/15%Ni

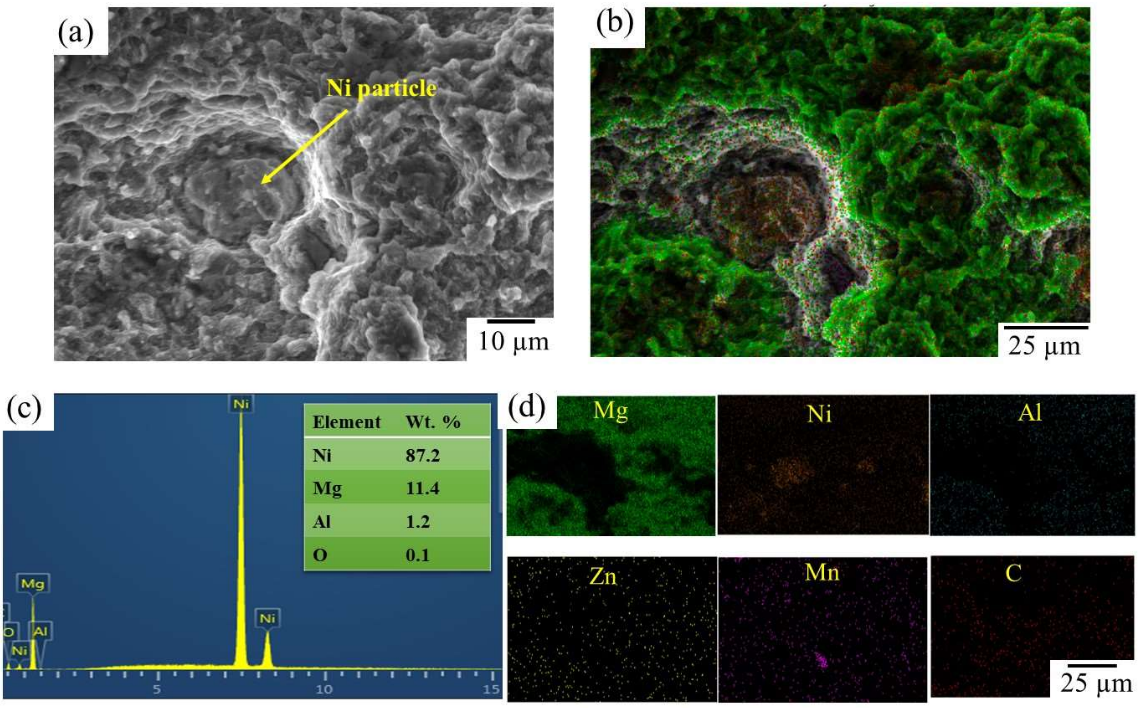

Fig. 4.20 (a) SEM micrograph of AZ31/15%Ni MMC. (b) EDS layered image during scanning. (c) Point EDS of AZ31/15%Ni MMC confirmed Ni particle. (d) EDS mapping represents various alloying elements present in the MMC.

As the number of passes impacts both the frictional heat and the action of mechanical stirring, which create residual stress, mechanical characteristics improve significantly as the volume fraction increases at multiple passes. Due to the homogenous dispersion of reinforced particles, FSP is one of the finest ways for forming MMCs. Multiple passes were used to get proper mixing of Ni particles in order to achieve a homogenous distribution. Frictional heat causes plasticization, which affects the size of the grains. Mechanical stirring, on the other hand, helps to distort the material, which affects particle mobility. FSP has provided a suitable particle distribution, which is beneficial for achieving improved characteristics. The presence of a significantly harder and stronger reinforcement phase, as well as tiny grain size, exacerbated the matrix's localised deformation during loading. The number of passes and nickel reinforcement were found to improve the characteristics of the AZ31 magnesium alloy in this research. The increased tensile strength is attributable to the combined effect of reinforcing particle dispersion in the magnesium matrix and grain refining. Grain refining was one of the most important strengthening mechanisms behind the increased tensile strength. The reinforcement particles are well-bonded and evenly distributed throughout the matrix, and the load is successfully transferred to them via the interface. The number of grain borders grows as the grain size decreases, resulting in the movement of dislocations stacked up at the grain boundary [82]. As a result, grain boundaries operate as a barrier to the dislocation's mobility in the grain refinement mechanism. As a result, the tensile strength of materials with refined grains rises when compared to those with coarser grain structures. However, the density of MMCs increases by approximately 13% when compared to the AZ31 alloy, while the strength increases by 25% with a small drop in ductility.

4.3.4 Fretting fatigue behavior of AZ31/Ni MMCs

The mechanical qualities of the composite made with several passes (4 pass) are better, which is why it was chosen for this experiment. The S-N curve in Fig. 4.21 represents the results of the fretting fatigue tests conducted in this investigation. The fatigue life has been shortened due to washer fretting with the specimen, as seen in the figure. In the instance of AZ31 magnesium alloy, the fatigue strength owing to fretting is reduced by more than 60% compared to the simple fatigue strength of the same alloy. According to the findings, the frictional stress along the contact boundary is significant due to the interaction of the washer (in a nut-bolt arrangement) with the specimen, causing severe surface damage and a decrease in fretting fatigue strength. Fig. 4.21(a) also represents the S-N curve for MMCs fabricated at various volume fraction of nickel particles. From the figure it is also observed that there is a significant improvement in the fatigue life of the AZ31 magnesium alloy due to the incorporation of nickel reinforced particles at multiple pass. The fretting fatigue life of the

MMCs increases as the volume fraction of nickel particle increases. By setting the run-out number of cycles to N = $2x10^6$, the apparent fatigue strength was calculated using the traditional staircase approach [78]. When N_f is $2x10^5$, the dependence of the stress amplitude on the number of cycles to failure, N_f, demonstrates a linear relationship. Due to the addition of nickel reinforced particles, the fretting fatigue life of the AZ31 magnesium alloy was increased from $8x10^5$ to$1.5x10^6$, which is approximately 2 times that of the AZ31 magnesium alloy. After the fatigue test, various broken samples for base alloy and MMCs at different volume fractions were shown in Fig. 4.21(b). The damage occurs beneath the washer, and the crack propagates from the washer's edge into the specimen, as shown in the diagram.

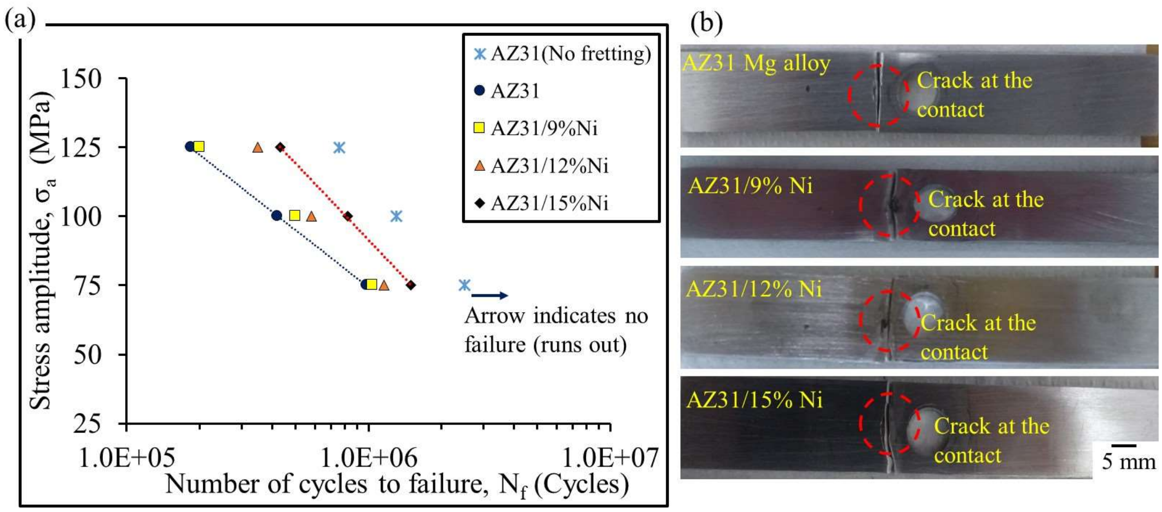

Fig. 4.21 (a) S-N curve for AZ31 Mg alloy and MMCs at different volume fraction. (b) Broken sample at different volume fraction after the test.

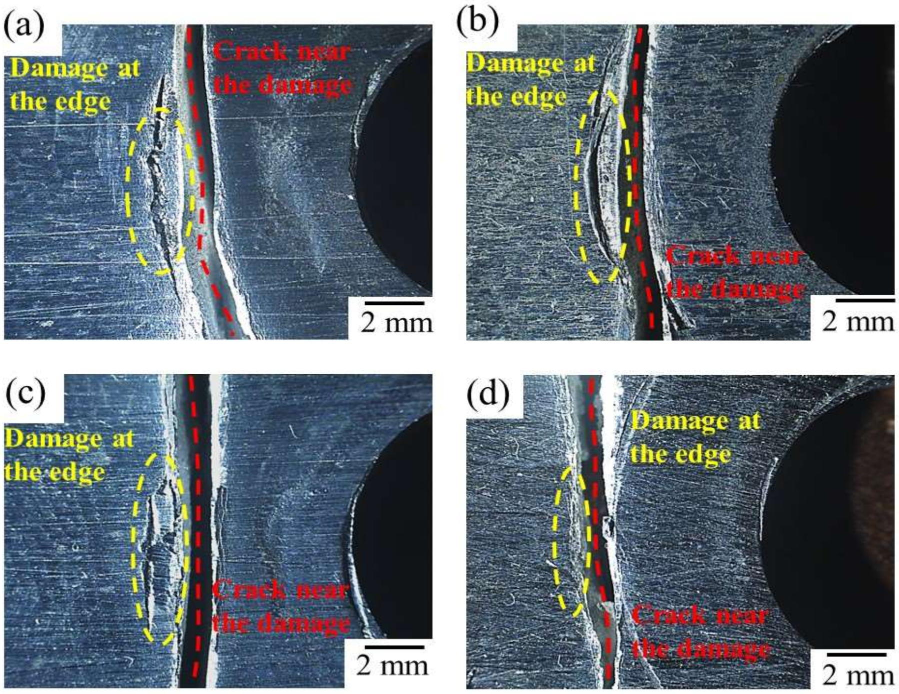

Fig. 4.22 Macroscopic images of the broken samples represents crack location and damage region under the contact.

The macroscopic images of the fractured samples, along with the position of the cracks, are shown in Fig. 4.22. The damage at the fretting location appears to decrease as the nickel volume percentage increases, as seen in the figures. The fracture that forms from the washer's outer edge during fretting damages the composite's surface, resulting in the production of microscopic cracks on the component's surface. These micro-cracks propagate and cause the component to fail due to the cyclic force required during fatigue testing.

The fracture surfaces of the AZ31 Mg alloy and the composites (AZ31/Ni) at different volume fractions were studied using SEM after the fretting fatigue test. Fig. 4.23(a), (b) and (c) represents the fracture surfaces of base Mg alloy at different magnification. The fracture surface image in Fig. 4.23(a) displayed crack initiation location with crack initiation and propagation. Fig. 4.23(b) and (c) represents the magnified fracture surface image at initiation region which shows flakes like structure and propagation region which represents rapid fracture. Fig. 4.23(d), (e) and (f) represents the fracture surfaces of AZ31/9%Ni MMC at different magnification. The fracture surface image in Fig. 4.23(d) displayed crack initiation and crack propagation region [80, 81]. Fig. 4.23(b) and (c) represents the magnified fracture surface image at different locations which shows particle cracking and the debonding of nickel particle. Fig. 4.23(g), (h) and (i) represents the fracture surfaces of AZ31/12%Ni MMC at different magnification. The fracture surface image in Fig. 4.23(g) displayed crack initiation and crack propagation region which confirmed that the crack initiate from the outer surface of the specimen. Fig. 4.23(h) and (i) represents the magnified fracture surface image at different locations which shows the breaking of nickel particles into the matrix with micro cracks. Fig. 4.23(j), (k) and (l) represents the fracture surfaces of AZ31/15%Ni MMC at different magnification. The fracture surface image in Fig. 4.23(j) displayed crack initiation and crack propagation region. Fig. 4.23(k) and (l) represents the magnified fracture surface image at different locations which shows high density of nickel particles into the matrix with micro cracks. The various element present in the composite was confirmed with the EDS mapping. Fig. 4.24 represents the EDS elemental mapping at different volume fraction after the fatigue test which confirmed the presence of different elements such Ni, Mg, Al and Zn.

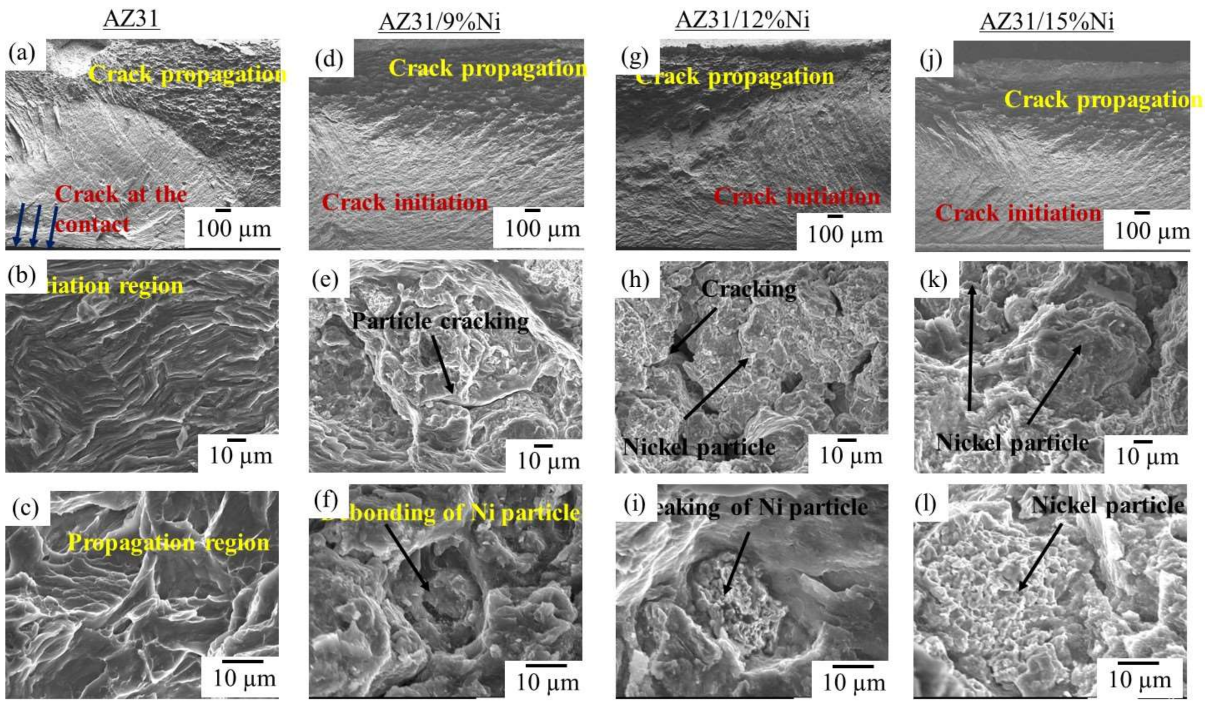

Fig. 4.23 The fracture surfaces of the AZ31 Mg alloy and the composites (AZ31/Ni) at different volume fractions using SEM after the fretting fatigue test. (a), (b) and (c) represents the fracture surfaces of AZ31 Mg alloy. (d), (e) and (f) represents AZ31/9%Ni MMC. (g), (h) and (i) represents AZ31/12%Ni MMC. (j), (k) and (l) represents AZ31/15%Ni MMC.

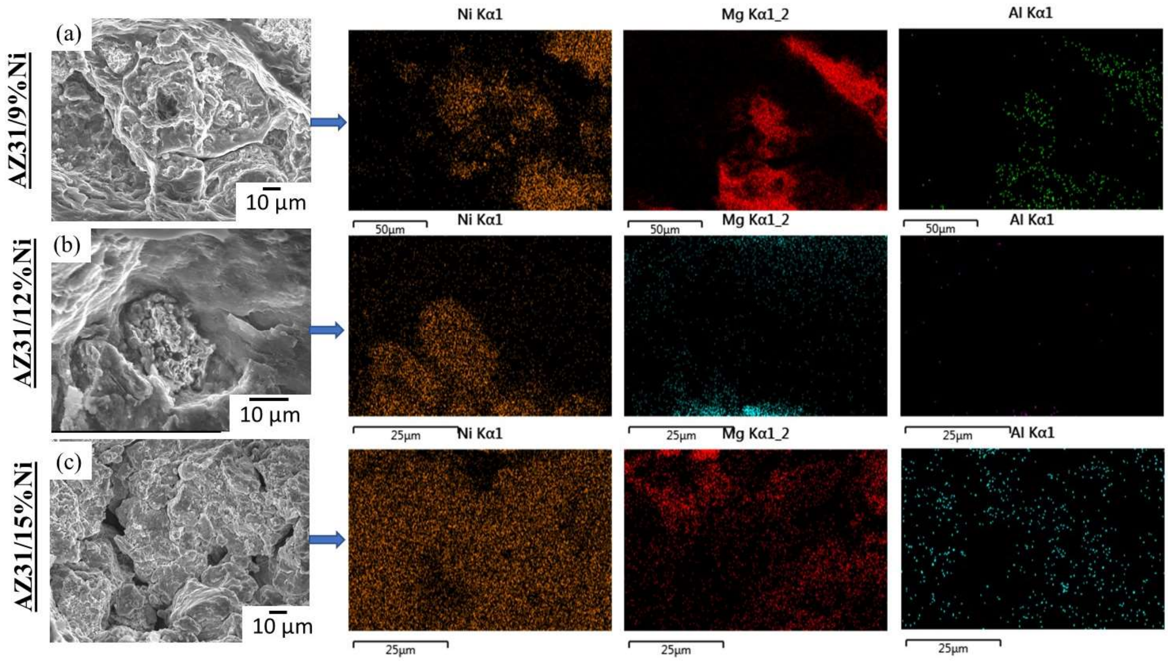

Fig. 4.24 The fracture surfaces of the AZ31/Ni MMC at different volume fractions with EDS. (a) AZ31/9%Ni MMC (b) AZ31/12%Ni MMC and (c) AZ31/15%Ni MMC.

The number of passes and the addition of nickel reinforcement to the AZ31 magnesium alloy were shown to improve its characteristics in this investigation. The dispersion of the reinforcing particles in the magnesium matrix, as well as grain refining, contribute to the increased tensile strength. The reinforcement particles are well-bonded and distributed evenly throughout the matrix, and the load is effectively transferred to them via the interface. The number of grain borders grows as a result of grain refining, and the movement of dislocations piled up at the grain boundary increases as a result [82, 83]. Because the number of passes impacts both the frictional heat and the action of mechanical stirring, which causes residual stress into the matrix, there is a significant improvement in mechanical characteristics and fretting fatigue life as the volume fraction increases at many passes. Because of the homogenous dispersion of reinforced particles, FSP is one of the best ways for forming MMCs. Multiple passes were used to change the volume percent of Ni particles in order to achieve a uniform distribution. Plasticization occurs as a result of the frictional heat changing the grain size. Mechanical stirring, on the other hand, aids in the deformation of the material, which affects particle mobility. FSP has provided a suitable particle distribution, which is beneficial for achieving improved characteristics. As the number of passes grows, the inter-particle spacing decreases, confirming the significant compressive residual stress and highlighting the homogenous distribution with grain refining. The presence of a significantly harder and stronger reinforcement phase, as well as tiny grain size, exacerbated the matrix's localized deformation during loading. The fretting fatigue life can be enhanced by producing MMCs using friction stir processing, according to this research.

4.4 Summary

Magnesium metal matrix composites were successfully produced using AZ31 magnesium alloy as matrix and Ni powder as reinforced particles using friction stir processing (FSP). Multiple passes were used, and the volume fraction was varied from 0 to 15 vol.% (0, 9, 12, and 15). The following conclusions were made from this study:

1. Homogeneous distribution of particles was observed in the MMCs with 4 passes at a 15% volume fraction of Ni particles. There was an appropriate bonding between the Ni reinforced particles and the magnesium alloy matrix at the interface without any reaction or formation of the intermetallic product.
2. The variation in volume fraction and number of passes caused different microstructural evolution within the processed zone. In the case of 2 passes, they were grouped into four different zones such as free zone, dispersed zone, layered zone, and cluster zone but in the case of 4 passes, there were no different zones formed except dispersed zone which might be due to proper dispersion of particles at a high number of passes.
3. From stress-strain results, there was a reduction of UTS from 196 MPa to 150 MPa and % elongation from 10.2% to 5% with 2 number of passes. However, there was an enhancement in UTS from 196 MPa to 254 MPa but a significant reduction in % elongation from 10.2% to 6.3% with 4 number of passes. In the case of 2 passes, the tensile behavior was adversely affected due to the poor distribution of particles. The increase in the number of passes (4 passes) and volume fraction of reinforcement improved the tensile behavior due to homogeneous distribution and grain refinement caused by frictional heat and mechanical stirring action.
4. The integration of Ni particles using FSP improves the hardness (55%) and ultimate tensile strength (25%) of magnesium alloy, according to the results. However, the ductility of the MMCs was unfavorably affected (reduced by 40%), but significantly better as compared to other reinforced particles used in prior studies. The MMC produced at 15% volume

fraction with 4 number of passes showed the highest tensile strength and hardness.

5. From the fatigue test results, the fatigue life was reduced due to fretting of washer with the specimen. The S-N curve for MMCs at various volume fraction of nickel particles obtained confirms there is a significant improvement in the fatigue life of the AZ31 magnesium alloy which is 2 times more due to the incorporation of nickel reinforced particles with induced residual stress which causes less surface damage and results in the increase in the fretting fatigue strength.
6. In the grain refinement, the grains size reduces because of this the number of grain boundaries increases, as result the movement of the dislocation piled up at the grain boundary. Hence, in the grain refinement mechanism, grain boundaries act as an obstacle for the motion of the dislocation. As result, the tensile strength increases in materials with refined grains as compared to the coarser grain structure materials. The fracture surface characterization of AZ31/Ni MMCs revealed that particle breakage is the primary cause of MMC failure under tensile loading, which explains why the base Mg alloy's fracture behavior changed from ductile to ductile-brittle, and how proper nickel particle bonding with the matrix improves the material's fatigue strength.

Chapter 5

Conclusions and Future Scope

5.1 Conclusions

To improve the fretting fatigue life of Titanium alloy, Ni-based superalloys and Magnesium alloy for aerospace and automobile applications, the studies related to fatigue strength enhancement through different contact pad geometry and fabrication of metal matrix composite through FSP technique have been successfully carried out in the current research work. The feasibility of FEA model has been investigated by optimizing the mesh size with various parameters and corelate experimental results with the FEA end results. Moreover, the effect of contact pad geometry, stress distribution along the contact pad, crack initiation and propagation, mechanical properties and fretting fatigue behavior have been examined in detail.

The overall results obtained from the current research work can be concluded as follows:

- It is confirmed that the geometry at the fretting contact plays a dominant role in the fretting fatigue behaviour of the component and by introducing grooves at the contact interface in fretting fatigue, fretting fatigue life can be significantly enhanced by reducing the stress concentration at the contact.
- For the fretting fatigue test with slit + porous pad, the tangential stress generated were less, surface damages were less compared to slit pad and flat pad. For both the Ni based super alloy used in the present study, the fretting fatigue lives were highest for fretting fatigue test with slit + porous pad. So, it is confirmed that by introducing porous material at the contact interface in fretting fatigue, the fretting fatigue lives can be significantly enhanced.

- From the FEA analysis results, it is confirmed that the tangential stress is highest for flat pad, followed by slit pad, followed by slit + porous pad. The slip + porous pad showed a lowest tangential stress value. For flat pad the tangential stress was highest near the external edge of contact. For slit pad the tangential stress was highest near the edge of first slit. For slit +porous pad the tangential stress was highest near the external edge of contact. The similar trends are observed for both Inconel 718 and CMSX-4 alloys. The location of maximum tangential stress identified using FEA matches well with the fracture location in the fretting fatigue tested specimens for all the types of contact pad in both the alloys.
- After fabricating MMCs, there was an improvement in UTS from 196 MPa to 254 MPa i.e., 25% but a significant reduction in percentage elongation from 10.2% to 6.3% i.e., 37% with 4 number of passes which is better as compared to other reinforced particles used in prior studies. The increase in the number of passes (4 passes) and volume fraction of reinforcement improved the tensile behavior due to homogeneous distribution and grain refinement caused by frictional heat and mechanical stirring action.
- The S-N curve for MMCs at various volume fraction of nickel particles obtained confirms there is a significant improvement in the fatigue life of the AZ31 magnesium alloy due to the incorporation of nickel reinforced particles with induced residual stress which causes less surface damage and results in the increase in the fretting fatigue strength of the component. It is confirmed that by introducing reinforced particles into the matrix through FSP, the fretting fatigue lives can be significantly enhanced.

6.2 Scope for future work

- From this study, it is confirmed that by introducing porous material at the contact interface in fretting fatigue, the fretting fatigue lives can be significantly enhanced. However, Titanium alloys and Ni-based superalloys most used in high temperature applications. So, it is very important to study the effect of fretting on fatigue behavior at high temperature conditions too.
- Further investigation can be done at different temperature by using proposed FEA model in the current study to understand the stress distribution along the contact pad at high temperature applications.
- From this study, it is confirmed that by fabricating metal matrix composite through FSP, the fretting fatigue strength can be improved. Therefore, different combination of powders can be used, or hybrid composites can be manufactured through FSP to improve the fretting fatigue life of the component in further studies.

References

[1] Waterhouse. R. B, Fretting, Treatise on Materials Science and Technology 13 (1979) 259-286.

[2] Hills. D. A, Nowell. D and O'Connor. J. J, On the Mechanics of Fretting Fatigue, Wear 125 (1988) 129-146.

[3] Waterhouse R. B, Fretting wear, wear 100 (1984) 107-118.

[4] Mutoh. Y, Mechanisms of fretting fatigue, JSME International Journal Series A 38 (1995) 405-415.

[5] Waterhouse. R. B, Fretting fatigue, International Materials Reviews 37 (1992) 77-98.

[6] Waterhouse. R. B, Fretting at high temperature, Tribology International 14 (1981) 203-207.

[7] Waterhouse. R. B and Lamb. M, Fretting Corrosion of Orthopedic Implant Materials by Bone Cement, wear 60 (1980) 357-368.

[8] Zheng. J. F and Luo. J, Fretting wear behaviors of a railway axle steel, Tribology International 43 (2010) 906-911.

[9] Jayaprakash. M, Mutoh. Y and Yoshii. K, Fretting fatigue behavior and life prediction of automotive steel bolted joint, Materials and Design 32 (2011) 3911-3919.

[10] Wang. D. G and Abdel Wahab. M, Finite Element Analysis of Fretting Fatigue of Fretted Wires, International Journal of Fracture Fatigue and Wear 3 (2015) 135-142.

[11] Daisuke Takazaki, Masanobu Kubota, Effect of Contact Pressure on Fretting Fatigue Failure of Oil-Well Pipe Material, International Journal of Fatigue 101 (2017) 67-74.

[12] Chao. J, Fretting-fatigue induced failure of a connecting rod, Engineering Failure Analysis 96 (2019) 186-201.

[13] Rahul Garg, Sudhakar Rao. G, Vikash Bhartia, Vakil Singh, Fretting Fatigue and Wear Behaviour of Timetal 834, Procedia Engineering 55 (2013) 661 – 665.

[14] Kartik Prasad, Abhaya. S, Amarendra. G, Vikas Kumar, Rajulapati. K. V, Bhanu Sankara Rao. K, Fatigue crack growth behavior of a near a titanium alloy

Timetal 834 at 450 ºC and 600 ºC, Engineering Fracture Mechanics 102 (2013) 194-206.
[15] Jayaprakash. M, Yoshiharu Mutoh, Effect of contact pad rigidity on fretting fatigue behavior of NiCrMoV turbine steel, International Journal of Fatigue 32 (2010) 1788-1794.
[16] Yoshiharu Mutoh, Jayaprakash. M, Tangential stress range–compressive stress range diagram for fretting fatigue design curve, Tribology International 44 (2011) 1394-1399.
[17] Jayaprakash. M, Anchalee. S, Otsuka. Y, Mutoh. Y, TSR–CSR diagram for 304 stainless steel, International Journal of Fatigue 54 (2013) 99-105.
[18] Jayaprakash Murugesan, Yoshiharu Mutoh, Fretting fatigue strength prediction of dovetail joint and bolted joint by using the generalized tangential stress range–compressive stress range diagram, Tribology International 76 (2014) 116-121.
[19] Noraphaiphipaksa. N, Kanchanomai. C, Mutoh. Y, Numerical and experimental investigations on fretting fatigue: Relative slip, crack path, and fatigue life, Engineering Fracture Mechanics 112 (2013) 58-71.
[20] Noraphaiphipaksa. N, Manonukul. A, Kanchanomai. C, Mutoh. Y, Fretting fatigue life prediction of 316L stainless steel based on elastic–plastic fracture mechanics approach, Tribology International 78 (2014) 84-93.
[21] Noraphaiphipaksa. N, Manonukul. A, Kanchanomai. C, Mutoh. Y, Fretting-contact-induced crack opening/closure behavior in fretting fatigue, International Journal of Fatigue 88 (2016) 185-196.
[22] Walvekar. A. A, Leonard. B. D, Sadeghi. F, Jalalahmadi. B, Bolander. N, An experimental study and fatigue damage model for fretting fatigue, Tribology International 79 (2014) 183-196.
[23] Jayaprakash. M, Komatsu. D, Okazaki. M, Miyashita. Y, Otsuka. Y, Mutoh. Y, High Temperature Fretting Fatigue Behavior of IMI 834 Titanium Alloy, Trans Indian Inst Met. 69(2) (2016) 439–444.
[24] Zobaer Shah, Quazi Md, Md Arefin Kowser, and Mohammad Asaduzzaman Chowdhury, Investigation of the combined effect of notch and fretting on bending fatigue, Theoretical and Applied Mechanics 47 (2020) 113-122.

[25] Xin Li, Zhengxing Zuo, Wenjie Qin, A fretting related damage parameter for fretting fatigue life prediction, International Journal of Fatigue 73 (2015) 110-118.
[26] Nadeem Ali Bhatti, Abdel Wahab. M, Fretting fatigue crack nucleation: A review, Tribology International 121 (2018) 121-138.
[27] Nadeem Ali Bhatti, K. Pereira, Magd Abdel Wahab, Effect of stress gradient and quadrant averaging on fretting fatigue crack initiation angle and life, Tribology International 131 (2019) 212-221.
[28] Diego Infante-Gracia, Eugenio Giner, Henar Miguelez, Magd Abdel Wahab, Numerical analysis of the influence of micro-voids on fretting fatigue crack initiation lifetime, Tribology International 135 (2019) 121-129.
[29] Guillaume Rousseau, Claudio Montebello, Yoann Guilhem, Sylvie Pommier, A novel approach to model fretting-fatigue in multi-axial and non-proportional loading conditions, International Journal of Fatigue 126 (2019) 79-89.
[30] Findley. W. N, A theory for the effect of mean stress on the fatigue of metals under combined torsion and axial load or bending, Journal of Engineering for Industry 81 (1959) 301-305.
[31] Szolwinski M P, Thomas N. Farris, Mechanics of fretting fatigue crack formation, Wear 198 (1996) 93-107.
[32] Pereira. K, Bhatti. N, Abdel Wahab. M, Prediction of fretting fatigue crack initiation location and direction using cohesive zone model, Tribology International 127 (2018) 245-254.
[33] Sumit Khot, Utpal Borah, Finite Element Analysis of Pin-on-Disc Tribology Test, International Journal of Science and Research 4 (2015) 1475-1481.
[34] Mahesh B Davanageri, Narendranath. S, Ravikiran Kadoli, Finite Element Wear Behaviour Modeling of Super duplex stainless steel AISI 2507 Using Ansys, Materials Science and Engineering 376 (2018) 1-13.
[35] John M. Thompson, Mary Kathryn Thompson, A Proposal for the Calculation of Wear, Mechanical Engineering Dept, MIT, International ANSYS Users Conference & Exhibition (2006).
[36] Archard.J.F and Hirst.W, The Wear of Metals under non-lubricated Conditions, Mathematical and Physical Sciences 236 (1956) 397-410.
[37] Shah, Quazi Md Zobaer, Md Arefin Kowser, and Mohammad Asaduzzaman

Chowdhury, Investigation on the Fretting Fatigue Failure Mechanism of Heat-Treated Al 6061-T6, Acta Technica Corviniensis-Bulletin of Engineering 12 (2019) 119-121.
[38] Shah, Quazi Md Zobaer, Mohammad Asaduzzaman Chowdhury, and Md Arefin Kowser. "Failure mechanism of polytetrafluoroethylene under friction fatigue." Journal of Failure Analysis and Prevention 19 (2019) 245-249.
[39] Shah, Quazi Md Zobaer, Md Asaduzzaman Chowdhury, and Md Arefin Kowser, On the diversity in design for different bending fretting fatigue mechanism, SN Applied Sciences 1(9) (2019)1-12.
[40] Chowdhury, Mohammad Asaduzzaman, Md Arefin Kowser, Quazi Md Zobaer Shah, and Suman Das, Characteristics and damage mechanisms of bending fretting fatigue of materials, International Journal of Damage Mechanics 27(4) (2018) 453-487.
[41] I. Llavori, A. Zabala, A coupled crack initiation and propagation numerical procedure for combined fretting wear and fretting fatigue lifetime assessment, Theoretical and Applied Fracture Mechanics 101 (2019) 294–305.
[42] K. Pereira, T. Yue, M. Abdel Wahab, Multiscale analysis of the effect of roughness on fretting wear, Tribology International 110 (2017) 222-231.
[43] L. Bohórquez, J. Vázquez, On the prediction of the crack initiation path in fretting fatigue, Theoretical and Applied Fracture Mechanics 99 (2019) 140-146.

[44] Tong Guo, Experimental study on fretting-fatigue of bridge cable wires, International Journal of Fatigue 131 (2020) 105321.
[45] Steffen Loen Sunde, Predicting fretting fatigue in engineering design, International Journal of Fatigue 117 (2018) 314-326.
[46] R.A. Cardoso, Wear numerical assessment for partial slip fretting fatigue conditions, Tribology International 136 (2019) 508-523.
[47] Aravind Vadiraj, M. Kamaraj, Effect of surface treatments on fretting fatigue damage of biomedical titanium alloys, Tribology International 40 (2007) 82–88.
[48] Kang Li, Xue-song Fu, A mechanism study on characteristic curve of residual stress field in Ti–6Al–4V induced by wet peening treatment, Materials and Design 86 (2015) 761-764.

[49] Qi Yang, Investigation of shot peening combined with plasma sprayed CuNiIn coating on the fretting fatigue behavior of Ti-6Al-4V dovetail joint specimens, Surface and Coatings Technology 358 (2019) 833-842.
[50] JSME Standard method of fretting fatigue testing, JSME S 015-2002. The Japan Society of Mechanical Engineers (2002).
[51] V. Sabelkin and S. Mall, Relative Slip-on Contact Surface under Partial Slip Fretting Fatigue Condition, Strain 42 (2006) 11–20.
[52] D.S. Mehta, S.H. Masood, W.Q. Song, Investigation of wear properties of magnesium and aluminum alloys for automotive applications, Journal of Materials Processing Technology 155 (2004) 1526–1531.
[53] B.R. Powell, P.E. Krajewski and A.A. Luo, Magnesium alloys for lightweight powertrains and automotive structures, Chapter 4, Materials, Design and Manufacturing for Lightweight Vehicles (2021) 125-186.
[54] al., 20th century uninterrupted growth in friction stir processing of lightweight composites and alloys, Materials chemistry and physics 266 (2021) 124572.
[55] S.F. Hassan and M. Gupta, Development of a novel magnesium/ nickel composite with improved mechanical properties, Journal of Alloys and Compounds 335 (2002) L10–L15.
[56] I. Bhiftime, Effect of wt.% SiCp and TiB on the mechanical properties in SiCp/AZ81A magnesium matrix composite by the method semi-solid stir casting, American Institute of Physics 1788 (2017) 030040.
[57] Li Huang, John Bonnen, John Lasecki, Haiding Guo, Xuming Su, Fatigue and fretting of mixed metal self-piercing riveted joint, International Journal of Fatigue 83 (2016) 230-239.

[58] Xiaofei Lei, Tianmo Liu, Microstructure and Mechanical Properties of Magnesium Alloy AZ31 Processed by Compound Channel Extrusion, Materials Transactions 52 (2011) 1082-1087.
[59] Dinaharan, S.C. Vettivel, M. Balakrishnan, E.T. Akinlabi, Influence of processing route on microstructure and wear resistance of fly ash reinforced AZ31 magnesium matrix composites, Journal of Magnesium and Alloys 7 (2019) 155-

165.
[60] Taito Hosakaa, Shoichiro Yoshihara, Influence of Grain Refinement and Residual Stress on Corrosion Behavior of AZ31 Magnesium Alloy Processed by ECAP in RPMI-1640 Medium, Procedia Engineering 184 (2017) 432 – 441.
[61] Asadi, G. Faraji, M.K. Besharati, Producing of AZ91/SiC composite by friction stir processing (FSP), Int. J. Adv. Manuf. Technol. 51 (2010) 247–260.
[62] Balakrishnan, I. Dinaharan, R. Palanivel, R. Sivaprakasam, Synthesize of AZ31/ TiC magnesium matrix composites using friction stir processing, Journal of Magnesium and Alloys 3 (2015) 76–78.
[63] Z.Y. Ma, Friction Stir Processing Technology: A Review, Metallurgical and Materials Transactions A 39 (2008) 642-658.
[64] R.S. Mishra, Sumit Jain, Friction stir processing of magnesium alloys used in automobile and aerospace applications, International Journal of Research in Engineering and Innovation 2(3) (2018) 241-248.
[65] Farzad Khodabakhshi and Adrian P. Gerlich, On the correlation between indentation hardness and tensile strength in friction stir processed materials, Materials Science & Engineering A 789 (2020) 139682.
[66] Isaac Dinaharan, and Shuai Zhang, Development of titanium particulate reinforced AZ31 magnesium matrix composites via friction stir processing, Journal of Alloys and Compounds 820 (2020) 153071.
[67] Isaac Dinaharan, and Shuai Zhang, Titanium particulate reinforced AZ31 magnesium matrix composites with improved ductility prepared using friction stir processing, Materials Science & Engineering A 772 (2020) 138793.
[68] Ho-Kyung Kim, Young-In Lee, and Chin-Sung Chung, Fatigue properties of a fine-grained magnesium alloy produced by equal channel angular pressing, Scripta Materialia 52 (2005) 473–477.
[69] Mariama, M. Afendia, M.S. Abdul Majida, M.J.M. Ridzuana, A.G. Gibson, Tensile and fatigue properties of single lap joints of aluminium alloy/glass fibre reinforced composites fabricated with different joining methods, Composites Structures 200 (2018) 647-658.

[70] F. Hassan, Effect of microstructure on the hydrogenation behavior of AZ61 magnesium alloy with silicon carbide and nickel additives, processed by equal channel angular pressing, International Journal of Hydrogen Energy 46 (2021) 4211-4221.
[71] Loreleï Commina, Myriam Dumont, Influence of the microstructural changes and induced residual stresses on tensile properties of wrought magnesium alloy friction stir welds, Materials Science and Engineering A 551 (2012) 288– 292.
[72] Zhichao M, Hongwei Zhao, Xiaoli Hu, Hongbing Cheng, Shuai Lu, Lin Zhang, Influences of tensile pre-strain and bending pre-deflection on bending and tensile behaviors of an extruded AZ31B magnesium alloy, Materials and Design 64 (2014) 566-572.
[73] Hai Zhi Ye, Xing Yang Liu, Review of Recent Studies In Magnesium Matrix Composites, Journal Of Materials Science 39 (2004) 6153 – 6171.
[74] Pedram Zamani, Abdolrahman Jaamialahmadi, Lucas F.M. da Silva, The influence of GNP and nano-silica additives on fatigue life and crack initiation phase of Al-GFRP bonded lap joints subjected to four-point bending, Composites Part B 207 (2021) 108589.
[75] Xiaomin Yuan, Jin Zhang, Research progress of residual stress determination in magnesium alloys, Journal of Magnesium and Alloys 6 (2018) 238–244.
[76] Dengfeng Wang, Wenchao Xu, Fatigue failure analysis and multi-objective optimisation for the hybrid (bolted/bonded) connection of magnesium–aluminium alloy assembled wheel, Engineering Failure Analysis 112 (2020) 104530.
[77] Abdul Kareem Abdul Jawwad, Nabeel ALShabatat, Mofid Mahdi, The effects of joint design, bolting procedure and load eccentricity on fatigue failure characteristics of high-strength steel bolts, Engineering Failure Analysis 122 (2021) 105279.
[78] Zeqing Xu, Hongxia Zhang, Zhifeng Yan, Fei Liu, Peter. K. Liaw, Wenxian Wang, Three-point-bending fatigue behavior of AZ31B magnesium alloy based on infrared thermography technology, International Journal of Fatigue 95 (2017) 156-167.
[79] M. Mariama, M. Afendia, M.S. Abdul Majida, M.J.M. Ridzuana, A.G. Gibson, Tensile and fatigue properties of single lap joints of aluminium

alloy/glass fibre reinforced composites fabricated with different joining methods, Composite Structures 200 (2018) 647-658.
[80] X. Song, P. Bayati, Fracture of magnesium matrix nanocomposites- A review, International Journal of Lightweight Materials and Manufacture 4 (2021) 67-98.
[81] Pedram Zamani, Abdolrahman Jaamialahmadi, Lucas F.M. da Silva, The influence of GNP and nano-silica additives on fatigue life and crack initiation phase of Al-GFRP bonded lap joints subjected to four-point bending, Composites Part B 207 (2021) 108589.

[82] Y. Wang, Q. Yan, Microstructure and strengthening mechanism of grain boundary strengthened W-ZrB2 alloy, J. Mater. Res. Technol. 9 (2020) 4007–4015.
[83] H. Hoche, H. Scheerer, Development of a plasma surface treatment for magnesium alloys to ensure sufficient wear and corrosion resistance, Surface, and Coatings Technology 174 (2003) 1018–1023.
[84] Ashish Kumar Srivastava, 20th century uninterrupted growth in friction stir processing of lightweight composites and alloys, Materials chemistry and physics 266 (2021) 124572.
[85] A. Nirala, S. Soren, Study of fabrication and mechanical characterization of magnesium metal matrix composites, Materials Science and Engineering 1149 (2021) 012006.
[86] Yong Liu, Bin Jin, Wear behavior of nanocrystalline structured magnesium alloy induced by surface mechanical attrition treatment, Surface & Coatings Technology 261 (2015) 219–226.
[87] M. Yue, A. H. Wang, and H. C. Man, Improvement in the corrosion resistance of magnesium ZK60/SiC composite by excimer laser surface treatment, Scripta Materials 38 (1998) 191-198.
[88] D. Lu, Y. Jiang, R. Zhou, Wear performance of nano-Al2O3 particles and CNTs reinforced magnesium matrix composites by friction stir processing, Wear 305 (2013) 286–290.
[89] B. Ratna Sunil, T.S. Sampath Kumar, U. Chakkingal, V. Nandakumar, M.

Doble, Friction stir processing of magnesium–nanohydroxyapatite composites with controlled in vitro degradation behavior, Mater. Sci. Eng. C 39 (2014) 315–324.
[90] M. Navazani, K. Dehghani, Fabrication of Mg-ZrO2 surface layer composites by friction stir processing, J. Mater. Process. Technol. 229 (2016) 439–449.
[91] D. Ahmadkhaniha, M. Heydarzadeh Sohi, A. Salehi, R. Tahavvori, Formations of AZ91/Al2O3 nano-composite layer by friction stir processing, Journal of Magnesium and Alloys 4 (2016) 314–318.
[92] W.L.E. Wong, M. Gupta, Development of Mg/Cu nanocomposites using microwave-assisted rapid sintering, Compos Sci Technol 67 (2007) 1541–1552.
[93] S.F. Hassan, M. Gupta, Development of ductile magnesium composite materials using titanium as reinforcement, J Alloys Compd. 345 (2002) 246–251.
[94] S.Fida Hassan, O.O. Nasirudeen, Magnesium-nickel composite: Preparation, microstructure and mechanical properties, Journal of Alloys and Compounds 646 (2015) 333-338.

[95] J. Babu, M. Anjaiah, Anoop Mathew, Experimental studies on friction stir processing of AZ31 magnesium alloy, Materials Today: Proceedings 5 (2018) 4515-4522.
[96] D. Khayyamin, A. Mostafapour, R. Keshmiri, The effect of process parameters on microstructural characteristics of AZ91/SiO2 composite fabricated by FSP, Mater. Sci. Eng. A 559 (2013) 217–221.
[97] J Shen, M. F. Zhang, and W. F. Ying, Processing, microstructure, and mechanical properties of bimodal size SiCp reinforced AZ31B magnesium matrix composites, Journal of Magnesium and Alloys 3 (2015) 162-167.
[98] Luo, Processing, Microstructure, and Mechanical behavior of cast magnesium metal matrix composites, Metallurgical and Materials Transactions A 26 (1995) 2445-2455.
[99] A. Heidarzadeh, S. Mironov, Friction stir welding/processing of metals and alloys: A comprehensive review on microstructural evaluation, Progress in Materials Science 117 (2021) 100752.

[100] K. K. OO, P. S. Ling and M. Gupta, Characteristics of Mg-based composites synthesized using a novel mechanical disintegration and deposition technique, Metallurgical and Materials Transactions A 31 (2000) 1873-1881.
[101] Jie Xu, Microhardness, microstructure, and tensile behavior of an AZ31 magnesium alloy processed by high-pressure torsion, J Mater Sci 50 (2015) 7424–7436.
[102] A. Simar, A. Mertens, S. Ryelandt, F. Delannay, L. Brassart, Mean-field model analysis of deformation and damage in friction stir processed Mg-C composites, Mater. Sci. Eng. A 723 (2018) 324–333.